Title

Advancing the study of fish populations in marine protected areas with passive acoustics and optical imaging

Author

Pagniello, Camille

Publication Date

2021

Peer reviewed|Thesis/dissertation

UNIVERSITY OF CALIFORNIA SAN DIEGO

Advancing the study of fish populations in marine protected areas with passive acoustics and optical imaging

A dissertation submitted in partial satisfaction of the requirements for the degree Doctor of Philosophy

in

Oceanography

by

Camille Pagniello

Committee in Charge:

Jules S. Jaffe, Chair
William A. Coles
Philip J. Hastings
William S. Hodgkiss
William A. Kuperman
P. Edward Parnell

2021

The Dissertation of Camille Pagniello is approved, and it is acceptable in quality and form for publication on microfilm and electronically.

University of California San Diego

2021

DEDICATION

To 12-year-old Camille, dreams do come true.

EPIGRAPH

The ocean is having a moment.

Margaret Leinen

Great periods of oceanography are defined by new kinds of instrumentation.

Roger Revelle

More and more students are playing it safe and not taking any risks. You might not succeed, but that's just part of the game.

Walter Munk

~~Play~~ Live with your heart.

Maman

TABLE OF CONTENTS

LIST OF FIGURES

LIST OF TABLES

ACKNOWLEDGEMENTS

It is slightly surreal to realize that I am finally at the end of a journey that is 17 years in the making. I am writing this last section of my doctoral dissertation, looking out at the Scripps Institution of Oceanography (SIO) pier, about to defend my PhD thesis in a few weeks' time. I have dreamt of and planned for this moment since I was 12 years old. I still cannot believe that I am about to become Dr. Camille Pagniello.

This journey has not been easy, but luckily, I have not been on it alone. First, I need to thank my advisor, mentor and friend Jules Jaffe. Your candor and support, both professionally and personally, have pushed me to be the best person and scientist I can be. You always find a way to make me laugh and have helped me establish a solid foundation upon which I will build the rest of my career. I will never be able to thank you enough for all you have done for me. Thank you to Edward Parnell for pushing me to think about the broader ecological applications of the tools and algorithms that I have developed. I strive to someday be able to orally replicate fish sounds with the same ridiculous accuracy as you. To Philip Hastings, thank you for teaching me about fish nomenclature and taxonomy. And finally, to the Bills. Thanks to William Kuperman for taking the time to teach me about ocean acoustics, even when I was the only student in the class. I hope that, after reading this dissertation, you realize that I have not been studying "whales in green stuff" over these past few years. Thank you to William Hodgkiss for entertaining my endless questions and always taking the time to discuss this research with me. Chapter 3 would not exist in its current form without both of your thoughtful input. To William Coles, thanks for our great pre-COVID conversations about acoustic propagation and for always tuning in from wherever you are in the world. A big thank you to Peter Franks, who should have been an official member of my thesis committee. Thank you for your endless wisdom and

willingness to share your insight into the bureaucratic side of academia. Your courses inspired me to explore research directions I had never considered. You are the best and my favorite professor that I have had the privilege of taking a course from during my entire post-secondary education. Finally, to Megan Cimino, thank you for leading and helping me through my first, first-author publication. I am incredibly lucky to have had you as my teammate.

This dissertation would not be possible without the assistance, guidance and support of Jack Butler. In you, I have found a mentor, collaborator and friend with a complementary skill set and who is always on the same wavelength as me. Our conservations have sparked endless research ideas that I cannot wait to pursue with you in the future. Thank you for teaching me many of the strange skills I have learned during this PhD including how to mix and pour concrete blocks and how to get your equipment off the seafloor.

I have had the privilege of advising and mentoring thirteen undergraduate and master's students who have assisted with and helped further this research. Thank you to Annie Rosen, Nicolas Jeffress, Annette Brennan, Addison Sherwood, Adithya Balaji, Helen Cai, Kian Bagheri, Mohammad Sederat, Sarah Reynolds, Gabriel Mink, Chad Mackie, Eamon Patamasing and Clare Walker. These students came with diverse backgrounds in a variety of disciplines (i.e., acoustics, engineering, machine learning, oceanography, marine biology, etc.). I am proud to say that most of them are now pursuing MSs and PhDs in top STEM graduate programs in the United States while others are now data scientists and engineers at top companies in the tech industry.

Thank you to the members of the Jaffe Laboratory for Underwater Imaging including Khalil Jackson, Pichaya Lertvilai, Eric Orenstein, Devin Ratelle, Paul Roberts, Hannah Walker and Joe Walter. Thank you to the members and groupies of the Franks Lab including Gabriella

Berman, Jessica Carrière-Garwood, Allison Cusick, Shailja Gangrade, Taylor Hernandez, Bryce Inman, Tammy Russell and Angela Szesciorka.

Thank you to the wonderful staff and faculty who have helped me along the way including Gilbert Bretado, Leslie Costi, Denise Darling, Tim DeBold, Benjamin Frable, Sarah Gille, Erilynn Heinrichsen, Beverly Kennedy, Margaret Leinen, Maureen McCormark, Maureen McGreevy, Art Miller, Ally Rice, Joshua Reeves, Jit Sarkar, Aaron Thode, Sienna Thomas and Shelley Weisel. To Drew Lucas and Kate Ricke, thank you for embracing me into your teaching team. Thanks to Adrian Castillo and Rials Christensen for supporting me as I learned how to be a lead instructor. Thank you to all the members of the SIO Unlearning Racism in Geoscience (URGE) Pod, especially my co-leaders Keiara Auzzene and Jamin Greenbaum, for our thoughtful discussions on racism and injustices impacting society and how they are perpetuated in academia. I hope that the anti-racist, institution-wide policies we drafted to improve accessibility, justice, equity, diversity and inclusion at SIO will soon be implemented.

During my time at SIO, I founded and chaired the Scripps Graduate Student Council. Thank you to all the student representatives and co-chairs who helped support this endeavor to advance the interests of all graduate students at SIO. Also, thank you to all the AOS and BO students during my tenure at SIO including Jennifer Brandon, Rebecca Cohen, Srishti Dasarathy, Lindsey Ekern, Natalya Gallo, Alfredo Girón-Nava, Regina Guazzo, Madeleine Harvey, Allison Ho, Mukta Kelkar, Anna Krumpel, Jennifer Le, Leah Lewis, Emma Ozanich, Goldie Phillips, Natalie Posdaljian, Edward Richards, Timothy Rowell, Hugh Runyan, Kerri Seger, Anne Simonis, Eric Snyder, Amy Van Cise, Christopher Verlinden and Morgan Ziegenhorn.

Most importantly, thank you to my friends and members of Team House and Associates, namely Matt Giddings, Jill Fader, Sarah Maher, Raul Martinez, Sarah Schwenck, Eadoh Reshef

and my nemesis Ashlyn Giddings. Without your friendship, I am certain that I would no longer be sane at the end of this journey. Thank you for being my family away from home and embracing my emphatic love of Canada. Thank you to members of my trivia team including Brianne Bozzella, Matthew Costa, Erica Ferrer, Andy Gross, Maitreyi Nagarkar and Ben Whitmore for all the free beer. A very special thank you to my K.C. and Ty Wilson. Thank you for celebrating my successes, listening to my sometimes-endless complaints and helping me explore San Diego. I hope that we will be life-long friends. To Kelley McBride, thanks for being an incredible friend that I can always count on. Also, thank you to Maya Becker, Irina Köster, Laura Lilly, Carrie McIntosh, Trevor Purdy and Kristen Zeiden for your friendship since day one. Finally, to Mary Munk, thank you for always checking-in on me. You and Walter welcomed me with open arms into the SIO and La Jolla community and showed me that I belonged at one of the most prestigious oceanographic institutions in the world. I cannot begin to thank you for your endless support and guidance.

Maman, Daddy, Céleste, Diane, Normand, Ernie et Grandmaman; Je suis vraiment chanceuse que vous êtes ma famille. Merci pour tout l'amour et l'encouragement au cours de ces 29 années. Sans vous, je ne serais pas ici aujourd'hui. Ma liste d'expérience, de réussite et de joie serait beaucoup plus courte. Merci de toujours soutenir mes rêves. Je vous aime beaucoup. Lastly, Dr. da Vinci, thank you for all the cuddles. You are by far the best decision I made during my time as a graduate student.

This dissertation reflects six years of work and too much Matlab® code written to process over 24 TB of acoustic recordings from six different sites and over 12 TB of images from four cameras. Thank you to all of the divers who helped collect this data, specifically Christian McDonald, Ashleigh Palinkas and Richard Walsh, who helped organize diving

operations. I cannot wait to continue to explore this dataset, as this dissertation only scratches the surface.

Most of the funding for this research was provided by the California Sea Grant College Program Project Award Number NA14OAR4170075 through NOAA'S National Sea Grant College Program, U.S. Dept. of Commerce. Funding was also provided by a Natural Sciences and Engineering Research Council of Canada (NSERC) Postgraduate Scholarship – Doctoral, Art Proceeds – SIO Graduate Fellowship, Greenridge Sciences Fellowship in Underwater Acoustics, H. William Menard Memorial Fellowship and Fleet Admiral Chester W. Nimitz Fellowship to me. Fieldwork aboard the R/V Robert Gordon Sproul was supported by a grant from the UC Ships Fund Program to me.

Chapter 1, in full, is a reprint of the material as it appears in *Frontiers in Marine Science*. Pagniello, Camille; Cimino, Megan; Terrill, Eric, 2019. The dissertation author was the primary investigator and author of this paper.

Chapter 2, in full, is a reprint of the material as it appears in *Oceanography*. Pagniello, Camille; Butler, Jack; Rosen, Annie; Sherwood, Addison; Roberts, Paul; Parnell, Edward; Jaffe, Jules; Širović, Ana, 2021. The dissertation author was the primary investigator and author of this paper.

Chapter 3, in part, is currently being prepared for submission for publication of the material. Pagniello, Camille. The dissertation author was the primary investigator and author of this paper.

VITA

2010 B.Sc. Honours Co-op, Marine Biology and Physics with minors in Mathematics and Ocean Sciences
Dalhousie University
Honours Thesis Title: "Spatial and temporal variation in water mass characteristics and the normalized zooplankton biomass size spectrum in the Northumberland Strait"

2016 M.Sc., Oceanography
Scripps Institution of Oceanography
University of California San Diego

2021 Ph.D., Oceanography
Scripps Institution of Oceanography
University of California San Diego
Dissertation Title: "Advancing the study of fish populations in marine protected areas with passive acoustics and optical imaging"

PUBLICATIONS

Pagniello, C.M.L.S. Three-dimensional localization and tracking of individual fish using *in situ* sound playbacks in a complex shallow-water environment. *In prep.*

Pagniello, C.M.L.S., Butler, J., Rosen, A., Sherwood, A., Roberts, P., Parnell, P.E., Jaffe, J.S., Širović, A. 2021. An optical imaging system to capture images in low-light aquatic habitats using only ambient light. *Oceanography* 34:3. doi:10.5670/oceanog.2021.305

Butler, J., Pagniello, C.M.L.S., Jaffe, J.S., Parnell, P.E., Širović, A. 2021. Diel and seasonal variability in kelp forest soundscapes off the Southern California coast. *Frontiers in Marine Science* 8:357. doi:10.3389/fmars.2021.629643

Pagniello, C.M.L.S., Cimino, M., Terrill, E. 2019. Mapping Fish Chorus Distributions in Southern California using an Autonomous Wave Glider. *Frontiers in Marine Science* 6:526. doi:10.3389/fmars.2019.00526

Cavole, L.M., Demko, A.M., Diner, R.E., Giddings, A., Koester, I., Pagniello, C.M.L.S., Paulsen, M.-L., Ramirez-Valdez, A., Schwenck, S.M., Yen, N.K., Zill, M.E., Franks, P.J.S. 2016. Biological Impacts of 2013-2015 Warm-Water Anomalies in the Northeast Pacific: Winners, Losers and the Future. *Oceanography* 29(2):273–285. doi:10.5670/oceanog.2016.32

Palmer, P.I., Parrington, M., Lee, J.D., Lewis, A.C., Rickard, A.R., Bernath, P.F., Duck, T.J., Waugh, D.L., Tarasick, D.W., Andrews, S., Aruffo, E., Bailey, L.J., Barrett, E., Bauguitte, J.-B.S., Curry, K.R., Di Carlo, P., Chisholm, L., Dan, L., Forster, G., Franklin, J.E., Gibson, M.D., Griffin, D., Helmig, D., Hopkins, J.R., Hopper, J.T., Jenkin, M.E., Kindred, D., Kliever, J., Le Breton, M., Matthiesen, S., Maurice, M., Moller, S., Moore, D.P., Oram, D.E., O'Shea, S.J., Owen, R.C., Pagniello, C.M.L.S., Pawson, S., Percival, C.J., Pierce, J.R., Punjabi, S., Purvis, R.M., Remedios, J.J., Rotermund, K.M., Sakamoto, K.M., Da Silva, A.M., Strawbridge, K.B., Strong, K., Taylor, J., Trigwell, R., Tereszchuk, K.A., Walker, K.A., Weaver, D., Whaley, C., Young, J.C.. 2013. Quantifying the impact of BOReal forest fires on Tropospheric oxidants over the Atlantic using Aircraft and Satellites (BORTAS) experiment: Design, execution and science overview. *Atmospheric Chemistry and Physics* 13(13):6239-6261. https://doi.org/10.5194/acp-13-6239-2013.

ABSTRACT OF THE DISSERTATION

Advancing the study of fish populations in marine protected areas with passive acoustics and optical imaging

by

Camille Pagniello

Doctor of Philosophy in Oceanography

University of California San Diego, 2021

Jules S. Jaffe, Chair

Marine protected areas (MPAs) have been established worldwide to protect coastal ecosystems and the species inhabiting them. However, it is difficult to quantify whether these areas are adequately protecting the targeted species. Current monitoring methods, such as diver surveys, allow fish species to be identified *in situ*, but are known to alter fish presence and behavior. Other methods, such as acoustic telemetry, are relatively invasive, requiring the implantation of a transmitter tag into the fish. Additionally, both these approaches are laborious and expensive, relying on good weather and a talented pool of fisherman and divers. Methods that are non-invasive, such as passive acoustics, offer good spatial and temporal coverage, but ascribing specific calls or sounds to the species creating them is difficult, particularly for fishes.

Camera deployments allow for *in situ* observations of behavior, diversity and frequency of occurrence of a wide variety of animals but are often hindered by low-light and battery limitations. Here, I developed passive acoustic and optical imaging tools to study sound-producing fish that allow improved performance over contemporary methods. These tools were used to study chorusing fish in protected kelp forests along the southern California coast. First, an autonomous Wave Glider was equipped with a passive acoustic recorder to map the distribution of five soniferous fish spawning aggregations. The fish choruses started near sunset and ended before sunrise, and were almost exclusively recorded offshore of kelp forests. Second, a low-cost underwater optical imaging system that utilizes a consumer-grade camera to capture high-quality images in low-light aquatic habitats without artificial lighting was designed and developed. The system was used to captured >1,500 images per day over 14 days, which revealed biologically important behaviors as well as daily patterns of presence/absence. Lastly, an underwater controlled source of known position was used to improve an acoustic localization algorithm to track fish to a resolution of a few meters. The fish remained outside of the MPA while vocalizing. This work demonstrates the promise of these tools to non-invasively monitor animal behavior, biodiversity and frequency of occurrence in MPAs as well as other nearshore areas.

Chapter 1: Mapping Fish Chorus Distributions in Southern California Using an Autonomous Wave Glider

frontiers in Marine Science

ORIGINAL RESEARCH
published: 29 August 2019
doi: 10.3389/fmars.2019.00526

Mapping Fish Chorus Distributions in Southern California Using an Autonomous Wave Glider

Camille M. L. S. Pagniello[1], Megan A. Cimino[1,2] and Eric Terrill[1]*

[1] Scripps Institution of Oceanography, University of California, San Diego, La Jolla, CA, United States, [2] Institute of Marine Sciences, University of California, Santa Cruz, Santa Cruz, CA, United States

Passive acoustics is a tool to monitor behavior, distributions, and biomass of marine invertebrates, fish, and mammals. Typically, fixed passive acoustic monitoring platforms are deployed, using *a priori* knowledge of the location of the target vocal species. Here, we demonstrate the ability to conduct coastal surveys of fish choruses, spatially mapping their distributions with an autonomous surface vehicle. For this study, we used an autonomous Liquid Robotics Wave Glider SV3 equipped with a Remora-ST underwater acoustic recorder and hydrophone. The exploratory 15-day deployment transited through three marine reserves, resulting in approx. 200 h of passive acoustic recordings, and revealed five distinct fish choruses from La Jolla to Capistrano Beach, CA (approx. 80 km separation), each with unique acoustic signatures. Choruses occurred in the evening hours, typically in the 40 to 1000 Hz band. There was a lack of both temporal and frequency partitioning amongst the choruses, but some choruses exhibited distinct spatial niches by latitude and water temperature. These results suggest that the mobility of the Wave Glider allows for persistent surveys and studies that otherwise may be too challenging or costly for stationary or ship-based sensors; a critical consideration for documenting biological activity over large spatiotemporal scales, or sampling of nearshore marine reserves.

Keywords: fish chorus, passive acoustics, Wave Glider, fisheries, autonomous platform, fish sounds

OPEN ACCESS

Edited by:
Leonard Pace, Schmidt Ocean Institute, United States

Reviewed by:
Robert McCauley, Curtin University, Australia
Miles James Parsons, Australian Institute of Marine Science (AIMS), Australia

****Correspondence:***
Camille M. L. S. Pagniello
cpagniello@ucsd.edu

Specialty section:
This article was submitted to Ocean Observation, a section of the journal Frontiers in Marine Science

Received: *15 November 2018*
Accepted: *12 August 2019*
Published: *29 August 2019*

Citation:
Pagniello CMLS, Cimino MA and Terrill E (2019) Mapping Fish Chorus Distributions in Southern California Using an Autonomous Wave Glider. Front. Mar. Sci. 6:526. doi: 10.3389/fmars.2019.00526

INTRODUCTION

Sound production plays an important role in the life history of many marine animals including invertebrates, fish and mammals (Tyack, 1998). Fish, in particular, are known to vocalize while defending their territory, feeding and spawning (Winn, 1964). Fish in some spawning aggregations are known to vocalize during certain time periods over a few hours (Cato, 1978). This "chorus" results in a significant increase in ambient sound pressure levels due to the large number of fishes producing sound at the same time. As such, fish choruses can be used to determine the timing of spawning seasons, species distributions and essential habitat (Gannon, 2008; Luczkovich et al., 2008).

Passive acoustics can be used to record sound production. It enables monitoring of soniferous animal presence and behavior over large temporal (i.e., on the order of years) and spatial (i.e., on the order of 10s km) scales because of the ocean's transparency to sound (Jensen et al., 2011). While passive acoustic monitoring can generate long temporal records at a single location, the spatial

coverage is small compared to those of interest to ecosystem managers that are required to monitor vast areas and entire coastlines. Given that passive acoustic recorders are traditionally deployed on stationary platforms (Mellinger et al., 2007; Sousa-Lima et al., 2013), there is a need for more instrument platforms that are mobile and capable of expanding the region that is monitored.

Recent studies show the increased deployment of passive acoustic recorders on autonomous mobile vehicles (e.g., Baumgartner and Fratantoni, 2008; Klinck et al., 2009; Wall et al., 2012). Slocum buoyancy gliders, for example, have been used to map the sound production of various fish species including red grouper (*Epinephelus morio*), toadfish (*Opsanus* spp.) and cusk eel (*Lepophidium* sp./*Ophidion* sp.) in the Gulf of Mexico (Wall et al., 2012, 2013, 2014) as well as various species of whales in the Gulf of Maine (Baumgartner et al., 2013). Similar to other autonomous vehicles, the Wave Glider (Hine et al., 2009) is a mobile platform that can be equipped with environmental sensors for measuring temperature, salinity, fluorescence, as well as acoustic doppler current profilers (ADCP), acoustic transponders and GPS motion sensors (e.g., Kraus and Bingham, 2011; Mullison et al., 2011; Bingham et al., 2012). It is unique in that it can harness ocean wave energy for forward platform propulsion, allowing for extended mission durations without the requirement for diving to depth, as is needed for buoyancy gliders. When equipped with passive acoustic recorders, Wave Gliders have been primarily used for the monitoring of marine mammals in deep water. Although the Wave Glider generates mostly low-frequency noise, the source level of low-frequency humpback whale vocalizations is high enough to enable the use of a Wave Glider to study the whale's acoustic behavior (Wiggins et al., 2010; Bingham et al., 2012). Soniferous fish, however, typically produce low-frequency sounds at source levels similar to or lower than marine mammals (Erisman and Rowell, 2017), making it a more challenging signal-to-noise environment for a Wave Glider to operate in.

The aim of this study was to determine if autonomous Wave Gliders can be used to record fish sounds and choruses in California nearshore environments, which are noisier and shallower than open ocean environments. A passive acoustic recorder was attached to a Wave Glider during an exploratory 15-day mission along the southern California coast. Recordings of different chorusing fish species collected during this study show that a Wave Glider equipped with passive acoustic monitoring capabilities enables scientists and managers to collect fisheries-independent data about the distribution of fish over large areas.

MATERIALS AND METHODS

Wave Glider and Sensors

The Wave Glider SV3 (Liquid Robotics, a Boeing company, Sunnyvale, CA, United States) is an autonomous surface platform with a tether that connects a surface float to a subsurface glider with articulating wings (hereafter referred to as the "sub") (**Figure 1**). The wings convert vertical wave motion into lift, resulting in forward propulsion. The surface float contains Iridium satellite communications and control computers as well as batteries charged by solar panels. The location and condition of the Wave Glider was recorded and telemetered every 5 min. The Wave Glider also has an Automatic Identification System (AIS) receiver, which was monitored closely in real-time for boat traffic to avoid collisions.

A Remora-ST underwater acoustic recorder (Loggerhead Instruments, Inc., Sarasota, FL, United States) was attached to custom made steel plates on the topside of the sub at 4 m depth (**Figure 1**). The recorder sampled at 48 kHz for 3 min every 5 min. The hydrophone had a typical sensitivity of −201 dB V/μPa and had a pre-amplifier of 33 dB gain. The acoustic recorder had a 16-bit analog-to-digital converter with a −1 to 1 V response. The passive acoustic recorder and hydrophone were factory calibrated and thus, no additional calibrations were conducted.

Study Area

The Wave Glider was deployed along the southern California coast from July 20 to August 3, 2017 (**Figure 2A**). The deployment started and ended in La Jolla, CA, where the vehicle ran inshore-offshore surveys near the kelp forests in the Matlahuayl State Marine Reserve (SMR), a habitat that supports a diverse assemblage of fishes. From July 26 to 30, 2017, the Wave Glider transited from La Jolla to Capistrano Beach, CA and back, passing through the San Diego-Scripps Coastal State Marine Conservation Area (SMCA) and the Swami's SMCA. The vehicle was constrained to waters greater than 10 m depth and approx. 2 km offshore to avoid entanglement in kelp forests, collisions with nearshore rocks and running aground in shallow waters. The Wave Glider track extended further offshore as it approached Oceanside Harbor, a high boat traffic area, and a restricted area within the Camp Pendleton Military exercise area. Overall, the Wave Glider traveled 296 km in a straight path along the coast at an average speed of 0.25 m/s. Locations along the track were not equally sampled during the day and night (**Figure 3**).

Acoustic Data Processing

Long-term spectral averages (LTSAs) of the passive acoustic recordings were computed using *Triton*, a Matlab-based (The Mathworks, Inc., Boston, MA, United States) acoustic data display and analysis software program (Wiggins, 2003). The program calculates fast Fourier transforms (FFTs), averages successive FFTs into a single spectral average and then, displays them as spectrograms (Wiggins and Hildebrand, 2007). FFTs were calculated using a Hanning window, 0% overlap and 1-Hz frequency bins. Successive FFTs were averaged over 5 s. LTSAs allowed for a visual scan of 199 h of recordings and to discern the start and end times of a chorus.

Choruses were divided into 10 s sub-samples. Spectrograms of each sub-sample were generated by dividing the time series into equal-length segments of 8192 samples having 90% overlap, applying a Kaiser-Bessel window of $\alpha = 2.5$ to each segment, taking the FFT of each segment, and averaging the squared magnitude of the FFT of overlapped, windowed segments. The overall sensitivity (−77.7 dB re 1 μPa/counts) of the acoustic recorder was applied to the spectrograms to yield

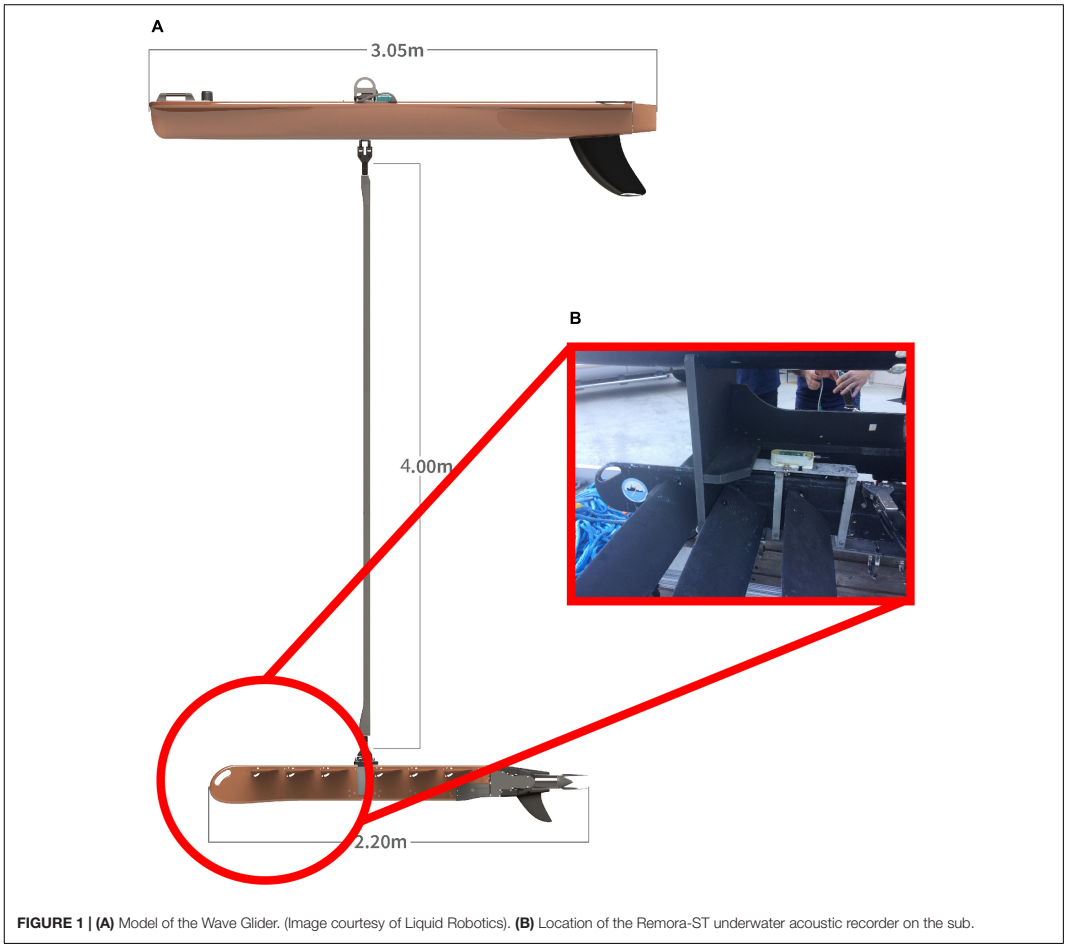

FIGURE 1 | (A) Model of the Wave Glider. (Image courtesy of Liquid Robotics). **(B)** Location of the Remora-ST underwater acoustic recorder on the sub.

calibrated values of spectral density (dB re 1 μPa^2/Hz). Frequency bandwidth (Hz) of each chorus was measured directly from spectrograms while peak frequency (Hz) was estimated from pressure spectral density curves. Received level (dB re 1 μPa peak-to-peak and rms) of each sub-sample was estimated to determine when the chorus reached its peak after sunset. When individual calls could be identified within a fish chorus, call duration (seconds) and frequency bandwidth (Hz) were measured directly from spectrograms. Peak frequency (Hz) of individual calls were estimated from pressure spectral density curves. Received level (dB re 1 μPa peak-to-peak and rms) of the individual calls was also calculated.

Choruses were classified as originating from fish based on the similarity of their acoustic characteristics to other reported fish calls and choruses (e.g., Parsons et al., 2016, 2017; McWilliam et al., 2018). A fish chorus was classified as a distinct type based on its frequency content, timing and location along the southern California coast as well as the duration and number of pulses of individual calls when possible.

Environmental Data

Environmental data was obtained to identify features that might be indicative of fish habitats. Bathymetric data for California that cover the continental shelf at 10 m contour resolution to a depth of 600 m were acquired from the California Department of Fish and Wildlife (CDFW)[1]. The union of kelp canopy data from 1989, 1999, 2002–2006, and 2008 collected during aerial surveys by the CDFW was used to show the persistent extent of kelp in California (i.e., a count of years of overlap per kelp bed)[1]. The images were processed and distributed

[1]https://www.wildlife.ca.gov/Conservation/Marine/GIS/Downloads

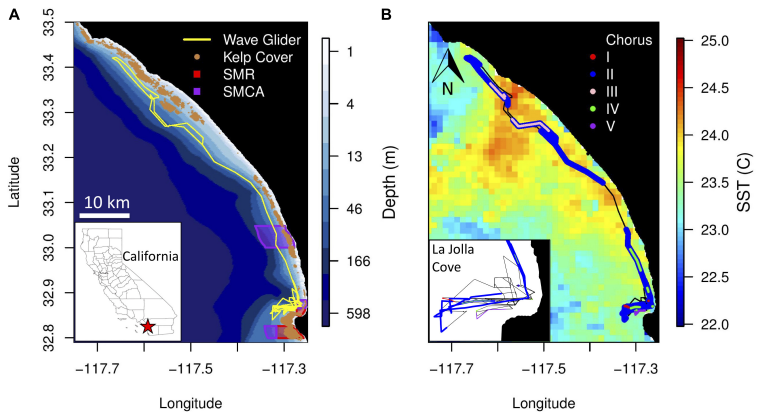

FIGURE 2 | (A) Bathymetry along the Wave Glider track (yellow line) from La Jolla Cove, San Diego, to Capistrano Beach, CA. Historical kelp cover is shown in brown. California State Marine Reserves (SMR) and State Marine Conservation Areas (SMCA) within the study area are shown in red and purple, respectively. **(B)** Average sea surface temperature (°C) during the Wave Glider deployment. The locations where the five fish choruses were recorded are shown in red (Type I), blue (Type II), light pink (Type III), green (Type IV) and purple (Type V). Each chorus is mapped separately in **Supplementary Figure S1**. (Inset) Zoomed in view of the location of the fish choruses recorded near La Jolla Cove.

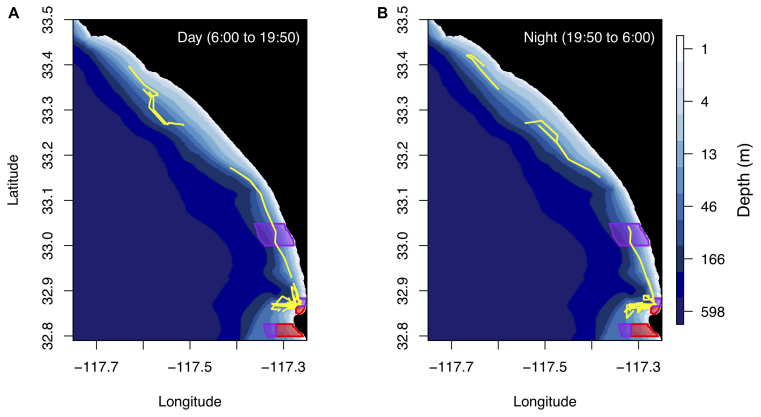

FIGURE 3 | (A) The Wave Glider track during the day from sunrise to sunset. **(B)** The Wave Glider track during the night from sunset to sunrise. Note, some areas were not sampled during both the day and night. Bathymetry along the Wave Glider track (yellow line) from La Jolla Cove, San Diego, to Capistrano Beach, CA and California SMR and SMCA within the study area are shown in red and purple, respectively. Average sunset and sunrise times are also shown on the maps. Times are reported in Pacific Standard Time.

by the CDFW Marine Region GIS Lab with a resolution of 2 m. Daily sea surface temperature (SST) measurements were made by an advanced very high-resolution radiometer aboard NOAA's Polar Operational Environmental Satellites (POES). The measurements have a 0.0125-degree resolution[2]. SST measurements were patchy due to cloud cover during the Wave Glider deployment; therefore, all measurements during the deployment were averaged to obtain a snapshot of surface water temperature along the coast.

RESULTS

Passive acoustic recordings from the 15-day deployment of the Wave Glider contained a diverse array of anthropogenic and biological sounds including surface crafts, dolphins, sea lions,

[2]https://coastwatch.pfeg.noaa.gov/erddap/griddap/erdATssta1day.html

snapping shrimp, and fish. Low-frequency noise originating from the Wave Glider (i.e., flow noise, the sub wings changing position, and tether strumming) was also recorded. Below 1500 Hz, the most notable sounds recorded are assumed to originate from fish based on the frequency, duration, received levels, and timing of the sound. We identified five distinct fish calls, but the species producing all but one of these choruses are unknown. The acoustic characteristics and spatiotemporal distribution of five different fish choruses (I–V) are described below. All times are reported in Pacific Standard Time.

Acoustic Characteristics and Spatiotemporal Distribution of Fish Choruses

Chorus I was the shortest chorus recorded, starting around 18:58 and ranging from 0.8 to 3.5 h (**Figures 4B**, **5A** and **Table 1**). It comprised of short-duration (0.25 ± 0.05 s, mean ± SD), mid-frequency (approx. 420–880 Hz) croaks (**Figures 5B,C** and **Table 2**). Individual calls were only observed during chorusing. Received levels reached a maximum of 107 ± 2 dB re 1 μPa rms approx. 12 min after sunset. Sunset throughout the deployment was around 19:50. The chorus was only recorded offshore of the La Jolla Cove kelp beds at approx. 32.85°N (**Figures 2B**, **4A**).

Chorus II was the longest chorus recorded, ranging from 6 to 13.5 h and started around 18:53 (**Table 1** and **Figure 4B**). Received levels were a maximum of 119 ± 7 dB re 1 μPa rms in two distinct frequency bands (i.e., approx. 300–600 Hz and 650–1000 Hz) during chorusing (**Figure 5D**). Chorus II was recorded most often (10 of the 14 nights) and was the only chorus recorded throughout the entire deployment from La Jolla to Capistrano Beach, CA (approx. 32.85 to 33.4°N), including both SMCAs (**Figures 2B**, **4A**). Individual calls were short-duration pulses of 0.19 ± 0.02 s (**Figures 5E,F**). Very few individual calls were recorded (**Table 2**). The presence of Chorus II does not appear to be related to the kelp distribution or SST.

Individual calls of Chorus III comprised of a pulse train, followed by zero to three short grunts (**Figures 5H,I**). When Chorus III occurred, its energy overlapped with energy from Chorus II in the 300 to 500 Hz frequency band. As such, calls recorded when Chorus II was not present displayed energy from approx. 60 to 540 Hz (**Table 2**). The chorus was only recorded twice when the Wave Glider transited near an area with elevated SST (**Figures 2B**, **4A**). This area was offshore of the historical kelp beds located 5 km south of San Onofre, CA (approx. 33.3°N). On both July 27 and 28, 2017, the chorus started slightly before 18:00 and lasted between 5 to 6 h (**Figures 4B**, **5G**). Received levels of the chorus peaked at 125 ± 8 dB re 1 μPa rms approx. 40 min before sunset (**Table 1**).

Chorus IV was recorded offshore of the La Jolla kelp beds up to Solana Beach, CA (approx. 32.85 to 32.99°N, **Figures 2B**, **4A**). Individual calls comprised of a grunt train of two to four grunts, with each grunt decreasing in duration (**Figures 5K,L**). More individual calls of Chorus IV were recorded compared to any other chorus (**Table 2**). This chorus started at around 20:20 and its received levels peaked at 119 ± 11 dB re 1 μPa rms on average 1.5 h after sunset (**Figures 4B**, **5J** and **Table 1**).

Chorus V was only recorded once on August 2, 2017 starting at ∼ 00:40 and lasted for 4 h (**Figures 4B**, **5M** and **Table 1**). It occurred approx. 2 km offshore of La Jolla Cove (approx. 32.85°N). The chorus comprised of one long, continuous tonal with multiple harmonics. No individual calls were recorded.

DISCUSSION

Knowledge of the location of fish choruses and their associated spawning aggregations is vital to the implementation of fisheries protection measures. Five distinct fish choruses were recorded by our Wave Glider equipped with a passive acoustic recorder transiting from La Jolla to Capistrano Beach, CA, confirming that the Wave Glider is a potential tool for future fisheries

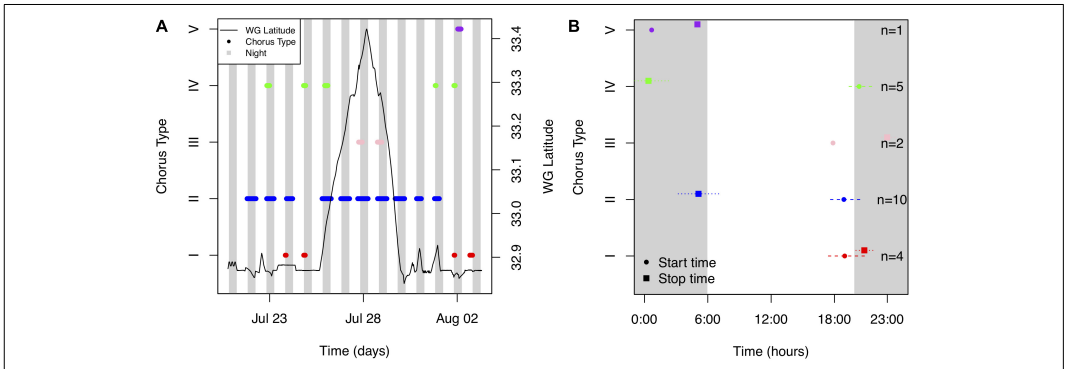

FIGURE 4 | (A) Occurrence of five fish choruses [red (Type I), blue (Type II), light pink (Type III), green (Type IV) and purple (Type V) dots] as a function of time (days) and latitude during the entire deployment. The latitude of the Wave Glider (WG) over time is shown as a solid black line. **(B)** The mean and standard deviation of start (circles) and end (squares) times of each chorus. The sample size (*n*) is shown. The time between sunset and sunrise (i.e., night) is shaded gray. Times are reported in Pacific Standard Time.

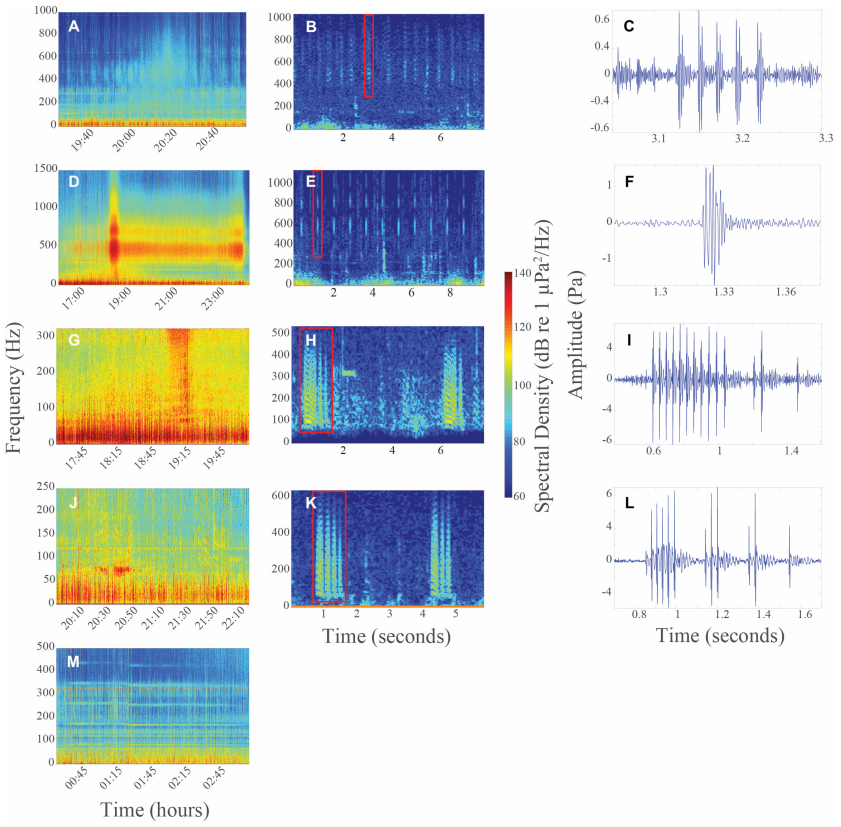

FIGURE 5 | (A) Long-term spectral average (LTSA) of Chorus I on 07/24/2017. **(B)** Spectrogram and **(C)** time series of individual call of Chorus I on 07/24/2017 at 21:10:25 (band pass filter = 395–1015 Hz). **(D)** LTSA of Chorus II on 07/27/2017. **(E)** Spectrogram and **(F)** time series of individual call of Chorus II on 07/26/2017 at 17:57:32 (band pass filter = 335–1115 Hz). **(G)** LTSA of Chorus III on 07/27/2017. **(H)** Spectrogram and **(I)** time series of individual call of Chorus III on 07/28/2017 at 19:15:04 (band pass filter = 40–535 Hz). **(J)** LTSA of Chorus IV on 07/22/2017. **(K)** Spectrogram and **(L)** time series of individual call of Chorus IV on 08/01/2017 at 21:25:42 (band pass filter = 25–635 Hz). **(M)** LTSA of Chorus V on 08/02/2017. All spectrograms used a Hanning window, f_s = 48 kHz, NFFT = 8192 and overlap = 90%. Time series are of the individual calls highlighted with a red box on each spectrogram. Color in all LTSAs and spectrograms represents spectral density (dB re 1 μPa^2/Hz), with red indicating highest received levels. Times are reported in Pacific Standard Time.

passive acoustic work in this region. The acoustic characteristics as well as the spatial and temporal occurrence of Chorus I are similar to the fish chorus reported by Butler et al., 2017 and Pagniello et al., 2017; however, individual calls recorded in our study did not provide clear confirmation that these are the same fish choruses. Chorus II is the same chorus first reported by Reshef et al., 2018 near Del Mar, CA. We are, however, the first to identify individual calls of this chorus. We are also the first to document Chorus III; although it is not the first fish chorus recorded near San Onofre, CA (D'Spain et al., 2013). Chorus IV is the same chorus that was recorded by Butler et al., 2017 further south offshore of Bird Rock, San Diego, CA. Given the large number of fish species that are reported to spawn during the summer months in this area (Love, 2011), it is impossible to identify the species of fish producing choruses I–IV with the currently available information. However, while the species for choruses I–IV are unknown, Chorus V is the hum of a plain midshipmen (*Porichthys notatus*) (Ibara et al., 1983).

While the Wave Glider survey occurred over a short timeframe and more data are needed to determine the full spatial extent and temporal boundaries of the choruses, initial observations suggested the choruses did not exhibit a distinct frequency or temporal niche, but spatial patterns by latitude and SST were observed. All choruses had high received levels primarily in 40 to 1000 Hz band and started near sunset. In

TABLE 1 | Frequency and temporal characteristics (mean ± standard deviation) of five distinct fish choruses.

Chorus type	Start time	Duration (hours)	Frequency band(s) (Hz)	Peak frequency (Hz)	Maximum received level (dB re 1 μPa rms)	Peak time post sunset (hours)	Number of occurrences (*n*)
I	18:58 ± 01:51	0.8–3.5	328 ± 21 to 773 ± 246	410 ± 55	107 ± 2	0.2 ± 1.7	4
II	18:53 ± 01:30	6–13.5	307 ± 31 to 596 ± 24; 651 ± 29 to 1002 ± 197	450 ± 44	119 ± 7	−3.8 ± 8.9	10
III	17:52 ± 00:00	4.7–5.7	55 ± 21 to 316 ± 13	128 ± 83	125 ± 8	−0.7 ± 1.0	2
IV	20:20 ± 01:11	1.1–4.2	42 ± 7 to 299 ± 30	66 ± 10	119 ± 11	1.5 ± 1.4	5
V	00:42	4.3	79, 167, 251, 339, 423	79	109	7.5	1

Start times are reported in Pacific Standard Time.

TABLE 2 | Frequency and temporal characteristics (mean ± standard deviation) of the individual calls of four distinct fish choruses.

Chorus type	Duration (seconds)	Frequency band(s) (Hz)	Peak frequency (Hz)	Received level (dB re 1 μPa peak-to-peak)	Received level (dB re 1 μPa rms)	Number of occurrences (*n*)
I	0.25 ± 0.05	419 ± 84 to 880 ± 96	548 ± 99	120 ± 2	99 ± 2	119
II	0.19 ± 0.02	435 ± 60 to 632 ± 66; 694 ± 55 to 853 ± 63	528 ± 65	127 ± 5	108 ± 6	29
III	0.78 ± 0.14	50 ± 12 to 297 ± 72	96 ± 38	135 ± 7	117 ± 6	286
IV	0.74 ± 0.13	45 ± 6 to 308 ± 104	80 ± 22	132 ± 4	114 ± 3	434

the southern region of the deployment, Choruses I, IV and V were only recorded offshore of La Jolla Cove. In comparison, Chorus III was only recorded further north near an area with elevated SST off San Onofre, CA. All choruses, except for Chorus II, were only recorded near historical kelp beds, suggesting kelp could be an important habitat. Chorus II displayed no spatial habitat preferences and was recorded throughout the entire deployment. Yet, Chorus II did not have the highest maximum received levels, suggesting the Wave Glider did not pass as close to Chorus II's location as to the location of other choruses, and thus, possibly explaining why few individual calls were recorded. In addition, we do acknowledge that in this study, all locations along the Wave Glider track were not surveyed at night (i.e., when most fish choruses tend to occur). Survey designs with equal day and night sampling at the same location would provide more insight into the temporal patterns in chorusing observed. Overall, however, our results demonstrate that the Wave Glider can be used for large-scale, exploratory missions to identify regions were soniferous fish are likely spawning.

Due to the constant motion of the Wave Glider and temporal variation in fish sound production, there are two important considerations when planning a survey. First, it is important to consider a chorus' received levels may not be constant throughout the chorusing period due to individual variation in sound production. Additionally, because the Wave Glider is constantly moving, it is impossible to decipher whether the maximum recorded received level was associated with the closest point of approach to the chorus or the most intense time of chorusing. A distinction between these two scenarios could be made by having the Wave Glider loiter in one location for an extended period of time during a chorus. Second, the exact start and end times (i.e., on the order of minutes) of the choruses were difficult to determine because the chorus signal fades in and out near the beginning and end of chorus. This signal fading is possibly due to the sub, where the hydrophone was attached, changing position in the water column as the Wave Glider moves, and thus, shadowing signal arrivals to the hydrophone. Therefore, these potential fish spawning locations could subsequently be targeted with stationary recorders to determine the long-term temporal patterns associated with spawning activity.

Our results suggest that Wave Gliders are an effective passive acoustic asset as either a stand-alone platform or to complement stationary passive acoustic recording platforms. If used as a stand-alone platform, Wave Gliders equipped with passive acoustic monitoring capabilities allow for the acoustic exploration of an extensive area. If a location of interest is identified, a Wave Glider could also be programed to "station-keep," and thus, acoustically monitor temporal patterns at a single location. As a precaution, Wave Gliders are not typically operated in shallow waters (<10 m) or in hazardous areas such as kelp beds, where fish choruses are most often reported to occur (e.g., Butler et al., 2017; Pagniello et al., 2017). Thus, strategic mission planning will ultimately be required to ensure that areas as close to the chorus as possible are surveyed during the expected chorusing time frame (i.e., at night). If a Wave Glider was paired with a stationary passive acoustic recording platform, long-term temporal patterns of occurrence as well as spatial extent of a fish

chorus could be defined. Both Wave Gliders and passive acoustic recorders with single hydrophones can be deployed for durations of up to 1 year. Such a dual platform approach to determine the location of chorusing may even eliminate the need of a multi-hydrophone passive acoustic array, which has significantly reduced recording durations compared to single hydrophone passive acoustic recorders. Additionally, this type of combined approach would address the two considerations detailed above (space and time). As such, an approach that uses both stationary and mobile platforms equipped with passive acoustic recorders and hydrophones in concert would be ideal.

Future studies that intend to use the Wave Glider as a platform for passive acoustic monitoring should consider integrating the passive acoustic recorder into glider's real-time system to allow for real-time feedback upon the detection of signals of interest. Furthermore, a wide range of acoustic arrays could be implemented to determine the direction of arriving signals of interest in real-time. Additionally, a depth logger and accelerometer could be attached to the sub to know the exact position of the hydrophone in the water column to determine if the fading chorus signal observed is due to the sub changing position in the water column, the propagation environment or is a natural phenomenon.

Even without these suggested platform improvements, we have shown that large-scale Wave Glider surveys in coastal environments can be used to identify the general location of fish spawning aggregations and to understand their relationships to the ocean's bio-physical properties. If paired with net sampling, diver surveys or cameras to identify the species producing these spawning sounds, the patterns we have documented could be used to create appropriate protected areas or fishing closure regions, if necessary. The Wave Glider's ability to be equipped with a wide variety of oceanographic sampling instruments enables the monitoring of all soniferous species as well as abiotic influences including anthropogenic activity, thus providing a full ecosystem view.

AUTHOR CONTRIBUTIONS

MC and ET designed the study. MC led mission programing and deployment of the Wave Glider and analyzed the Wave Glider data, environmental data and created the maps. CP processed and visualized the passive acoustic data. CP wrote the initial manuscript with contributions from MC, and all authors read and helped and revise the final version.

FUNDING

CP was supported in part by a Natural Sciences and Engineering Research Council (NSERC) of Canada Postgraduate Scholarship – Doctoral Program and the Fleet Admiral Chester W. Nimitz Fund.

ACKNOWLEDGMENTS

We are grateful to staff at the Coastal Observing Research and Development Center at Scripps Institution of Oceanography, especially Nixon Carruthers, Daniel Bedenko, Michael Jilka, and Robert Hess for help in Wave Glider programming, setup and deployment. We are also wish to acknowledge the U.S. Office of Naval Research DURIP program for supporting the research instrumentation used in this program and their long term commitment to development of unmanned systems, as well as the support of the Friedkin Foundation for research support.

SUPPLEMENTARY MATERIAL

The Supplementary Material for this article can be found online at: https://www.frontiersin.org/articles/10.3389/fmars.2019.00526/full#supplementary-material

REFERENCES

Baumgartner, M. F., and Fratantoni, D. M. (2008). Diel periodicity in both sei whale vocalization rates and the vertical migration of their copepod prey observed from ocean gliders. *Limnol. Oceanogr.* 53, 2197–2209. doi: 10.4319/lo.2008.53.5_part_2.2197

Baumgartner, M. F., Fratantoni, D. M., Hurst, T. P., Brown, M. W., Cole, T. V. N., Van Parijs, S. M., et al. (2013). Real-time reporting of baleen whale passive acoustic detections from ocean gliders. *J. Acoust. Soc. Am.* 134, 1814–1823. doi: 10.1121/1.4816406

Bingham, B., Kraus, N., Howe, B., Freitag, L., Ball, K., Koski, P., et al. (2012). Passive and active acoustics using an autonomous wave glider. *J. F. Robot.* 29, 911–923. doi: 10.1002/rob.21424

Butler, J., Parnell, E., and Širović, A. (2017). Who's making all that racket? Seasonal variability in kelp forest soundscapes. *J. Acoust. Soc. Am.* 141:3864. doi: 10.1121/1.4988635

Cato, D. H. (1978). Marine biological choruses observed in tropical waters near Australia. *J. Acoust. Soc. Am.* 64, 736–743. doi: 10.1121/1.382038

D'Spain, G. L., Batchelor, H., Helble, T. A., and McCarty, P. (2013). New observations and modeling of an unusual spatiotemporal pattern of fish chorusing off the southern California coast. *Proc. Meetings Acoust.* 19, 1–7. doi: 10.1121/1.4800997

Erisman, B. E., and Rowell, T. J. (2017). A sound worth saving: acoustic characteristics of a massive fish spawning aggregation. *Biol. Lett.* 13:20170656. doi: 10.1098/rsbl.2017.0656

Gannon, D. P. (2008). Passive acoustic techniques in fisheries science: a review and prospectus. *Trans. Am. Fish. Soc.* 137, 638–656. doi: 10.1577/T04-142.1

Hine, R., Willcox, S., Hine, G., and Richardson, T. (2009). "The wave glider: a wave-powered autonomous marine vehicle," in *Proceedings of the MTS/IEEE OCEANS Conference*, (Biloxi, MS), 1–6.

Ibara, R. M., Penny, L. T., Ebeling, A. W., van Dykhuizen, G., and Cailliet, G. (1983). "The mating call of the plainfin midshipman fish, *Porichthys notatus*," in *Predators and Prey in Fishes*, eds D. L. G. Noakes, D. G. Lindquist, G. S. Helfman, and J. A. Ward (The Hague: Dr W. Junk Publishers), 205–212. doi: 10.1007/978-94-009-7296-4_22

Jensen, F. B., Kuperman, W. A., Porter, M. B., and Schmidt, H. (2011). *Computational Ocean Acoustics*, 2nd Edn. New York, NY: Springer New York.

Klinck, H., Stelzer, R., Jafarmadar, K., and Mellinger, D. K. (2009). "AAS Endurance: an autonomous acoustic sailboat for marine mammal research," in *Proceedings of International Robotic Sailing Conference*, (Matosinhos), 43–48.

Kraus, N., and Bingham, B. (2011). "Estimation of wave glider dynamics for precise positioning," in *Proceedings of the MTS/IEEE OCEANS Conference*, (Kona), 1–9.

Love, M. (2011). *Certainly More Than You Want to Know About the Fishes of the Pacific Coast: A Postmodern Experience*. Santa Barbara, CA: Really Big Press.

Luczkovich, J. J., Mann, D. A., and Rountree, R. A. (2008). Passive acoustics as a tool in fisheries science. *Trans. Am. Fish. Soc.* 137, 533–541. doi: 10.1577/T06-258.1

McWilliam, J. N., McCauley, R. D., Erbe, C., and Parsons, M. J. G. (2018). Soundscape diversity in the Great Barrier Reef: Lizard Island, a case study. *Bioacoustics* 27, 295–311. doi: 10.1080/09524622.2017.1344930

Mellinger, D., Stafford, K., Moore, S., Dziak, R., and Matsumoto, H. (2007). An overview of fixed passive acoustic observation methods for cetaceans. *Oceanography* 20, 36–45. doi: 10.5670/oceanog.2007.03

Mullison, J., Symonds, D., and Trenaman, N. (2011). "ADCP data collected from a liquid robotics wave glider," in *Proceedings of the 2011 IEEE/OES 10th Current, Waves and Turbulence Measurements (CWTM)*, (Monterey, CA), 266–272.

Pagniello, C. M., Butler, J., D'Spain, G. L., Jaffe, J., Parnell, E., and Širović, A. (2017). Soundscape fishing: spatial variability in a low-frequency fish chorus in the southern California kelp forest. *J. Acoust. Soc. Am.* 142:2503. doi: 10.1121/1.5014140

Parsons, M. J. G., Salgado Kent, C. P., Recalde-Salas, A., and McCauley, R. D. (2017). Fish choruses off port Hedland. *Western Aust. Bioacoust.* 26, 135–152. doi: 10.1080/09524622.2016.1227940

Parsons, M. J. G., Salgado-Kent, C. P., Marley, S. A., Gavrilov, A. N., and McCauley, R. D. (2016). Characterizing diversity and variation in fish choruses in Darwin Harbour. *ICES J. Mar. Sci.* 73, 2058–2074. doi: 10.1093/icesjms/fsw037

Reshef, E. S., Demer, D. A., Wiggins, S., and Baumann-Pickering, S. (2018). *Chorusing Fish Behavioral Changes Potentially Linked to Climate Variability. in 2018 Ocean Sciences Meeting F14A-0718*. Available at: https://agu.confex.com/agu/os18/meetingapp.cgi/Paper/324358 (accessed February 12, 2018).

Sousa-Lima, R. S., Norris, T. F., Oswald, J. N., and Fernandes, D. P. (2013). A review and inventory of fixed autonomous recorders for passive acoustic monitoring of marine mammals. *Aquat. Mamm.* 39, 23–53. doi: 10.1578/AM.39.1.2013.23

Tyack, P. L. (1998). "Acoustic communication under the sea," in *Animal Acoustic Communication: Sound Analysis and Research Methods*, eds S. L. Hopp, M. J. Owren, and C. S. Evans (Berlin: Springer), 163–220. doi: 10.1007/978-3-642-76220-8_6

Wall, C. C., Lembke, C., Hu, C., and Mann, D. A. (2014). Fish sound production in the presence of harmful algal blooms in the Eastern Gulf of Mexico. *PLoS One* 9:e114893. doi: 10.1371/journal.pone.0114893

Wall, C. C., Lembke, C., and Mann, D. A. (2012). Shelf-scale mapping of sound production by fishes in the eastern Gulf of Mexico, using autonomous glider technology. *Mar. Ecol. Prog. Ser.* 449, 55–64. doi: 10.3354/meps09549

Wall, C. C., Simard, P., Lembke, C., and Mann, D. A. (2013). Large-scale passive acoustic monitoring of fish sound production on the West Florida Shelf. *Mar. Ecol. Prog. Ser.* 484, 173–188. doi: 10.3354/meps10268

Wiggins, S. (2003). Autonomous acoustic recording packages (ARPs) for long-term monitoring of whale sounds. *Mar. Technol. Soc. J.* 37, 13–22. doi: 10.4031/002533203787537375

Wiggins, S., Manley, J., Brager, E., and Woolhiser, B. (2010). "Monitoring marine mammal acoustics using Wave Glider," in *Proceedings of the MTS/IEEE OCEANS Conference*, (Washington, DC), 1–4.

Wiggins, S. M., and Hildebrand, J. A. (2007). "High-frequency acoustic recording package (HARP) for broad-band, long-term marine mammal monitoring," in *Proceedings of the 2007 Symposium on Underwater Technology and Workshop on Scientific Use of Submarine Cables and Related Technologies*, (Tokyo: IEEE), 551–557.

Winn, H. E. (1964). "The biological significance of fish sounds," in *Marine Bio-Acoustics*, ed. W. N. Tavolga (Oxford, UK: Pergamon Press), 213–231.

Conflict of Interest Statement: The authors declare that the research was conducted in the absence of any commercial or financial relationships that could be construed as a potential conflict of interest.

frontiers

Supplementary Material

1 Supplementary Figures

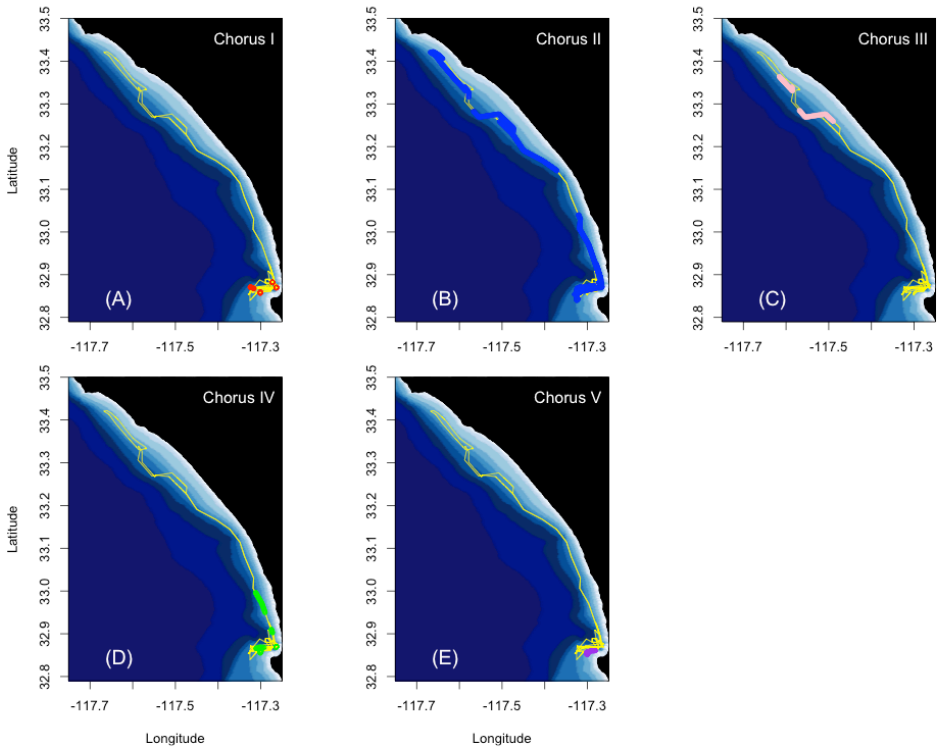

Supplementary Figure S1. Bathymetry along the Wave Glider track (yellow line) from La Jolla Cove, San Diego, to Capistrano Beach, CA and the (A) location (red) of Chorus I, (B) location (blue) of Chorus II, (C) location (light pink) of Chorus III, (D) location (green) of Chorus IV, and (E) location (purple) of Chorus V.

Chapter 1, in full, is a reprint of the material as it appears in Frontiers in Marine Science. Pagniello, Camille; Cimino, Megan; Terrill, Eric, 2019. The dissertation author was the primary investigator and author of this paper.

Chapter 2: An Optical Imaging System for Capturing Images in Low-Light Aquatic Habitats Using Only Ambient Light

An Optical Imaging System for Capturing Images in Low-Light Aquatic Habitats Using Only Ambient Light

By Camille M.L.S. Pagniello, Jack Butler, Annie Rosen, Addison Sherwood, Paul L.D. Roberts, P. Edward Parnell, Jules S. Jaffe, and Ana Širović

ABSTRACT. It is preferable that methods for monitoring fish behavior, diversity, and abundance be noninvasive to avoid potential bias. Optical imaging facilitates the noninvasive monitoring of underwater environments and is best conducted without the use of artificial lighting. Here, we describe a custom-designed optical imaging system that utilizes a consumer-grade camera to capture images in situ in ambient light. This diver-deployed system can be used to collect time series of occurrences of animals while concurrently obtaining behavioral observations for two weeks to a month (depending on the sampling rate). It has also been configured to be paired with a passive acoustic system to record time-synchronized image and acoustic data. The system was deployed in a protected kelp forest off southern California and captured >1,500 high-quality images per day over 14 days. The images revealed numerous fish species exhibiting biologically important behaviors as well as daily patterns of presence/absence. The optical imaging system is a cost-effective tool that can be easily fabricated and improves upon many of the limitations of previous systems, including deployment length and image quality in low-light and limited-visibility conditions. The system provides a relatively noninvasive way to monitor shallow marine habitats, including protected areas, and can augment traditional survey methods by providing nearly continuous observations and thus yield increased statistical power.

INTRODUCTION

Optics-based technology has become a powerful monitoring method for marine ecologists and managers (Bicknell et al., 2016). Cameras are relatively noninvasive when compared to other monitoring methods (Chaudoin et al., 2015), and they permit in situ observations of behavior (Bouchet and Meeuwig, 2015; Parnell et al., 2017), diversity (Favaro et al., 2012), and abundance (McLean et al., 2010) of a wide variety of marine animals. Despite recent advancements in underwater housings, image quality, and data storage, low-cost (i.e., <$5,000) optical imaging systems (OISs) are still challenged by power and light limitations (Balazy et al., 2018). Most battery-powered OISs that sample nearly continuously are only capable of a few hours of image or video capture (e.g., Favaro et al., 2012; Mallet and Pelletier, 2014; Wilby et al., 2016). OISs capable of longer deployments are often part of seafloor ocean observatories that are powered from shore (Aguzzi et al., 2011; Vardaro et al., 2013). Additionally, behavioral observations using OISs should be made without artificial lighting, as many fish species exhibit behavior patterns that are regulated by ambient light levels (Potts, 1990), so artificial lighting can alter behavior (Nightingale et al., 2006). However, to capture high-quality images during crepuscular periods, OISs for studies of fish are often equipped with artificial lights (e.g., Harvey et al., 2012; Fitzpatrick et al., 2013; Myers et al., 2016). Others who have not used artificial lighting simply do not record any observations during the hours near sunrise and sunset (Chaudoin et al., 2015).

Studies to monitor fish crepuscular behavior have mostly been conducted in coral reef environments (Potts, 1990), where the abundance of ambient light allows for extended observation periods. However, temperate fish species that inhabit environments such as kelp forests also display light-dependent behaviors (Hobson et al., 1981). The scotopic pigments responsible for low-light vision in many of these temperate fish species cluster about wavelengths that are spectrally similar to ambient light during twilight (Hobson et al., 1981), suggesting increased visual sensitivity during crepuscular periods when the risks and opportunities of predation are greatest (Munz and McFarland, 1973). While the complex three-dimensional habitat of kelp forests provides additional refuge to its inhabitants from visual predators (Schiel and Foster, 2015), it also presents a significant challenge to monitoring animal biodiversity using cameras without artificial light due to the decreased ambient light levels near the seafloor. Changing ocean conditions are threatening kelp forests' diverse and productive communities (Krumhansl et al., 2016), and many are now safeguarded within marine protected areas (MPAs) to ensure their persistence and resiliency. However, it is challenging and expensive to gauge the efficacy of MPAs utilizing traditional methodology (Pendleton et al., 2018).

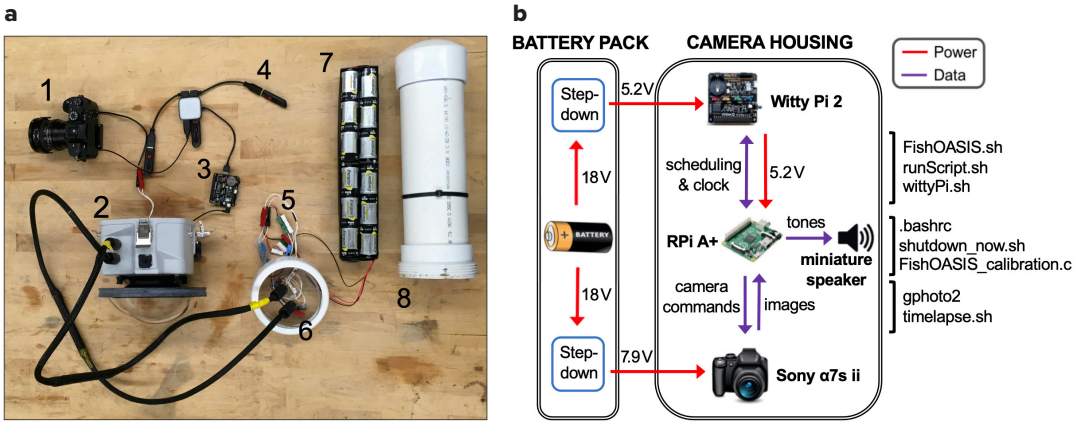

FIGURE 1. (a) Optical imaging system hardware components: (1) Sony α7s II camera with fisheye lens. (2) Ikelite camera housing. (3) Raspberry Pi A+ with Witty Pi 2 real-time clock and power management board. (4) USB flash data storage. (5) Step-down converters. (6) Wet-mateable bulkhead connectors. (7) Battery bank. (8) PVC battery housing. Note that the pictured battery bank (7) allowed for a 7-day deployment of the optical imaging system, while the battery bank that allowed for a 14-day deployment is twice as long. The miniature speaker that is soldered onto the Raspberry Pi A+ and used to produce synchronization tones is not pictured. (b) Schematic of the optical imaging system showing the flows of power (red lines) and data (purple lines) within and between the battery pack and the camera housing. Bourne shell code files (.sh) noted in the image can be found at https://github.com/cpagniel/FishOASIS/.

Traditional monitoring methods, such as diver surveys, allow species to be identified in situ; yet, these surveys are laborious, expensive, time-limited, weather-dependent, and reliant on a talented pool of divers. Additionally, a diver's presence can alter animal behavior (Dickens et al., 2011). Other monitoring methods, such as acoustic telemetry, are relatively invasive, requiring, for example, the implantation of a transmitter tag into the fish of interest. Methods that are noninvasive, such as passive acoustics, currently do not allow assignment of in situ observations to a particular species (Pagniello et al., 2019; Butler et al., 2021), as catalogues of fish sounds are either incomplete or nonexistent in most aquatic environments (Rountree et al., 2006). Given the limitations of these methods, optical imaging systems have become an increasingly popular, noninvasive, in situ monitoring method to quantify species diversity and abundance in and around MPAs (e.g., Langlois et al., 2006; Pelletier et al., 2011; Bouchet and Meeuwig, 2015).

Here, we describe the development and proof-of-concept of a novel, cost-effective OIS to enhance the efficient identification of fishes to a species level in low-light environments without artificial light. We review the capabilities of this new system and provide results from a deployment in the kelp forests within the South La Jolla State Marine Reserve (SMR). Given the performance and relatively low price of the system, this OIS has the potential to become a valuable tool for monitoring biodiversity, animal behavior, and presence/absence patterns in a host of aquatic environments. Details about the components, assembly steps, and software for the OIS are available online in this GitHub repository: https://github.com/cpagniel/FishOASIS/.

DESIGN OF THE OPTICAL IMAGING SYSTEM

The hardware for the OIS was assembled with off-the-shelf products (Figure 1a), based on a Sony α7S II (ILCE-7SM2) camera (Sony, Tokyo, JP) capable of capturing still frame images with 4,240 × 2,380 pixel resolution. The camera was fitted with a Rokinon 12 mm F2.8 fisheye lens (Elite Brands Inc., New York, NY) to provide a hemispherical field of view whose depth, and hence the imaging volume, depended on the water turbidity and ambient light. The OIS did not have stereoscopic capability.

The camera was set to "PC Remote" interface mode so that it could be controlled by a Raspberry Pi Model A+ single-board computer (SBC; Raspberry Pi Foundation, Cambridge, UK) equipped with a Witty Pi 2 real-time clock and power management (RTC/PM) board (UUGear, Prague, CZ). Bourne shell (.sh) scripts on the SBC managed camera actuation, sampling, and data storage (Figure 1b). The open-source command-line client *gphoto2* (http://gphoto.org/), which allows the camera to be controlled by the SBC via USB, was used to capture an image and download it to one of three SanDisk Cruzer 256 GB USB 3.0 flash drives (SanDisk, Milpitas, CA). If the OIS's total data storage capacity was exceeded, new images captured were not saved. The RTC/PM board kept the correct time without using network time protocol over the internet by using the accurate temperature-compensated real-time clock DS3231 (Maxim Integrated, San Jose, CA) and synched the time to the SBC clock. It also scheduled the start-up/

shutdown sequence of the SBC with a Bourne shell script. After shutdown, the power to the SBC and all its USB peripherals was fully cut by the RTC/PM board.

To enable the co-deployment of the OIS and a passive acoustic system (PAS), a miniature 8 Ω, 0.5 W metal speaker (Adafruit, New York, NY) was soldered to the SBC's general-purpose input/output (GPIO) pin 22 and ground pin. The GPIO access library WiringPi (http://wiringpi.com/) was used to output simple synchronization tones alternating between 610 Hz and 690 Hz on the startup of the SBC through the speaker. The camera, SBC, data storage, speaker, and other hardware described above were all placed in a custom-ordered camera housing with an 8-inch dome port and a 3.5-inch port extension (Ikelite, Indianapolis, IN), which was depth-rated to 60 m.

An external battery pack consisting of 48 industrial D-cell alkaline batteries (Energizer, St. Louis, MO) housed in a 30-inch PVC tube was used to power the OIS. Four banks, each consisting of 12 batteries wired in series, were wired in parallel to create a 720 Wh battery pack that outputs a nominal 18 V. Two DC-DC step-down converters (RioRand, Richmond, BC) were used to output voltages of 5.2 V and 7.9 V to power the SBC and the camera, respectively. The positive and negative output wires of each converter were soldered to a MCBH4M 4-pin micro bulkhead connector (SEACON, San Diego, CA) to connect the battery pack to the camera housing via a wet-mateable connection consisting of two MCIL4F 4-socket micro in-line connectors. This battery pack enabled the OIS to operate for 16 hours per day over 14 days, capturing a burst of 24 images taken over 2 minutes in a 12-minute cycle.

The total cost of the hardware components of the optical imaging system, including the camera, the SBC, and the housing, was approximately $4,350 (USD in 2017) at the time of fabrication (Table 1). A recent survey of components suggests that the cost of the OIS in 2021 is around $4,900 due to the significant increase in the price of bulkhead connectors.

OPTICAL IMAGING SYSTEM PERFORMANCE

Power Consumption

This OIS takes advantage of contemporary hardware that requires little power for extended use, enabling deployment lengths on the order of days to months (depending on the sampling rate) without a connection to shore for power (Table S1). The lower limit of power consumption for the system is set by the Sony camera because the camera's proximity sensor always remains activated by the housing. As a result, the camera does not enter the no-power sleep mode until 5 minutes and 4 seconds after the SBC has shut down. Given that the battery pack provides a total of 720 Wh, the camera can capture images for approximately 14.1 days with a 24 image/12-minute duty cycle over 16 operational hours per day. This is based on the 0.28 Wh power consumption of one on/off cycle of the SBC during which one image is captured and the camera sleeps. Specifically, each instance of the startup of the SBC and the capture of one image by the camera consumes on average 0.02 Wh. In addition, throughout an entire cycle, the SBC draws 0.42 A. After the SBC is shut down and prior to entering sleep mode, the camera consumes an additional 0.19 Wh. As the number of images captured during each 12-minute cycle is increased, the OIS shifts from battery limitation to storage limitation (Table S1). An .xlsx sheet with these power and data calculations is provided in the GitHub repository to help users calculate their own recording durations.

TABLE 1. Estimated cost (USD in 2017) of the major hardware components of the optical imaging system.

COMPONENTS	COST
Sony α7S II E-mount Camera with Full-Frame Sensor	$2,335
Rokinon 12 mm F2.8 Full Frame Fisheye Lens	$350
Custom Ikelite Camera Housing with 8-inch Dome Port, 3.5-inch Port Extension	$980
Battery System	$405
Raspberry Pi Model A+, 512MB RAM	$25
Witty Pi 2: Real Time Clock and Power Management	$23
SanDisk – Extreme PLUS 32 GB microSDHC UHS-I Memory Card	$25
Mini Metal Speaker with Wires 8 ohm, 0.5 W	$2
SanDisk Cruzer Glide USB 3.0, 256 GB (quantity: 3)	$150
Misc. Electronics (e.g., USB Cables, USB Hub, Molex Connectors, etc.)	$55
Total	**$4,350**

Clock Synchronization Between Optical Imaging and Passive Acoustic Systems

The OIS has a built-in method for time-aligning the OIS and an independent PAS. Given that the OIS is programmed to take only still images, a traditional clapboard cannot be used for the time synchronization between systems. In order to synchronize the OIS with a passive acoustic system, the miniature speaker that was attached to the SBC in the OIS was used to play synchronization tones at the start of each image capture sequence. These tones could be clearly identified in spectrograms of the acoustic data captured by the hydrophone co-located with the OIS (Figure S2a). While the clocks of both the passive acoustic and the optical imaging systems were synchronized before a deployment, the clocks linearly drifted apart at a rate of approximately 41.5 seconds per day (Figure S2b). Further testing of the OIS

indicated that its clock drifts less than a second in 14 days, so the majority of the drift between the systems was due to the PAS's clock. In addition to the sound produced by the miniature speaker, the sound produced by the actuation of the camera shutter could also be clearly identified in a spectrogram, providing an exact time stamp as to when an image was captured (Figure S2a). This feature could be used for future deployments without the need for a speaker if the OIS were placed within 0.5 m of a hydrophone and could thus enable users to establish species-sound associations for soniferous fishes in situ.

FIELD APPLICATION

Details about the underwater operation of the OIS, its deployment in the kelp forests on the northern edge of the South La Jolla SMR in approximately 14 m water depth from July 10–23, 2018, and post-deployment data analysis can be found in the online supplementary materials.

Fish Species Identification Using the OIS

Fish often display crepuscular behaviors that have been historically difficult to observe and characterize in temperate marine habitats (Potts, 1990). This OIS captured images with sufficient quality to permit identification of fish species without artificial lighting before sunrise (approximately 05:30 PDT) and after sunset (approximately 20:30 PDT), when light availability was extremely low (Figure 2). Images captured between these hours had the best signal-to-noise ratio, with no visible pixelation and exposure times less than 1/60 seconds and ISOs less than 128,000. Only about 80 of the 1,500 images per day were deemed unusable as they were too dark to identify any fishes. Remarkably, the system appeared to out-perform the ability of divers to visually observe animals underwater. When divers reported "poor visibility" (i.e., visibility that was <2 m), the system was capable of acquiring usable images at ranges of 3–4 m.

Overall, the high image quality reduced the need for a highly specialized expert analyst, as many different fish species can easily be distinguished based on coloration and shape, even before sunrise and after sunset. Other factors that affected identification of fish species in the images included the distance of the fish from the system, the size of the fish, and the vertical position of the fish within the water column. In general, with moderate amounts of ambient light (i.e., between 90 and 130 lux), fishes could be identified to a species level at distances of up to 8 m and to a family level at 10 m (Figure S3). However, identification of the species of a distant fish was also dependent on the shape, coloration, and size of the fish. We estimate that the OIS can resolve fishes as small as 10 cm if they are located within 2 m of the system. Additionally, fishes located higher in the water column were also more difficult to identify to species or family because the system provided a silhouetted, more ventral view of the fish.

Behavioral and Presence/Absence Observations from the South La Jolla SMR Kelp Forest

From July 10 to July 23, 2018, in the South La Jolla SMR kelp forest, a total of 17,101 images in which fish species could be identified were captured. A total of 9,601 fish across 20 species were manually identified (Table S2) by a team of analysts. Often, it was also possible to identify life stages of different fish. In this deployment, only 11% of fish were not identifiable.

Images captured various species of fish exhibiting a range of biologically important behaviors. Aggregations of kelp bass (*Paralabrax clathratus*) were observed

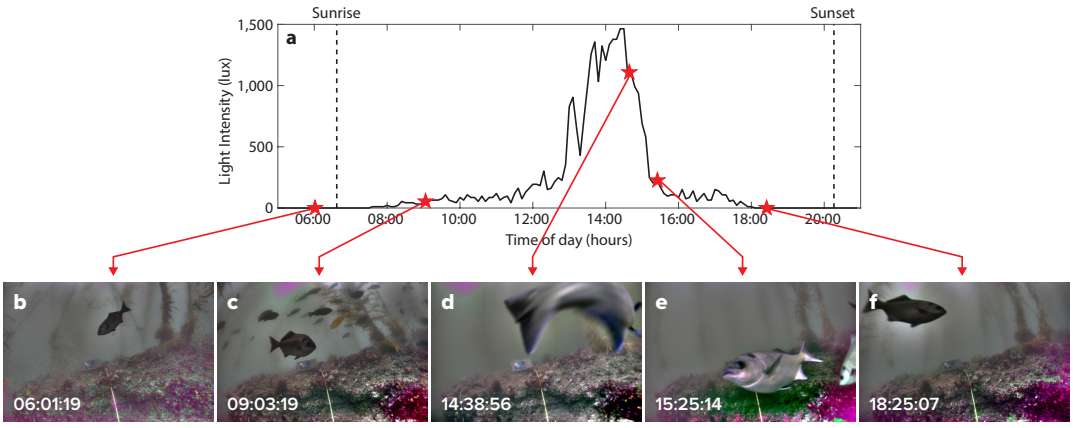

FIGURE 2. (a) Light intensity (lux) from 05:00 to 21:00 on July 12, 2018, in the South La Jolla State Marine Reserve. Images of halfmoon fish taken using the optical imaging system at (b) 06:01:19, (c) 09:03:19, (d) 14:38:56, (e) 15:25:14, and (f) 18:25:07 on July 12, 2018, at the same location. All times are local (Pacific Daylight Time).

potentially engaging in the spawning behavior described by Erisman and Allen (2006; Figure 3a). Terminal adult male California sheephead (*Semicossyphus pulcher*) were seen chasing other adult conspecifics, possibly to defend their territory (Figure 3b). Halfmoon (*Medialuna californiensis*) were often photographed within 0.5 m of the system, with many appearing to brush up against the lens dome (Figure 3c). Larger and rarer animals such as broadnose sevengill sharks (*Notorynchus cepedianus*) were also photographed (Figure 3d).

Fishes were present in the kelp forest throughout each day (Figure 4a). Adult señorita (*Oxyjulis californica*) were observed most frequently, comprising over 46% of the fish identified to a species level (Table S2). Schools of señorita were present every day during daylight hours (Figure 4b). Other species exhibited temporal variability in their presence. For example, Blacksmith (*Chromis punctipinnis*), the second most encountered fish species, were plentiful on some days, but nearly absent from images on others (Figure 4b). Rock wrasse (*Halichoeres semicinctus)* were almost exclusively identified in images before 12:00 PDT, whereas kelp bass were generally identified after 12:00 PDT (Figure 4c). Though both species are known to form schools, most of these fishes were imaged as individuals. Note, these counts of fish occurrence do not account for the presence of the same individual of a species appearing on multiple images throughout the deployment. This is an ongoing problem with optically based surveys, which Willis et al. (2000), for example, addressed by only choosing images with the maximum number of fish. We are not proposing that this OIS solves this over-counting problem. Thus, counts of fish occurrence reported here should be considered as inflated measures of "abundance."

FUTURE MODIFICATIONS

We have identified three limitations of the OIS that could be addressed in future system upgrades. First, the Sony camera remains energized for an additional five minutes after the system captures its final image and the SBC shuts down because the camera's proximity sensor is always activated inside the housing. To further extend recording durations, addition of an n-channel MOSFET switch could be considered so that the SBC could fully cut power to the camera after it has captured the images. Secondly, the camera encounters errors when an image has not been downloaded before *gphoto2* actuates the camera to capture a subsequent image. Because the camera automatically selects its own shutter speed based on available light and *gphoto2* actuates the camera at a predefined interval, the shutter speed can be longer than the predefined interval between images, leading to a situation where the SBC signals the camera to capture another image while it is still capturing the previous image. Thus, the camera is unable to continuously capture images without encountering an error when this situation occurs. Changing the camera actuation interval based on the time of day (a proxy for available light) or incorporating a light sensor could enable continuous image capture in the future. Finally, the OIS is not a completely noninvasive monitoring system. We captured a high number of images where halfmoon were located less than 0.5 m away from the camera. Often referred to as the "reef effect," the aggregation response of fish to the addition of an artificial structure, including a camera, to their habitat has been well documented (Vardaro et al., 2007). In our case, we hypothesize that halfmoon may be attracted to the sound of the camera shutter or are simply attracted to the OIS itself. The potential change in behavior due to the presence of the OIS may lead to the overestimation of halfmoon occurrence or incorrect interpretations of their behavior.

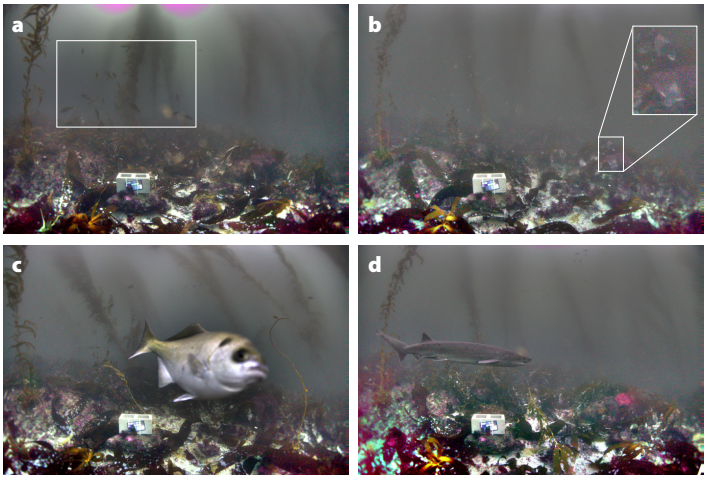

FIGURE 3. Examples of fish behaviors and species diversity captured with the optical imaging system. (a) Possible spawning aggregation of kelp bass. (b) A terminal adult California sheephead defending his territory. (c) Halfmoon close approach to the imaging system. (d) Broadnose sevengill shark.

CONCLUSIONS

We have designed and deployed an optical imaging system that captures high-quality images in low-light conditions, can be deployed for two weeks to a month (depending on the sampling rate), and includes a built-in method for synchronizing its clock with that of a passive acoustic system. Unlike other OISs, this one also provides the user with maximum system flexibility. All of the OIS's Bourne

shell scripts can easily be modified to alter the sampling rate or to capture video instead of still frame images and to run on any computer with a Unix-like operating system. Many of the hardware components can be interchanged as the command-line client *gphoto2*, used by the SBC to control the camera, is compatible with 574 unique camera models. Therefore, the Sony α7S II camera could be interchanged with a less expensive camera for use in higher ambient light environments (e.g., coral reefs). This built-in flexibility and interchangeability allow users to select the best settings and configurations based on their deployment objectives and budgets.

In 14 days, the OIS captured 40% of the fish species recorded during 500 dive transects conducted in the same region over a different three-year period, with similar rank-order abundances (Hastings et al., 2014). The OIS also captured almost the same diversity of fish species reported by recreational anglers in the area (Parnell et al., 2010). We estimated a diver-based approach at the same study site in the kelp forest with six 25 m dive transects per day (or approximately 3 dive hours per day) over 14 days would cost approximately US$10,000 in 2020 (including boat time and gas, scuba equipment, and personnel salary). This is about 2.3 times greater than the initial acquisition cost of the OIS (~US$4,350 in 2017), with the diver-based approach costing approximately $240 per monitoring hour and the camera-based approach costing about $130 per monitoring hour (including dives to deploy and recover the system). The cost of a camera-based approach drops substantially to only $15 per monitoring hour when the acquisition cost of the OIS is removed, illustrating the improved cost-efficiency of the OIS over extended uses in addition to the greater temporal spread of observations (i.e., observations for 2 minutes every 12 minutes over 16 hours per day) captured using the OIS compared to traditional methods. The availability of a consumer-grade camera with the ability to produce high-quality images in low-light levels without artificial lighting was key to extending the price-performance ratio of this system.

With our successful deployment in the kelp forest, we show that this OIS provides a novel, cost-effective scientific approach for monitoring the behavior, diversity, and frequency of occurrence of fish species in MPAs as well as other nearshore areas, and that it maintains its efficacy near sunrise and sunset when biological activity intensifies. Furthermore, the OIS is minimally invasive, and it captures presence/absence patterns that are similar to those captured by traditional methods but with much greater temporal resolution and duration. The OIS's capability to collect data at larger sample sizes provides high statistical power at specific locations and increases our ability to accurately detect population trends. Note, OIS deployment locations should be chosen to be representative of the larger surveyed areas of dive transects. We anticipate that ongoing developments in consumer-grade cameras will continue to improve the price-performance ratio of OISs, creating more opportunities in the future. We are hopeful that this OIS will become a highly utilized tool by researchers to study fish communities in MPAs, given its advantages over traditional MPA monitoring methods.

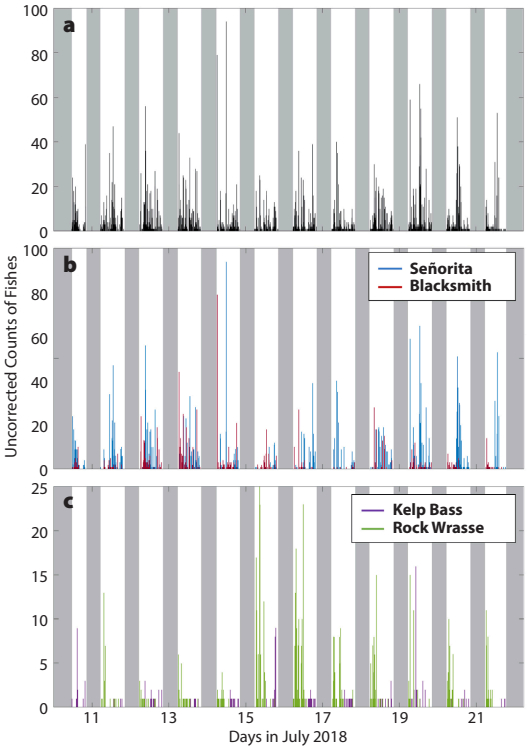

FIGURE 4. (a) Total number of all fishes (black) and counts of occurrences of (b) señorita (blue) and blacksmith (red), and (c) kelp bass (purple) and rock wrasse (green) captured in images from July 11, 2018, through July 21, 2018, in the kelp forest. All counts are uncorrected for the amount of ambient light available at the time of image capture and do not account for recurring individual fish in multiple images. All life stages of each species are included. Gray areas represent times when there were no usable images or when the camera was not operational.

SUPPLEMENTARY MATERIALS

The supplementary materials are available online at https://doi.org/10.5670/oceanog.2021.305.

REFERENCES

Aguzzi, J., A. Mànuel, F. Condal, J. Guillén, M. Nogueras, J. Del Rio, C. Costa, P. Menesatti, P. Puig, F. Sardà, D. Toma, and A. Palanques. 2011. The new seafloor observatory (OBSEA) for remote and long-term coastal ecosystem monitoring. *Sensors* 11(6):5,850–5,872, https://doi.org/10.3390/s110605850.

Balazy, P., P. Kuklinski, and J. Berge. 2018. Diver deployed autonomous time-lapse camera systems for ecological studies. *Journal of Marine Engineering and Technology* 17(3):137–142, https://doi.org/10.1080/20464177.2017.1357164.

Bicknell, A.W.J., B.J. Godley, E.V. Sheehan, S.C. Votier, and M.J. Witt. 2016. Camera technology for monitoring marine biodiversity and human impact. *Frontiers in Ecology and the Environment* 14(8):424–432, https://doi.org/10.1002/fee.1322.

Bouchet, P.J., and J.J. Meeuwig. 2015. Drifting baited stereo-videography: A novel sampling tool for surveying pelagic wildlife in offshore marine reserves. *Ecosphere* 6(8):1–29, https://doi.org/10.1890/ES14-00380.1.

Butler, J., C.M.L.S. Pagniello, J.S. Jaffe, P.E. Parnell, and A. Širović. 2021. Diel and seasonal variability in kelp forest soundscapes off the southern California coast. *Frontiers in Marine Science* 8:629643, https://doi.org/10.3389/fmars.2021.629643.

Chaudoin, A.L., O.G. Feuerbacher, S.A. Bonar, and P.J. Barrett. 2015. Underwater videography outperforms above-water videography and in-person surveys for monitoring the spawning of devils hole pupfish. *North American Journal of Fisheries Management* 35(6):1,252–1,262, https://doi.org/10.1080/02755947.2015.1094155.

Dickens, L.C., C.H.R. Goatley, J.K. Tanner, and D.R. Bellwood. 2011. Quantifying relative diver effects in underwater visual censuses. *PLoS ONE* 6(4):e18965, https://doi.org/10.1371/journal.pone.0018965.

Erisman, B.E., and L.G. Allen. 2006. Reproductive behaviour of a temperate serranid fish, *Paralabrax clathratus* (Girard), from Santa Catalina Island, California, U.S.A. *Journal of Fish Biology* 68:157–184, https://doi.org/10.1111/j.0022-1112.2006.00886.x.

Favaro, B., C. Lichota, I.M. Côté, and S.D. Duff. 2012. TrapCam: An inexpensive camera system for studying deep-water animals. *Methods in Ecology and Evolution* 3(1):39–46, https://doi.org/10.1111/j.2041-210X.2011.00128.x.

Fitzpatrick, C., D. McLean, and E.S. Harvey. 2013. Using artificial illumination to survey nocturnal reef fish. *Fisheries Research* 146:41–50, https://doi.org/10.1016/j.fishres.2013.03.016.

Harvey, E.S., J.J. Butler, D.L. McLean, and J. Shand. 2012. Contrasting habitat use of diurnal and nocturnal fish assemblages in temperate Western Australia. *Journal of Experimental Marine Biology and Ecology* 426–427:78–86, https://doi.org/10.1016/j.jembe.2012.05.019.

Hastings, P.A., M.T. Craig, B.E. Erisman, J.R. Hyde, and H.J. Walker. 2014. Fishes of marine protected areas Near La Jolla, California. *Bulletin, Southern California Academy of Sciences* 113(3):200–231, https://doi.org/10.3160/0038-3872-113.3.200.

Hobson, E.S., W.N. McFarland, and J.R. Chess. 1981. Crepuscular and nocturnal activities of Californian nearshore fishes, with consideration of their scotopic visual pigments and the photic environment. *Fishery Bulletin* 79(1):1–30.

Krumhansl, K.A., D.K. Okamoto, A. Rassweiler, M. Novak, J.J. Bolton, K.C. Cavanaugh, S.D. Connell, C.R. Johnson, B. Konar, S.D. Ling, and others. 2016. Global patterns of kelp forest change over the past half-century. *Proceedings of the National Academy of Sciences of the United States of America* 113(48):13,785–13,790, https://doi.org/10.1073/pnas.1606102113.

Langlois, T., P. Chabanet, D. Pelletier, and E. Harvey. 2006. Baited underwater video for assessing reef fish populations in marine reserves. *SPC Fisheries Newsletter* 118(September):53–57.

Mallet, D., and D. Pelletier. 2014. Underwater video techniques for observing coastal marine biodiversity: A review of sixty years of publications (1952–2012). *Fisheries Research* 154:44–62, https://doi.org/10.1016/j.fishres.2014.01.019.

McLean, D.L., E.S. Harvey, D.V. Fairclough, and S.J. Newman. 2010. Large decline in the abundance of a targeted tropical lethrinid in areas open and closed to fishing. *Marine Ecology Progress Series* 418:189–199, https://doi.org/10.3354/meps08834.

Munz, F.W., and W.N. McFarland. 1973. The significance of spectral position in the rhodopsins of tropical marine fishes. *Vision Research* 13(10):1,829–1,874, https://doi.org/10.1016/0042-6989(73)90060-6.

Myers, E.M.V., E.S. Harvey, B.J. Saunders, and M.J. Travers. 2016. Fine-scale patterns in the day, night and crepuscular composition of a temperate reef fish assemblage. *Marine Ecology* 37(3):668–678, https://doi.org/10.1111/maec.12336.

Nightingale, B., T. Longcore, and C.A. Simenstad. 2006. Artificial night lighting and fishes. Pp. 257–276 in *Ecological Consequences of Artificial Night Lighting*. C. Rich and T. Longcore, eds, Island Press, Washington, DC.

Pagniello, C.M.L.S., M.A. Cimino, and E. Terrill. 2019. Mapping fish chorus distributions in southern California using an autonomous wave glider. *Frontiers in Marine Science* 6:526, https://doi.org/10.3389/fmars.2019.00526.

Parnell, P.E., P.K. Dayton, R.A. Fisher, C.C. Loarie, and R.D. Darrow. 2010. Spatial patterns of fishing effort off San Diego: Implications for zonal management and ecosystem function. *Ecological Applications* 20(8):2,203–2,222, https://doi.org/10.1890/09-1543.1.

Parnell, P.E., J.T. Fumo, C.E. Lennert-Cody, S.C. Schroeter, and P.K. Dayton. 2017. Sea urchin behavior in a southern California kelp forest: Food, fear, behavioral niches, and scaling up individual behavior. *Journal of Shellfish Research* 36(2):529–543, https://doi.org/10.2983/035.036.0224.

Pelletier, D., K. Leleu, G. Mou-Tham, N. Guillemot, and P. Chabanet. 2011. Comparison of visual census and high definition video transects for monitoring coral reef fish assemblages. *Fisheries Research* 107(1–3):84–93, https://doi.org/10.1016/j.fishres.2010.10.011.

Pendleton, L.H., G.N. Ahmadia, H.I. Browman, R.H. Thurstan, D.M. Kaplan, and V. Bartolino. 2018. Debating the effectiveness of marine protected areas. *ICES Journal of Marine Science* 75(3):1,156–1,159, https://doi.org/10.1093/icesjms/fsx154.

Potts, G.W. 1990. Crepuscular behaviour of marine fishes. Pp. 221–228 in *Light and Life in the Sea*. P.J. Herring, A.K. Campbell, M. Whitfield, and L. Maddock, eds, Cambridge University Press, Cambridge, UK.

Rountree, R.A., R.G. Gilmore, C.A. Goudey, A.D. Hawkins, J.J. Luczkovich, and D.A. Mann. 2006. Listening to fish: Applications of passive acoustics to fisheries science. *Fisheries* 31(9):433–446, https://doi.org/10.1577/1548-8446(2006)31[433:LTF]2.0.CO;2.

Schiel, D.R., and M.S. Foster. 2015. *The Biology and Ecology of Giant Kelp Forests*. University of California Press, 416 pp.

Vardaro, M.F., D. Parmley, and K.L. Smith. 2007. A study of possible "reef effects" caused by a long-term time-lapse camera in the deep North Pacific. *Deep Sea Research Part I* 54(8):1,231–1,240, https://doi.org/10.1016/j.dsr.2007.05.004.

Vardaro, M.F., P.M. Bagley, D.M. Bailey, B.J. Bett, D.O.B. Jones, R.J. Milligan, I.G. Priede, C.M. Risien, G.T. Rowe, H.A. Ruhl, and others. 2013. A Southeast Atlantic deep-ocean observatory: First experiences and results. *Limnology and Oceanography: Methods* 11(6):304–315, https://doi.org/10.4319/lom.2013.11.304.

Wilby, A., R. Kastner, A. Hostler, and E. Slattery. 2016. Design of a low-cost and extensible acoustically-triggered camera system for marine population monitoring. *OCEANS 2016 MTS/IEEE Monterey*, https://doi.org/10.1109/OCEANS.2016.7761320.

Willis, T.J., R.B. Millar, and R.C. Babcock. 2000. Detection of spatial variability in relative density of fishes: Comparison of visual census, angling, and baited underwater video. *Marine Ecology Progress Series* 198:249–260, https://doi.org/10.3354/meps198249.

ACKNOWLEDGMENTS

Thank you to I. Arzeno, K. Bagheri, D. Bevans, A. Brennan, J. Busch, S. Brody, M. Cimino, M. Costa, A. Cusick, B. Frable, M. Harvey, P. Lertvilai, C. McDonald, A. Palinkas, K. Pederson, B. Pickering, M. Sedarat, R. Walsh, K.C. Wilson, K. Wilson, and W. Wolfe for assistance in the field. Thank you to D. Akkaynak for generating the color-corrected images using the Sea-thru method. Thank you to B. Frable and P. Hastings for assistance in identifying fish species in images. Thank you to R. Walsh for assistance with diver survey cost estimates.

Funding was provided by California Sea Grant College Program Project Award Number NA14OAR4170075 to AŠ, JSJ and PEP, through NOAA'S National Sea Grant College Program, US Department of Commerce. CMLSP was also supported in part by a Natural Sciences and Engineering Research Council (NSERC) of Canada Postgraduate Scholarship-Doctoral Program.

AUTHORS

Camille M.L.S. Pagniello (cpagniel@ucsd.edu) is PhD Candidate, Scripps Institution of Oceanography, University of California San Diego (SIO-UCSD), La Jolla, CA, USA. **Jack Butler** is Postdoctoral Researcher, SIO-UCSD, La Jolla, CA, USA, and Institute of Environment, Florida International University, North Miami, FL, USA. **Annie Rosen** and **Addison Sherwood** are interns at SIO-UCSD, La Jolla, CA, USA. **Paul L.D. Roberts** is Research Engineer, SIO-UCSD, La Jolla, CA, USA, and Monterey Bay Aquarium Research Institute, Moss Landing, CA, USA. **P. Edward Parnell** is Associate Researcher and **Jules S. Jaffe** is Research Oceanographer, both at SIO-UCSD, La Jolla, CA, USA. **Ana Širović** is Associate Professor, SIO-UCSD, La Jolla, CA, USA, and Department of Marine Biology, Texas A&M University Galveston, Galveston, TX, USA.

ARTICLE CITATION

Pagniello, C.M.L.S., J. Butler, A. Rosen, A. Sherwood, P.L.D. Roberts, P.E. Parnell, J.S. Jaffe, and A. Širovic. 2021. An optical imaging system for capturing images in low-light aquatic habitats using only ambient light. *Oceanography* 34(3), https://doi.org/10.5670/oceanog.2021.305.

COPYRIGHT & USAGE

SUPPLEMENTARY MATERIALS FOR

An Optical Imaging System for Capturing Images in Low-Light Aquatic Habitats Using Only Ambient Light

By Camille M.L.S. Pagniello, Jack Butler, Annie Rosen, Addison Sherwood, Paul L.D. Roberts, P. Edward Parnell, Jules S. Jaffe, and Ana Širović

S1. DEPLOYMENT AND UNDERWATER OPERATION

The optical imaging system (OIS) was deployed in the kelp forests on the northern edge of the South La Jolla State Marine Reserve (SMR; 32.8263°N, 117.2901°W) in approximately 14 m water depth from July 10 to 23, 2018 (Figure S1a). It captured 24 images every 12 minutes between 05:00 and 21:00 (i.e., at least one hour before sunrise and after sunset) to ensure that no potentially usable light conditions were missed for image acquisition. Images were captured under aperture priority mode (aperture: *f*2.8) as uncompressed, raw image files with a 16:9 aspect ratio. The focusing distance of the lens was set at 0.3 m in air so that a fish one meter away from the camera in water would be in focus. This was determined using equations in Jenkins and White (2001) to compute the focusing distance for thick lenses, and we have included a MATLAB R2016b (MathWorks, Natick, MA) script to calculate this in the GitHub repository (https://github.com/cpagniel/FishOASIS/blob/master/hardware/FishOASIS_lens_focusing_dist_code.m). The ISO (International Standards Organization) sensitivity of each image was automatically set by the camera between 50 and 409,600. The white balance was also automatically set by the camera.

The OIS was mounted by divers to an L-bracket (for landscape images) on a 1 m tall u-post set in a 50 × 50 × 10 cm concrete block (Figure S1b). It could also be mounted directly to the stand for portrait images. The battery pack was placed on the concrete block and cable-tied to two eyebolts set in the concrete block. A HOBO Pendant temperature/light 8K data logger (Onset Computer Corporation, Bourne, MA) was attached to the camera housing to measure seawater temperature (in °C) and ambient light (in lux). To correct for the ambient light spectra, a DGK Color Tools WDKK Waterproof Color Chart was deployed in the field of view of the camera at a distance of 2 m. To approximate the distance of fishes from the camera, distances to various stationary objects always visible in the images (e.g., rocks, kelp holdfasts, cinderblocks) from the camera were measured using a transect tape.

To demonstrate the OIS's ability to synchronize its clock with that of a passive acoustic recorder, the OIS was deployed alongside a SoundTrap ST4300 (Ocean Instruments, Auckland, NZ) four-channel acoustic recorder equipped

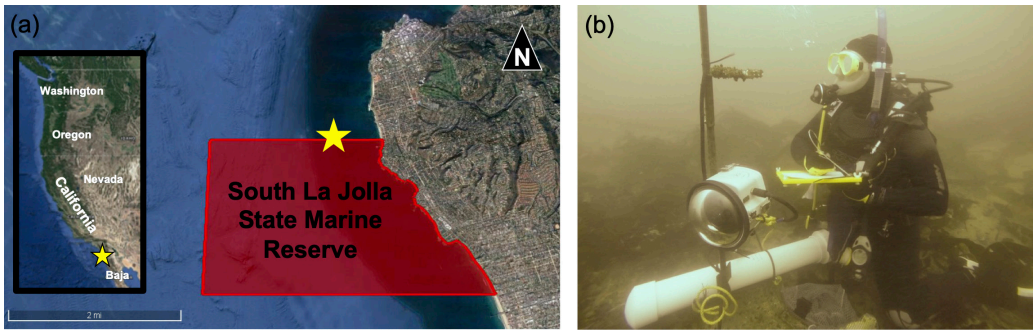

FIGURE S1. (a) Location of deployment of optical imaging system off the coast of La Jolla, California, on the northern edge of the South La Jolla SMR (yellow pentagram). In the inset, the location of the larger map is shown as a yellow star off the coast of southern California. (b) Optical imaging system deployed by a diver. *Image credit: A. Cusick*

https://doi.org/10.5670/oceanog.2021.3xx

with four HTI-96-MIN hydrophones (High Tech Inc., Long Beach, MS), whose sensitivity was –201 dB V/µPa with 36 dB pre-amplifier gain. The acoustic recorder sampled continuously at 48 kHz.

S2. DATA ANALYSIS

All of the data analysis described below was performed offline (i.e., after the data had been downloaded from the OIS).

S2.1 Image Analysis

All raw images were color-corrected using a modified version of the Sea-thru method (Akkaynak and Treibitz, 2019). This method requires a range map of the scene from raw images and uses an updated underwater image formation model (Akkaynak and Treibitz, 2018) to estimate distinct backscatter and attenuation coefficients for all colors. For our images, we were only able to obtain range maps for pixels very close to the camera. Because our goal was to improve visibility (and not to obtain accurate color reconstruction), we extrapolated range information for the rest of the scene.

Fishes in these images were manually identified to the species level (when possible) by an analyst using a custom-built MATLAB R2016b graphical user interface. The analyst used contextual information such as the fish's shape and position in the water column as well as preceding and succeeding images and a list of expected species in the deployment location to identify each fish. Images of individual fish were extracted from the raw images so that another analyst could review the initial species identification. When the analyst was unsure of the fish species, a professional fish taxonomist from the Scripps Institution of Oceanography Marine Vertebrate Collection was consulted. Image quality was classified based on the ability of the trained analyst, not the professional fish taxonomist, to identify a fish to the species level. If the species of the majority of the fish in an image could easily be identified, the image was considered of high quality. All post-processing tools are available online from https://github.com/cpagniel/FishOASIS/.

S2.2 Acoustic Analysis

Because the frequency of fish sounds previously recorded in this area generally does not exceed 2 kHz (Pagniello et al., 2019), acoustic data were decimated from 48 kHz to 4 kHz by first lowpass filtering the data with a Chebyshev Type I infinite impulse response filter (8^{th} order, normalized cutoff frequency of 0.8/12, passband ripple of 0.05 dB) and subsequently down-sampling the filtered data. Spectrograms of the acoustic data were generated by dividing the time series into equal-length segments of 512 samples having 90% overlap, applying a Kaiser-Bessel window of $\alpha = 2.5$ to each segment, taking the fast Fourier transform (FFT) of each segment, and averaging the squared magnitude of the FFT of overlapped, windowed segments. The overall sensitivity (–78 dB re 1 µPa/counts) of the PAS was applied to the spectrograms to yield calibrated values of spectral density (dB re 1 $\mu Pa^2/Hz$). Spectrograms of all the acoustic data between 05:00 and 21:00 were manually reviewed for the 610 Hz and 690 Hz synchronization tones played by the miniature speaker as well as the sound produced by the actuation of the camera shutter. The start time, duration, and frequency bandwidth of these sounds were logged using the logger feature of the MATLAB R2013b program Triton (Wiggins, 2003).

REFERENCES

Akkaynak, D., and T. Treibitz. 2018. A revised underwater image formation model. *The IEEE Conference on Computer Vision and Pattern Recognition (CVPR)*, June 18–23, 2018, Salt Lake City, UT, https://doi.org/10.1109/CVPR.2018.00703.

Akkaynak, D., and T. Treibitz. 2019. Sea-thru: A method for removing water from underwater images. *The IEEE Conference on Computer Vision and Pattern Recognition (CVPR)*, held June 15–20, 2019, Long Beach, CA, https://doi.org/10.1109/CVPR.2019.00178.

Jenkins, F.A., and H.E. White. 2001. *Fundamentals of Optics*, 4th ed. McGraw-Hill Education, 768 pp.

Pagniello, C.M.L.S., M.A. Cimino, and E. Terrill. 2019. Mapping fish chorus distributions in southern California using an autonomous wave glider. *Frontiers in Marine Science* 6:526, https://doi.org/10.3389/fmars.2019.00526.

Wiggins, S. 2003. Autonomous Acoustic Recording Packages (ARPs) for long-term monitoring of whale sounds. *Marine Technology Society Journal* 37(2):13–22, https://doi.org/10.4031/002533203787537375.

TABLE S1. Approximate recording duration (days) for different data storage capacities and sampling rate combinations estimated from power consumption of 720 Wh battery pack and image size

	1 img/12 min	12 img/12 min	24 img/12 min
256 GB	32.3[a]	9.4[b]	4.7[b]
512 GB	32.3[a]	18.9[b]	9.4[b]
768 GB	32.3[a]	22.3[a]	14.1[b]

[a] indicates the optical system would be battery limited
[b] indicates storage limited.

TABLE S2. Fish species photographed during a 14-day camera deployment in the South La Jolla State Marine Reserve kelp forest from July 10 to July 23, 2018. Taxa are listed in order of decreasing total counts.

Common and Scientific Name	Life Stage	Life Stage Counts	Total Counts
Señorita (*Oxyjulis californica)*	Adult	4,421	4,421
Blacksmith (*Chromis punctipinnis)*	Adult	18	2,739
	Juvenile	2,698	
	Unknown	23	
Unidentifiable Fishes		1,191	1,191
Rock Wrasse (*Notorynchus cepedianus)*	Adult	1,120	1,120
Kelp Bass (*Paralabrax clathratus)*	Adult	420	420
Opaleye (*Girella nigricans)*	Adult	295	295
California Sheephead (*Semicossyphus pulcher)*	Terminal	118	234
	Initial	114	
	Unknown	2	
Halfmoon (*Medialuna californiensis)*	Adult	78	78
Kelp Perch (*Brachyistius frenatus)*	Adult	74	74
Bait Ball (> 20 Fish) of Unidentifiable Fishes	Unknown	73	73
Kyphosidae	Unknown	71	71
Pacific Barracuda (*Sphyraena argentea)*	Adult	6	58
	Juvenile	52	
Pacific/California Jack Mackerel (*Trachurus symmetricus)*	Adult	24	57
	Unknown	33	
Sargo (*Anisotremus davidsonii)*	Adult	30	30
Garibaldi (*Hypsypops rubicundus)*	Adult	22	25
	Juvenile	3	
Broadnose Sevengill Shark (*Notorynchus cepedianus)*	Adult	24	24
Black Surfperch (*Embiotoca jacksoni)*	Adult	8	8
Yellowtail Amberjack (*Seriola dorsalis)*	Adult	5	6
	Juvenile	1	
Bat Ray (*Myliobatis californica)*	Adult	5	5
White Seabass (*Atractoscion nobilis*)	Juvenile	1	3
	Unknown	2	
Barred Sand Bass (*Paralabrax nebulifer)*	Adult	2	2
Sebastidae	Unknown	2	2
Painted Greenling (*Oxylebius pictus)*	Adult	1	1
Shovelnose Guitarfish (*Rhinobatos productus)*	Adult	1	1

Total Fishes:	**10,938**
Total Fishes Identified to Species Level:	9,601
Total Fishes Identified to Family Level:	73
Total Unidentifiable Fishes:	1,264
Total Adult Fishes:	6,786
Total Juvenile Fishes:	2,755
Total Unknown Life Stage Fishes:	60

| https://doi.org/10.5670/oceanog.2021.3xx

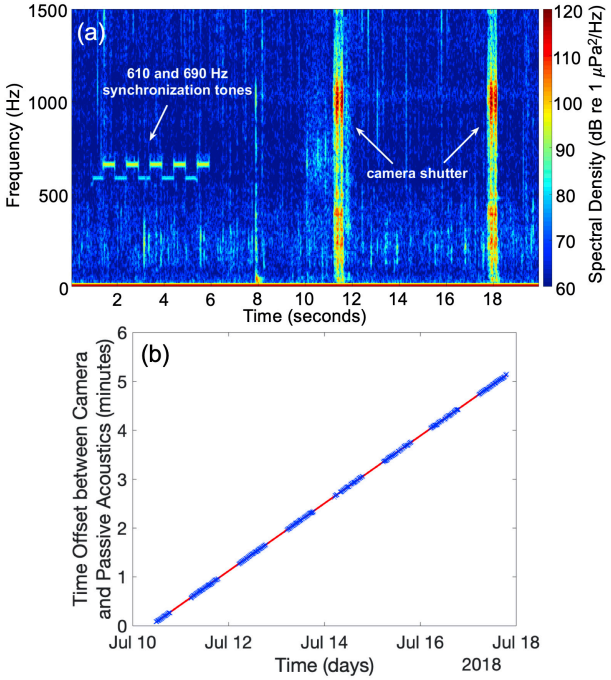

FIGURE S2. (a) Spectrogram showing 610 and 690 Hz tones used to synchronize optical imaging system and passive acoustic system clocks as well as sound produced when the camera shutter was actuated. (Spectrogram parameters: Kaiser-Bessel window with a = 2.5, sample rate = 4 kHz, 512-point fast Fourier transform with 90% overlap. Color represents spectral density (dB re 1 mPa^2/Hz).) (b) Clock drift of passive acoustic recorder relative to the clock time of the optical imaging system. Blue crosses indicate the times of the first 610 Hz inter-calibration tones of each sequence during which camera was operational. Demonstrating the linearity of the drift is the red least-squares fit line (y = 0.00048001x + 0.075834) in units of minutes since July 10, 2018, at 11:36:51 PST (i.e., the start of the deployment).

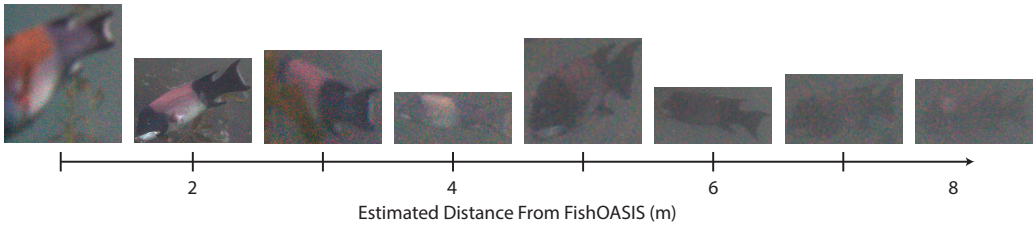

FIGURE S3. Image quality of terminal adult California sheephead at increasing distances from the optical imaging system. All images were captured between 10:30 and 11:15 local Pacific standard time. Fish were at about the same depth at all times.

Chapter 2, in full, is a reprint of the material as it appears in Oceanography. Pagniello, Camille; Butler, Jack; Rosen, Annie; Sherwood, Addison; Roberts, Paul; Parnell, Edward; Jaffe, Jules; Širović, A, 2021. The dissertation author was the primary investigator and author of this paper.

Three-dimensional localization and tracking of individual fish using *in situ* sound playbacks in a complex shallow-water environment

Camille M.L.S. Pagniello*

Scripps Institution of Oceanography, University of California San Diego, La Jolla, California 92093-0205, USA

* corresponding author, cpagniel@ucsd.edu

Abstract

1. Passive acoustics is a promising tool to study the movement ecology of sound-producing animals, including fish, as multi-element receiver arrays can be used to determine the location of an individual animal. However, to enable accurate and precise localization, models that account for the propagation physics of sound in the shallow-water environments that fish inhabit are needed. Additionally, error associated with location estimates should be quantified to draw biologically-relevant conclusions about an animal's behavior.
2. We describe an approach for quantifying and reducing localization error for position estimates of animals that uses an underwater source to create a data-derived library of time-difference-of-arrivals (TDOAs). To accomplish this, a fish call was played at GPS-located positions and two depths around a four-element array. A grid-search algorithm was used to estimate the source's position, which was compared to its GPS-based position to evaluate localization error. Performance of this new approach was compared to that of modeled TDOA estimates that assumed an iso-velocity, straight-line propagation environment. Predictive intervals were also computed from these *in situ* playbacks and applied to localized position estimates of living, vocalizing fish.
3. Approximately 48% of playbacks were localized within ±5 m from their true position using modeled replica fields. This improved to 87% using data-derived replicas, with 44% located within ±1 m. Deeper sources located within the footprint of the array were much closer to their true positions than sources located higher in the water column or outside the array. Modeled replicas captured the general trajectory of a swimming

fish. However, only data-derived replicas accurately captured the fish's position when it was relatively stationary, enabling estimates of its general pattern of activity.

4. Fish movement studies are critical to understanding the small-scale movements of fish in and around marine protected areas (MPAs) and to ensure effective protections. Existing methods, such as acoustic telemetry with implanted tags, are time-consuming and expensive. This non-invasive approach for improved localization of vocalizing fishes in complex habitats is a key step towards better understanding the behavior of fishes *in situ* and how fishes interact with MPA boundaries.

Keywords
error estimation; experimental method; fish behavior; fish sounds; marine protected area; localization; passive acoustics; shallow-water environment; sound playbacks

1. Introduction

Passive acoustics has proven to be a useful tool to study the ecology of sound-producing animals in the ocean (Tyack, 1998). Marine ecological studies that employ passive acoustic techniques typically use only single-element recorders (i.e., acoustic recorders with a single hydrophone). However, since sound propagates rapidly and over large distances in the ocean, passive acoustic arrays with multiple elements can be used to find the precise location of soniferous animals. Knowledge of the animal's location can be used, for example, to determine critical habitat (Simard, Bahoura, & Roy, 2004). If the animal produces multiple, successive calls over time, animals can be tracked to learn about their movement patterns (e.g., Tiemann, Porter, & Frazer, 2004; Guazzo et al., 2017). Additionally, the identification of individuals through localization and tracking has allowed for population abundance estimates of endangered population (Kim et al., 2018). Since many of these sounds are related to reproductive behavior (e.g., K. C. Wilson, Semmens, Pattengill-Semmens, McCoy, & Širović, 2020), the ability to determine an animal's location is crucial for managing the impact of anthropogenic activities on an individual- and population-level.

It is becoming increasingly popular to monitor fish populations with passive acoustics. Over 800 species of fish are known to produce sound (Kaatz, 2002; Rountree et al., 2006). Fish produce sound for several important biological functions including territorial defense and spawning (Winn, 1964). Yet, there are limited published studies that localize individual fish using their sounds (Table 3.1). Results from these studies are promising and suggest that passive acoustic monitoring could be used to learn about the behavior and estimate the abundance of many commercially and recreationally important soniferous fish populations.

Challenges associated with estimating the position of a fish from their vocalizations primarily arise due to the difficulty associated with modeling the shallow-water environments that fish often inhabit (Larsen & Radford, 2018). The inability to properly characterize the environment, specifically the sound speed profile in the water column (i.e., how the speed of sound varies vertically at a location), geoacoustic properties (e.g., stratification of sediment layers as well as density, attenuation and compressional sound speed in each layer) and bathymetry, can introduce significant error (i.e., bias and variance) in position estimates (Spiesberger & Fristrup, 1990). Uncertainties in array geometry (i.e., location of receivers in array) and acoustic properties of the signal of interest (e.g., frequency, bandwidth, duration, signal-to-noise ratio (SNR), etc.) can also contribute to error in position estimates. Even if environmental fluctuations are ignored and errors in array geometry are small, choosing the appropriate localization method is not trivial. Beamforming (Van Veen & Buckley, 1988) and Matched Field Processing (MFP) (Baggeroer, Kuperman, & Mikhalevsky, 1993) methods require modeled replica fields that can be matched to the received data across the array. Hyperbolic cross-fixing and other time-differences of arrival (TDOAs)-based methods exploit the geometric properties of triangles to determine the originating location of the signal (Urazghildiiev & Clark, 2013). All localization methods rely on several underlying assumptions and approximations that can result in differences in the estimated location of the animal. Given the inherent variability in each of these potential sources of error and methods, if biologically-relevant conclusions are to be drawn from animal locations estimated via passive acoustics, a quantitative evaluation of localization performance should accompany every report of an animal's location. As such, an approach that considers all of these factors (i.e., environment,

array geometry, signal of interest, localization method, etc.) to determine prediction intervals for position estimates is needed.

Here, we present an experimental approach to localize individual marine animals that directly addresses many of the challenges associated with estimating source position in shallow-water environments. We quantified localization performance and applied prediction intervals computed using a controlled underwater source to estimates of the position of living, vocalizing fishes. This localization method is a key step towards better characterizing the small-scale spawning movements of soniferous fishes with high precision and accuracy.

2. Methods

2.1 Experimental Setup

A SoundTrap ST4300 (Ocean Instruments, Auckland, NZ) four-channel ($M = 4$) passive acoustic recorder sampling continuously at 48 kHz was deployed from September 6-13, 2019 in the kelp forests off La Jolla, California (Fig. 3.1a). A large sand channel cuts through the middle of the receiver array, in what is an area otherwise dominated by a hard-bottom substratum with small scattered rocky reefs. The acoustic recorder has four 16-bit analog-to-digital converter with a ±1.5 V response. Four HTI-96-MIN hydrophones (High Tech Inc., Long Beach, MS) were arranged in the geometry shown in Fig. 3.1b in 13 to 17 m water depth. The average hydrophone sensitivity was -201 dB V/µPa, with 36 dB gain from a pre-amplifier (Table 3.2). Weighted surface buoys were placed by divers next to each receiver on the seafloor to record their location by taking a GPS measurement of the buoy at the surface using a handheld Garmin GPSMAP 78SC (Table 3.2).

On September 7, 2019, a controlled source, whose GPS location was known, was used to play a fish call previously recorded at this site (Fig. 3.2). The call's frequency and temporal

characteristics were initially reported in Pagniello, Cimino, & Terrill (2019) as Chorus Type I calls. This fish call is hypothesized to be that of either the Spotfin (*Roncador stearnsii*), Black (*Cheilotrema saturnum*) or Yellowfin Croaker (*Umbrina roncador*) (Johnson, 1948). Spearfisherman have also reported that Sargo (*Anisotremus davidsonii*) produce a frog-like croak and could be the source of this call. The call was played at various locations within 60 m of the center of the array at two depths: approximately 5 or 13 m (Fig. 3.1b). Hereafter, "shallow" sources refer to playbacks at depths around 5 m, whereas "deep" sources refer to playbacks at depths around 13 m. The controlled source was a Lubell Labs LL916C full-range pistonic piezoelectric underwater loudspeaker, whose mean ± standard deviation (SD) output source level (SL) was 155.6 ± 0.6 dB re: 1 μPa at 1 m RMS from 245 to 1255 Hz for the fish call. A conductivity, temperature and depth (CTD) sensor was placed 29 cm above the center of the source to measure the exact depth of the source as well as the sound speed at that depth, which varied between 1505.2 and 1531.8 m/s with a harmonic average of 1516.0 m/s (Fig. 3.3).

2.2 Localization Method

The method described below and illustrated in Fig. 3.4 was used to determine the location of the controlled underwater source as well as sounds produced by living fishes. Details about the coordinate system, planned array geometry, processing of acoustic data, localization performance metrics, combined replica library used to localize living fishes as well as call parameters and behavioral metrics can be found in the Supporting Information.

2.2.1 Numerical Setup

We defined a 481x481x2-point spatial search grid where x and y range between –60 and 60 m. The z dimension was restricted to two depths, 5 and 13 m. To determine the appropriate

grid resolution in the x and y dimensions, we estimated the theoretical timing error in the time domain. This is defined by Woodward (1964) as:

$$\sigma_t = \frac{1}{(f_2 - f_1)\sqrt{RL/NL}}, \quad (1)$$

where $f_2 - f_1$ is the bandwidth of the signal and RL/NL is the signal to noise ratio (SNR). Details about how received (RL) and noise (NL) were computed are included in the Supporting Information. For playbacks of the fish call, we used a bandwidth of 1010 Hz. The median SNR of the fish call was approximately 12 dB and σ_t was approximately 0.49 ms. As such, we selected a 0.25-m resolution grid (i.e., half of the corresponding timing error based on a harmonic average sound speed of 1516.0 m/s).

2.2.2 Modeled and Data-Derived Replica Fields

Two different types of replica fields were used to localize the signal of interest (i.e., either playback or fish call). The first was a modeled replica field that assumed a homogenous sound speed profile and a direct-path travel time between the source and receiver. No bathymetric effects were considered. The calculated propagation time $\hat{T}_m$ between the modeled source position $\vec{q}(x, y, z)$ and the m^{th} receiver is defined as:

$$\hat{T}_m(\vec{q}) = \frac{\|\vec{q} - \vec{p}_m\|}{c}. \quad (2)$$

As such, the modeled estimate of TDOA $\Delta\hat{t}_{nm}(\vec{q})$ between two receivers *m* and *n* is defined as:

$$\Delta\hat{t}_{nm}(\vec{q}) = \hat{T}_n(\vec{q}) - \hat{T}_m(\vec{q}) \quad (3)$$

Modeled estimates of TDOAs were computed for all possible pairs of receivers in the array. For this experimental setup, six TDOA pairs exist at each point in the 481x481x2-point search grid.

The second set of replica fields was derived from the *in situ* playbacks of a fish call using the controlled underwater source. Data-derived estimates of TDOAs between playbacks recorded

at the *m*th and *n*th receivers were computed using the smoothed coherence transform (SCOT) (Carter, Nuttall, & Cable, 1973). The SCOT $C(\tau)$ was computed by taking the inverse fast Fourier transform of the complex coherence function $\gamma(f)$:

$$C(\tau) = \int_{-\infty}^{\infty} W(f)\gamma(f)e^{i2\pi f\tau}\, df, \tag{4}$$

where $W(f)$ is a Kaiser-Bessel window of $\alpha = 2.5$, f is the frequency and τ is the lag variable (i.e., the next "step" between data points), which is constrained to be an integer. The auto spectra $G_n(f)$ and $G_m(f)$ for two signals $x_n(t)$ and $x_m(t)$, respectively, and their cross spectrum $G_{nm}(f)$ were used to calculate $\gamma(f)$:

$$\gamma(f) = \frac{G_{nm}(f)}{\sqrt{G_n(f)G_m(f)}}. \tag{5}$$

The data-derived estimate of TDOA for the *m*th and *n*th receiver pair $\Delta\hat{t}_{nm}$ was computed by dividing the value of lag variable τ when the absolute value of SCOT sequence $C(\tau)$ is maximized by the sampling frequency f_s of the signal (Fig. 3.5). The SCOT was used to determine TDOAs instead of cross-correlation because it performs optimally for weak, broad-band signals and allows signals with different frequency spectra to be compared. TDOAs were bounded by the largest possible time delay between receivers in an iso-velocity, straight-line propagation environment. The SCOT vectors containing the six TDOA pairs for each playback were georeferenced with latitude, longitude, and depth. This approach is similar to that described by Verlinden, Sarkar, Hodgkiss, Kuperman, & Sabra (2015) for passive acoustic localization using sources of opportunity.

To create a data-derived replica library that has the same extent as the 481x481x2x6 modeled replica library and thus, increase grid density between source playbacks, a natural neighbor interpolation method was used to compute TDOA values in locations within the

numerical search grid where no playbacks occurred. This local interpolation method uses only the points that immediately surround a query point and weighs them according to proportionate areas to interpolate a value (Sibson, 1981). Each interpolated surface (i.e., one for each of the six TDOA pairs) was re-sampled at points within numerical search grid to create the data-derived replica library. Note, TDOAs associated with the signal of interest (i.e., the playback whose position we were attempting to estimate) were omitted from the replica library. More details on the effect of interpolation in addition to how the modeled and data-derived replica libraries were combined to localize living, vocalizing fishes are included in the Supporting Information.

2.2.3 Measured Estimates of TDOA

The six measured estimates of TDOAs Δt_{nm} for the signal of interest were computed using the SCOT in the same manner described above for the data-derived replica fields. TDOAs for all pairs of receivers in the array were computed only if the signal of interest was detected on all receivers.

2.4.4 Maximum Likelihood Estimate of Source Position and Construction of Ambiguity Surfaces

Localization is a parameter estimation problem. A maximum likelihood (ML) estimate of source position is considered an ideal localization algorithm when estimation errors are independent, zero-mean Gaussian variables with the same distribution for all receivers (Van Trees, 2001). This is because, asymptotically, the variance of an ML estimate approaches the Cramer-Rao bound (i.e., the lower bound of the parameter estimation error). Mathematically, when this assumption holds, an ML estimate is equivalent to the minimization of a least-squares (LS) difference. In this case, $LS(\vec{q})$ is a 481x481x2 matrix computed by taking the sum of the squared difference between the 6x1 measured estimates of TDOAs and 6x1 modeled or data-

derived estimates of TDOAs at each of the 462,722 possible source positions $\vec{q}$ in the 481x481x2 search grid:

$$LS(\vec{q}) = \sum_{m}^{M} \sum_{n}^{M-1} \frac{-1}{2\sigma_{nm}^2} \left(\Delta t_{nm} - \Delta \hat{t}_{nm}(\vec{q})\right)^2 . \quad (6)$$

The variance σ_{nm}^2 accounts for uncertainties in receiver position and synchronization, measured estimates of call times and sound speed profile (Nosal, 2013). To compute the ML estimate of source position, a nonlinear optimization problem must be solved; hence the use of a grid search approach described above. Note, the assumption that the TDOA estimation errors are independent, identically distributed Gaussian variables is a simplification which does not always hold, especially for sub-optimal array geometries. As discussed by Baggenstoss (2011), overall, this simplification should not have a significant impact on a localization algorithm's performance.

To generate a location estimate of the source, an ambiguity surface was constructed by plotting the normalized $LS(\vec{q})$ value computed with equation (6) at each candidate source position in the search grid. Ambiguity surfaces, like those shown in Fig. 3.6, visualize the probability that the source is at a hypothesized location and will have a minimum where the measured and modeled or data-derived estimates of TDOAs agree best. The minimum of the $LS(\vec{q})$ matrix is taken as the estimate of the source position.

2.3 Error Budget

We defined the estimated position as the localization-derived position of the source and the true position as the GPS- and ambient pressure-derived position of the source. A general error budget for a localization-derived position in our experiment is defined as:

$$\vec{q}_{true} \pm \sqrt{\sigma_{GPS}^2 + \sigma_{source}^2} = \vec{q}_{estimated} \pm \sqrt{\sigma_{receiver}^2 + \sigma_{sync}^2 + \sigma_c^2 + \sigma_t^2 + \sigma_{multi}^2 + \sigma_{ray}^2}. \quad (7)$$

Descriptions and estimates of these sources of error are included in Table 3.3. Equation (7) can be further simplified as total receiver position error ($\sigma_{receiver}$) is comprised of both GPS error (σ_{GPS}) and error due to the displacement of the surface buoy by currents (σ_{buoy}). Additionally, receiver synchronization error (σ_{sync}) is zero as all receivers are connected to a single passive acoustic recorder. As such, for modeled replicas fields, the error budget is defined as:

$$\vec{q}_{true} \pm \sqrt{\sigma^2_{source}} = \vec{q}_{estimated} \pm \sqrt{\sigma^2_{buoy} + \sigma^2_c + \sigma^2_t + \sigma^2_{multi} + \sigma^2_{ray}}. \quad (8)$$

The error budget for data-derived replicas fields is defined as:

$$\vec{q}_{true} \pm \sqrt{\sigma^2_{source}} = \vec{q}_{estimated} \pm \sqrt{\sigma^2_{buoy} + \sigma^2_t}\,, \quad (9)$$

because the data-derived replicas account for the downward-refracting sound speed profile and the multi-path arrival structure.

3. Results

3.1 Localization of Controlled Underwater Source

Overall, using data-derived rather than modeled replica fields improved localization performance. However, error in the estimates of the source's position varied in each Cartesian dimension (Table 3.4, Figs. 7-8). Performance was best in x- and y-dimensions when data-derived replicas were used, with a median ($\tilde{x}$) error of 0.01 m and median absolute deviation (MAD) of 0.61 m in the x-dimension (Fig. 3.7a) and 0.05 ± 0.59 m ($\tilde{x}$ ± MAD) in the y-dimension (Fig. 3.7b). In this case, localization error in each dimension was less than or equal to 1 m for 81% of source locations, respectively. Approximately 87% of sources were located within 5 m of their true positions, with 44% located within 1 m (1.20 ± 0.72 m, $\tilde{x}$ ± MAD; Fig. 3.7e). The concordance of the GPS-derived true positions to the position estimates using data-derived replicas was 0.97 in the x-dimension (Fig. 3.8d) and 0.98 in the y-dimension (Fig. 3.8e).

As per the cutoffs proposed by McBride (2005), this indicates substantial concordance. However, there was only moderate concordance of true positions to estimated positions when modeled replica fields were used (CCC in x = 0.92, CCC in y = 0.93; Fig. 3.8a-b). In this case, a large bias occurred in the x-dimension ($\tilde{x}$ = -1.30 m) and the spread of the distributions in both horizontal dimensions was much larger (MAD in x = 1.56 m, MAD in y = 2.13 m; Fig. 3.7a-b). Approximately 44% of sources were located within 5 m of their true positions, with only 4% of sources were located to within 1 m. Additionally, only 66% of z-position estimates were correctly resolved using modeled replicas. This improved when data-derived replicas were used as the correct depth bin was estimated 94% of the time. Yet, concordance was poor in the z-dimension using either type of replica. However, positions estimates using data-derived replicas demonstrated a much greater degree of concordance (CCC = 0.88; Fig. 3.8c) than those using modeled replicas (CCC = 0.31; Fig. 3.8f).

Localization performance was also affected by source depth and varied based on source distance to the center of the receiver array (Supplementary Table 3.1, Supplementary Fig. 3.3-4). When data-derived replicas were used, the MAD of error distributions in the horizontal dimensions was approximately 50% less for deep sources. Concordance of the true to estimated positions in the x- and y-dimensions was almost perfect for deep sources but was only substantial for shallow sources. When sources were deep, 99% of the z-positions were estimated correctly compared to 91% when sources were shallow. Much larger biases in the error distributions of the horizonal dimensions occurred for deep when modeled replicas were used. Localization performance was much worse in the z-dimension, with only 50% and 78% of z-positions estimated correctly for deep and shallow sources, respectively. As the source moved further away from the center of the array, localization error in the x- and y-dimensions significantly

increased when modeled replicas were used. Approximately 75% of the sources located inside the array, but only 42% of the sources located outside the array were localized to within 5 m of their true xy-position. Additionally, position estimates of sources located outside the array using modeled replicas were always located closer to the center of the array than their true positions (Fig. 3.9a). Modeled replicas captured the general shape and trajectory of speaker playbacks, but often were offset by over 5 m from the true position both inside the array and near its perimeter (Fig. 3.9b-c). Much of the vertical departure from the 1:1 line of agreement observed when sources were outside the array ($d > 22.8$ m) disappeared when data-derived replicas were used (Fig. 3.8). In this case, concordance was almost perfect outside of the array and substantial inside of the array in the horizontal dimensions. About 92% of sources located inside the array and 85% of sources located outside the array were localized to within 5 m of their true xy-position. Z-position accuracy was high, with over 94% estimated correctly regardless of source distance from the array. Concordance to the true z-position was poor regardless of source depth, distance from the center of the array and type of replica field, though a much greater degree of concordance occurred when data-derived replicas were used. There was no relationship between localization error and SNR or the strength of SCOT peak using either type of replica.

3.2 Localization of Living, Vocalizing Fishes

In order to illustrate the effectiveness of our approach, we analyzed the calls of two different fish that were manually identified and then localized. They consisted of a variable number short of pulses that combined to form calls of 0.29 ± 0.02 and 0.32 ± 0.03 (mean ± standard deviation) seconds in duration, respectively (Table 3.5). Fish #1 waited on average between 2.30 ± 0.91 seconds before producing a subsequent call, while Fish #2 waited slightly

longer at 2.74 ± 1.47 seconds. The peak frequency of the calls ranged between 240 and 533 Hz. The SL of calls ranged from 118 to 142 dB re: 1 μPa at 1 m RMS from 245 to 1255 Hz.

Fish #1 called between 22:13:59 and 22:27:54 on September 7, 2019. Only 336 of the 395 calls were localized as many were obstructed by noise on one or more receivers. TDOAs of these calls varied very little over time (Fig. 3.10a). When data-derived replicas were used to localize the calls (Fig. 3.10c), Fish #1's total activity space was 387 m^2, with 220 calls falling in a single numerical bin creating a core activity space of 79 m^2 (Table 3.6, Fig. 3.10e). However, when modeled replicas were used (Fig. 3.10b), its total and core activity space were over twice these sizes with only 10 calls falling in a single numerical bin (Fig. 3.10d). Fish #1 never entered the South La Jolla State Marine Reserve (SMR).

Fish #2 called between 21:18:38 and 21:33:06 on September 6, 2019. It started calling about 20 m due east of receiver $\vec{p}_0$ (Figs 11b-c). After approximately two minutes, it traveled along the boundary of the South La Jolla SMR due west to receiver $\vec{p}_0$, where it changed direction and started swimming northward towards receiver $\vec{p}_3$. Position estimates computed using modeled replicas suggest that the fish continued along this northward trajectory, past receiver $\vec{p}_3$, at an average speed of 209 cm/s for an additional 5 minutes until it exited the footprint of the array (Table 3.6, Fig. 3.11b). However, position estimates computed with data-derived replicas suggest that the fish most likely remained halfway between receiver $\vec{p}_0$ and $\vec{p}_3$ for 7 minutes, slowly making its way towards $\vec{p}_3$ at an average speed of 164 cm/s (Table 3.6, Fig. 3.11c). Outside the array, the fish shifted its trajectory slightly to the NNE direction before it stopped calling or calls could no longer be detected. As such, the fish's total and core activity spaces were both approximately 24% smaller when computed using data-derived rather than modeled replica fields (Table 3.6; Fig. 3.11d-e).

4. Discussion

Here, we show that *in situ* sound playbacks can be used to not only quantify passive acoustic localization performance, but also to reduce localization error. We found that localization performance is a complicated function of position from the receiver array to the source that varies in all three Cartesian dimensions rather than concentric rings of constant location uncertainty often reported when small perturbations are applied to TDOAs for localization error analysis (e.g., K. C. Wilson et al., 2019). Additionally, using data-derived replica fields that accounted for the path-to-path variations in sound speed and multi-path arrival structure instead of modeled replica fields significantly decreased localization error in all dimensions. This improved localization accuracy and precision can be used to localize and track individual fish and compute more realistic behavioral metrics from their vocalizations.

The spatial variability in localization performance observed in the xy-plane is, in part, due to the underwater configuration of the receiver array. Unfortunately, the array was not a two-dimensional tetrahedron as planned (Supplementary Fig. 3.1b); therefore, its localization performance was not omni-directional. Further, error associated with using a (nominally) two-dimensional receiver array to localize a source in all three Cartesian dimensions decreases as the source approaches the center of the array and/or as source depth approaches the plane of the array (Spiesberger, 2019). We found that position estimates of sources located inside the array ($d \leq 22.8$ m) and deeper ($z = 13$ m) were much closer to their GPS- and ambient pressure-derived true positions than sources located inside the array and shallower ($z = 5$ m) as well as all sources located outside the array ($d > 22.8$ m). Additionally, when a source is located within the footprint of the array and at a similar depth to the receivers, the direct-path from the source to the receivers is typically the strongest arrival and thus, bathymetric effects can largely be ignored. In

this case, localization performance is good regardless of replica type as representing the environment with an iso-velocity, straight-line propagation model is appropriate (Tiemann et al., 2004). If the source is higher in the water column or located further than one or two water depths from the array, surface and bottom interactions become important, especially for low-frequency sounds. This is due to the downward-refracting sound speed profile typical of shallow-water environments. We were only able to accurately resolve the depth of the source using data-derived replicas. Despite only two options in source depth, only 66% of z-positions were estimated correctly using modeled replicas. Given that all receivers were at a similar depth, this observation is not unexpected as it is common for depth estimates to be associated with much larger errors than those of the corresponding horizontal position estimates (Baggenstoss, 2011).

To our knowledge, Parsons et al. (2009) is the only other study that has used *in situ* playbacks of fish calls to quantify localization error. However, they only described broad patterns of localization performance (e.g., decreased localization performance with range) due to a limited number of playbacks ($n < 20$) and thus, a limited spatial coverage throughout the array. We suggest that studies that aim to localize individual animals conduct a survey with a controlled source within the numerical search grid and with high of resolution as possible in all three dimensions. This could be accomplished by looping the signal of interest, attaching the source to a slowly drifting platform, such as a small vessel, and repeating this survey at different depths. Additionally, repeating these playbacks multiple times at each point in the numerical search grid would provide sufficient spatial resolution to fully characterize the horizontal spatial variability in localization error we observed.

Replica fields that correctly characterize the spatially and temporally varying surface, volume and bottom properties of the environment are needed to accurately and precisely locate

sources higher in the water column and outside the footprint of the array. If the geoacoustic properties within the study area were known, we could have used acoustic propagation models such as Kraken, a normal mode propagation algorithm, or RAMGeo, which uses a parabolic equation approximation to the acoustic wave equation, to compute such replica fields. Unfortunately, values for the sediment geoacoustics properties are not readily available in many coastal areas. Additionally, they are difficult and costly to obtain, requiring coring, which is not permitted within a marine protected area (MPA), and subsequent laboratory analysis. Shallow-water, coastal habitats also often have fine-scale and complex bathymetry (e.g., scattered rocky reefs) as well as spatially and temporally varying bottom sediment composition (e.g., sand, hard-bottom) that would need to be accounted for in the model. The presence of biologics in the water column (e.g., kelp, seagrass) could also influence sound propagation (C. J. Wilson, Wilson, Greene, & Dunton, 2013). As such, a simple range-independent model with a flat bottom approximation would not be sufficient to capture the complexity of the environment at an appropriate resolution.

Shallow-water environments create diverse and unique replica fields that can be exploited to improve localization performance. By using data-derived instead of simple modeled replicas, we accounted for the two primary types of error that can negatively impact localization performance. First, we accounted for any potential mismatch between the true and modeled environment. We also eliminated the need to explicitly define the sound speed profile, geoacoustic properties and bathymetry as this information is embedded within the replicas. Second, data-derived replicas also accounted for any multi-path arrival structure. Multi-path signal propagation causes multiple peaks in the SCOT sequence, which can be of higher magnitude than the peak from the direct-path (Spiesberger, 1998). This can lead to erroneous

TDOAs because a direct-path signal at one receiver could be associated with a reflected signal on another or two reflected signals could be associated with each other (Nosal, 2013). This was commonly observed for shallow sources, whose TDOAs often scattered far from the expected TDOA based on the known trajectory of the source (Fig. 3.4). However, TDOAs were mostly consistent within each numerical grid cell, even if they were erroneous. As such, we did not attempt to correct replicas based on erroneous TDOAs; though this could be accomplished by deconvolving the signal of interest to estimate the TDOAs of multi-path path arrivals. Uncertainties in the location of the receivers and true source position from drift are not accounted for in the data-derived replica fields; hence why localization error is never zero.

Small localization error (i.e., on the order of <5 m) is needed to localize individual fish, as their body size and distance traveled from one call to the next might be smaller than the error. We showed that the substantial improvement in localization performance obtained when using data-derived replicas can be used to localize living fishes that live in these complex, shallow-water habitats without the use of sophisticated acoustic propagation models. Data-derived replicas accurately captured the relatively stationary behavior of a living, vocalizing fish. If modeled replicas had been used, we would have incorrectly assumed that the fish occupied a much larger space. While modeled replicas captured the general trajectory of a moving fish, they failed to capture when the fish stopped and swam around a small area for a significant period of time and overestimated swimming speeds. When data-derived replicas were used and localization error was accounted for, calculated swimming speeds were consistent with those estimated for White Croaker (*Genyonemus lineatus*), a species closely related to the species of fish that are potential producing this sound (Dorn, Johnson, & Darby, 1979). We also found that fishes were likely located closer to the surface than the seafloor. This is consistent with

observations that the ambient SLs in this region during summer, evening chorusing are higher near the thermocline (~5-8 m) (pers. obs.). Additionally, given the high SL of these fish calls such that they could be detected on all four receivers at distances greater than one or two water depths, it is important to use replicas, such as those derived from *in situ* playbacks, that capture all of the complexity of the acoustic environment as we have shown that an iso-velocity, straight-line propagation model is not sufficient to accurately and precisely localize such sources that are higher in the water column and located outside the receiver array perimeter. Notably, only Fish #2 produced some calls originating from within the borders of the South La Jolla SMR. This suggests that the MPA in its current location may not be providing adequate protection to this species of fish when it is spawning. The improved localization performance provided by data-derived replicas enables future research to distinguish between two individual vocalizing fish, even if they are close together, leading to estimates of abundance and density of populations as well as *in situ* observations as to how fishes interact with each other.

Using *in situ* sound playbacks to quantify and reduce localization error is a robust and simple method that can be easily added after the deployment of a receiver array. With the continued development of low-cost instrumentation and available open source guides to build underwater speakers (e.g., Hopton & Cui, 2020), the deployment of a controlled source to characterize error and construct data-derived replicas should become standard practice for all passive acoustic localization studies in complex, shallow-water environments, particularly those aiming to study animal movement ecology. Such practice enables researchers to verify their localization algorithm and generate more accurate and precise estimates of an animal's location. While we used the same call in our playbacks as we localized, the data-derived replicas generated in this experiment could be used to localize any other sound recorded during the

deployment, even those with different spectral characteristics because we used TDOAs instead of the signal of interest itself for matching. This approach could be extended to improve the accuracy and precision of location estimates derived from acoustic telemetry, which are typically used to study fish movement, by using the acoustic tag as the controlled source. While this approach enabled us to characterize the spatial variability of localization performance, further research is needed to investigate the sensitivity of the data-derived replicas to temporal environmental variation. This will define how long the replicas can be used to localize an animal before the physical oceanographic conditions have changed sufficiently such that localization error is increased significantly.

Acknowledgements

The author would like to thank D. Bedenko, M. Costa, PE. Parnell and R. Walsh for assistance in the field. A special thank you to J. Butler for building the underwater source and for providing feedback on an early draft of the manuscript. Thank you to G. D'Spain and W. Hodgkiss for fruitful discussions about quantifying localization error and error budgets, to W. Kuperman for guidance on the use of data-derived replica fields for acoustic localization, and J. Jaffe for guidance on experimental setup and additional financial support to conduct the experiment. CMLSP was supported in part by a Natural Sciences and Engineering Research Council (NSERC) of Canada Postgraduate Scholarship – Doctoral Program as well as the Fleet Admiral Chester W. Nimitz Fellowship and H. William Menard Memorial Fellowship awarded by Scripps Institution of Oceanography. Funding to acquire the passive acoustic receiver array and the underwater source was provided by the California Sea Grant College Program Project Award Number NA14OAR4170075, through NOAA'S National Sea Grant College Program, U.S. Dept. of Commerce.

Authors' Contributions

Data Accessibility

All software and data will be accessible on the project's associated GitHub page.

References

Baggenstoss, P. M. (2011). An algorithm for the localization of multiple interfering sperm whales using multi-sensor time difference of arrival. *The Journal of the Acoustical Society of America*, *130*(1), 102–112. doi:10.1121/1.3598454

Baggeroer, A. B., Kuperman, W. A., & Mikhalevsky, P. N. (1993). An overview of matched field methods in ocean acoustics. *IEEE Journal of Oceanic Engineering*, *18*(4), 401–424. doi:10.1109/48.262292

Carter, G. C., Nuttall, A. H., & Cable, P. G. (1973). The smoothed coherence transform. *Proceedings of the IEEE*, *61*(10), 1497–1498. doi:10.1109/PROC.1973.9300

Cummings, W. C., Brahy, B. D., & Herrnkind, W. F. (1964). The Occurrence of Underwater Sounds of Biological Origin off the West Coast of Bimini, Bahamas. In W. N. Tavolga (Ed.), *Marine Bio-Acoustics. Proceedings of a Symposium held at the Lerner Marine Laboratory, Bimini, Bahamas, April 11 to 13, 1963.* (pp. 27–43). Oxford, UK: Pergamon Press.

Dorn, P., Johnson, L., & Darby, C. (1979). The Swimming Performance of Nine Species of Common California Inshore Fishes. *Transactions of the American Fisheries Society*, *108*(4), 366–372. doi:10.1577/1548-8659(1979)108<366:tspons>2.0.co;2

Guazzo, R. A., Helble, T. A., D'Spain, G. L., Weller, D. W., Wiggins, S. M., & Hildebrand, J. A. (2017). Migratory behavior of eastern North Pacific gray whales tracked using a hydrophone array. *PLoS ONE*, *12*(10), 1–29. doi:10.1371/journal.pone.0185585

Hopton, T., & Cui, F. (2020). AusOcean Underwater Speaker Guide. Retrieved from https://docs.google.com/document/d/e/2PACX-1vQMI4_PIhiV4XEZmS4epEmmz1yxPt_6szFSWTjjOur-h8RFDdeLlyCaVIuYpUX4xGcYvs2RIQiwdugr/pub

Johnson, M. W. (1948). Sound As a Tool in Marine Ecology, From Data on Biological Noises and the Deep Scattering Layer. *Journal of Marine Research*, *7*(03–26), 443–458.

Kaatz, I. M. (2002). Multiple sound-producing mechanisms in teleost fishes and hypotheses regarding their behavioural significance. *Bioacoustics*, *12*(2–3), 230–233. doi:10.1080/09524622.2002.9753705

Kim, K. H., Thomas, L., Marques, T. A., Harris, D., Oedekoven, C. S., Cheoo, G., … Conrad, A. (2018). An evaluation of density estimation methods using a multiyear dataset of localized bowhead whale calls. *The Journal of the Acoustical Society of America*, *144*(3), 1850. doi:10.1121/1.5068143

Larsen, O. N., & Radford, C. (2018). Acoustic Conditions Affecting Sound Communication in Air and Underwater. In H. Slabbekoorn, R. Dooling, A. Popper, & R. R. Fay (Eds.), *Effects of Anthropogenic Noise on Animals* (pp. 109–144). New York, NY: Springer. doi:10.1007/978-1-4939-8574-6_5

Locascio, J. V., & Mann, D. A. (2011). Localization and source level estimates of black drum (*Pogonias cromis*) calls. *The Journal of the Acoustical Society of America*, *130*(4), 1868–1879. doi:10.1121/1.3621514

McBride, G. (2005). *A proposal for strength-of-agreement criteria for Lin's concordance correlation coefficient*. Hamilton, New Zealand. Retrieved from https://www.medcalc.org/download/pdf/McBride2005.pdf

Mouy, X., Rountree, R., Juanes, F., & Dosso, S. E. (2018). Cataloging fish sounds in the wild using combined acoustic and video recordings. *Journal of the Acoustical Society of America*, *143*(4), EL333. doi:10.1121/1.5037359

Nosal, E.-M. (2013). Methods for tracking multiple marine mammals with wide-baseline passive acoustic arrays. *The Journal of the Acoustical Society of America*, *134*(3), 2383–2392. doi:10.1121/1.4816549

Pagniello, C. M. L. S., Cimino, M. A., & Terrill, E. (2019). Mapping Fish Chorus Distributions in Southern California Using an Autonmous Wave Glider. *Frontiers in Marine Science*, *6*, 526. doi:10.3389/fmars.2019.00526

Parsons, M. J. G., McCauley, R. D., Mackie, M. C., & Duncan, A. J. (2010). A comparison of techniques for ranging close-proximity mulloway (*Argyrosomus Japonicus*) calls with a single hydrophone. *Acoustics Australia*, *38*(3), 145–151.

Parsons, M. J. G., McCauley, R. D., Mackie, M. C., Siwabessy, P., & Duncan, A. J. (2009). Localization of individual mulloway (*Argyrosomus japonicus*) within a spawning aggregation and their behaviour throughout a diel spawning period. *ICES Journal of Marine Science*, *66*(6), 1007–1014. doi:10.1093/icesjms/fsp016

Putland, R. L., Mackiewicz, A. G., & Mensinger, A. F. (2018). Localizing individual soniferous fish using passive acoustic monitoring. *Ecological Informatics*, *48*(July 2019), 60–68. doi:10.1016/j.ecoinf.2018.08.004

Rountree, R. A., Gilmore, R. G., Goudey, C. A., Hawkins, A. D., Luczkovich, J. J., & Mann, D. A. (2006). Listening to Fish: Applications of Passive Acoustics to Fisheries Science. *Fisheries*, *31*(9), 433–446. doi:10.1577/1548-8446(2006)31

Sibson, R. (1981). A Brief Description of Natural Neighbour Interpolation. In *Interpolating Multivariate Data* (pp. 21–36). New York, NY: John Wiley & Sons.

Simard, Y., Bahoura, M., & Roy, N. (2004). Acoustic detection and localization of whales in bay of fundy and St. Lawrence estuary critical habitats. *Canadian Acoustics - Acoustique Canadienne*, *32*(2), 107–116.

Spiesberger, J. L. (1998). Linking auto- and cross-correlation functions with correlation equations: Application to estimating the relative travel times and amplitudes of multipath. *The Journal of the Acoustical Society of America*, *104*(1), 300–312. doi:10.1121/1.423257

Spiesberger, J. L. (2019). Locating calling mammals with signal times amongst shadows and black holes in two-dimensional models. *The Journal of the Acoustical Society of America*, *146*(4), 2770. doi:10.1121/1.5136597

Spiesberger, J. L., & Fristrup, K. M. (1990). Passive Localization of Calling Animals and Sensing of their Acoustic Environment Using Acoustic Tomography. *The American Naturalist*, *135*(1), 107–153.

Tiemann, C. O., Porter, M. B., & Frazer, L. N. (2004). Localization of marine mammals near Hawaii using an acoustic propagation model. *The Journal of the Acoustical Society of America*, *115*(6), 2834–2843. doi:10.1121/1.1643368

Tyack, P. L. (1998). Acoustic communication under the sea. In S. Hopp, M. Owren, & C. Evans (Eds.), *Animal acoustic communication* (pp. 163–220). Berlin, Germany: Springer.

Urazghildiiev, I. R., & Clark, C. W. (2013). Comparative analysis of localization algorithms with application to passive acoustic monitoring. *The Journal of the Acoustical Society of America*, *134*(6), 4418–4426. doi:10.1121/1.4824683

Van Trees, H. L. (2001). *Detection, Estimation, and Modulation Theory, Part I*. New York, NY: Wiley. doi:10.1002/0471221082

Van Veen, B. D., & Buckley, K. M. (1988). Beamforming: A Versatile Approach to Spatial Filtering. *IEEE ASSP Magazine*, *5*(2), 4–24. doi:10.1109/53.665

Verlinden, C. M. A., Sarkar, J., Hodgkiss, W. S., Kuperman, W. A., & Sabra, K. G. (2015). Passive acoustic source localization using sources of opportunity. *The Journal of the Acoustical Society of America*, *138*(1), EL54–EL59. doi:10.1121/1.4922763

Wilson, C. J., Wilson, P. S., Greene, C. A., & Dunton, K. H. (2013). Seagrass meadows provide an acoustic refuge for estuarine fish. *Marine Ecology Progress Series*, *472*, 117–127. doi:10.3354/meps10045

Wilson, K. C., Semmens, B. X., Gittings, S. R., Pattengill-Semmens, C., & Širović, A. (2019). Development and evaluation of a passive acoustic localization method to monitor fish spawning aggregations and measure source levels. *OCEANS 2019 MTS/IEEE Seattle, OCEANS 2019*, 0–6. doi:10.23919/OCEANS40490.2019.8962663

Wilson, K. C., Semmens, B. X., Pattengill-Semmens, C. V., McCoy, C., & Širović, A. (2020). Potential for grouper acoustic competition and partitioning at a multispecies spawning site off Little Cayman, Cayman Islands. *Marine Ecology Progress Series*, *634*, 127–146. doi:10.3354/meps13181

Winn, H. E. (1964). The biological significance of fish sounds. In W. N. Tavolga (Ed.), *Marine Bio-Acoustics. Proceedings of a Symposium held at the Lerner Marine Laboratory, Bimini, Bahamas, April 11 to 13, 1963.* (pp. 213–231). Oxford, UK: Pergamon Press.

Woodward, P. M. (1964). Probability and Information Theory, with Applications to Radar. In D.

W. Fry & W. Higinbothan (Eds.), *vol. 3 of International Series of Monographs on Electronics and Instrumentation* (2nd ed, p. 136). Pergamon Press. doi:10.1057/jors.1977.45

Yamato, K., Matsuo, I., Takahashi, R., Matsubara, N., & Yasuma, H. (2017). Localization method of fish by using fish call sounds recorded by two stereo underwater sound recorders. *Techno-Ocean 2016: Return to the Oceans*, 556–561. doi:10.1109/Techno-Ocean.2016.7890717

Figures and Tables

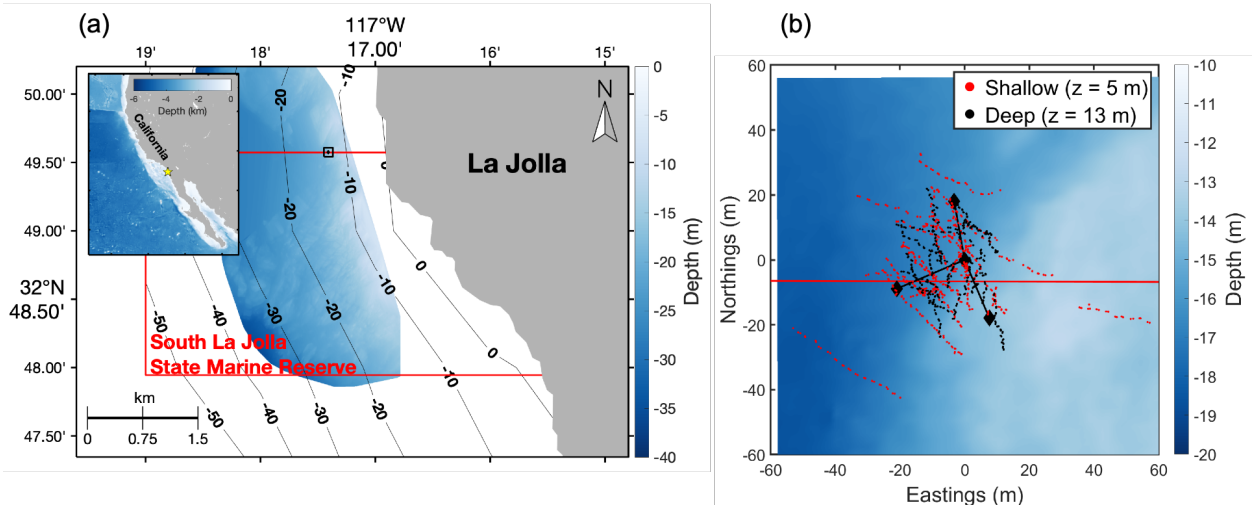

Figure 3.1. (a) Location of deployment of passive acoustic array (black diamond) and extent of numerical search grid (black square) off the coast of La Jolla, California on the northern edge of the South La Jolla State Marine Reserve (boundaries shown in red). In the top-left inset, location of the larger map is shown as yellow star off the coast of southern California. (b) Playback locations for fish call at shallow (z = 5 m) (red circles) and deep (z = 12 m) (black circles) depths within the numerical search grid. Black diamonds are receiver locations.

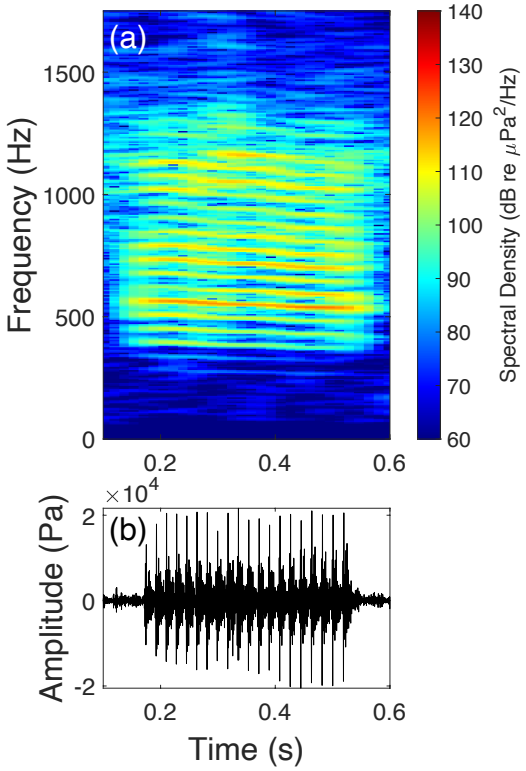

Figure 3.2. (a) Spectrogram and (b) timeseries of fish call used for *in situ* playbacks. (Spectrogram parameters: Kaiser-Bessel window with $\alpha = 2.5$, sample rate = 48 kHz, 8192-point fast Fourier transform with 90% overlap. Color represents spectral density (dB re 1 $\mu Pa^2/Hz$).)

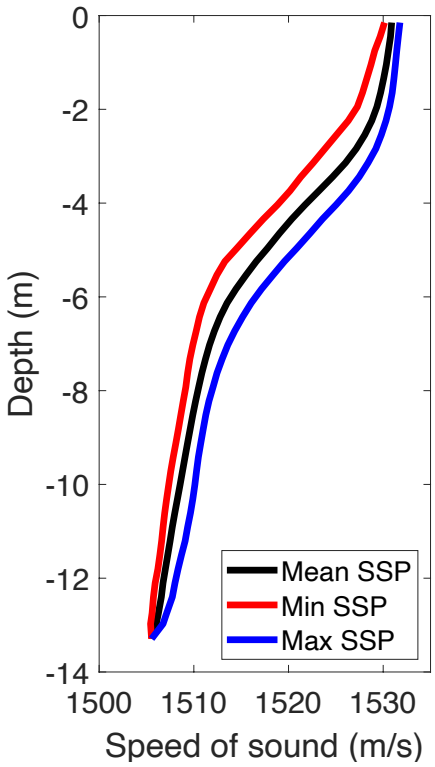

Figure 3.3. Mean (black line), minimum (red line) and maximum (blue line) sound speed profile (SSP).

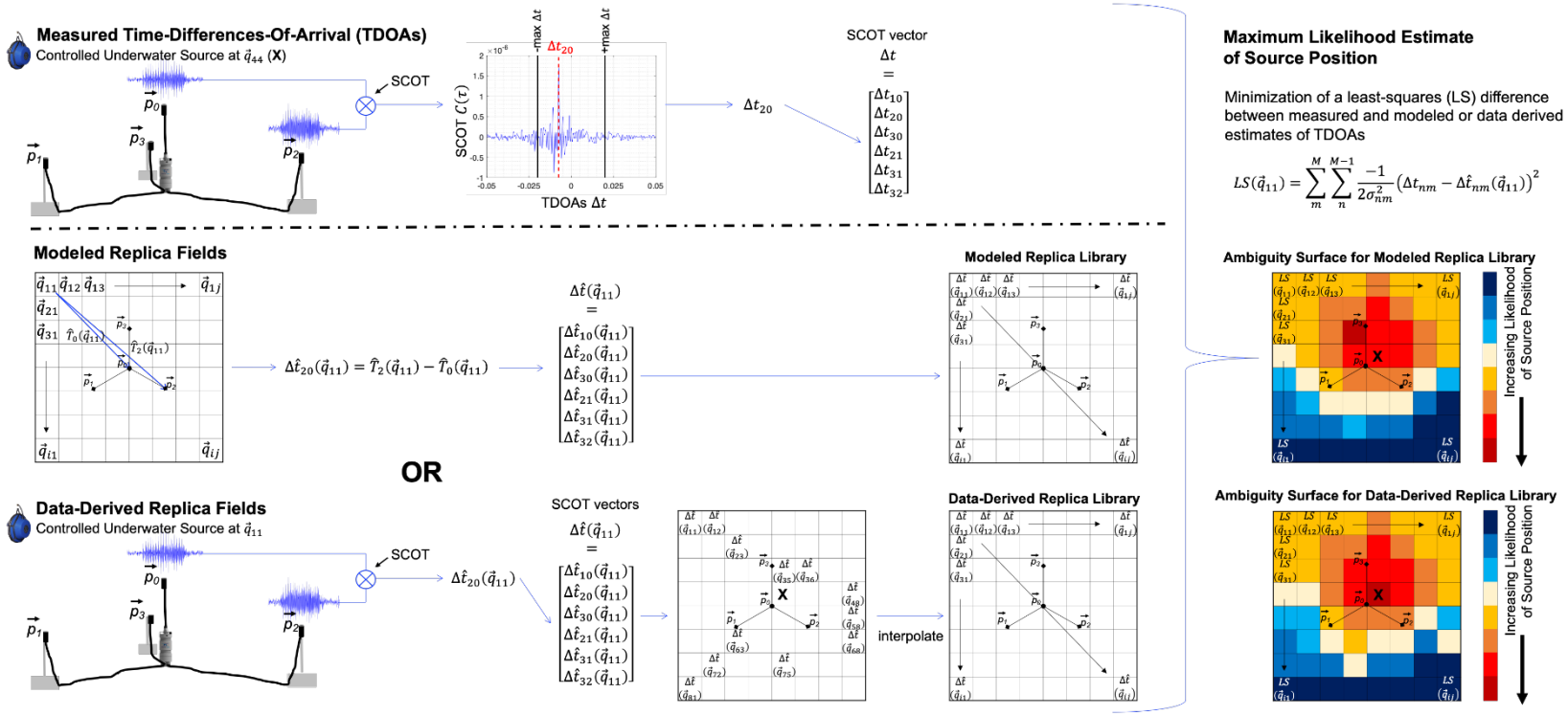

Figure 3.4. A schematic illustrating the steps of the acoustic localization method.

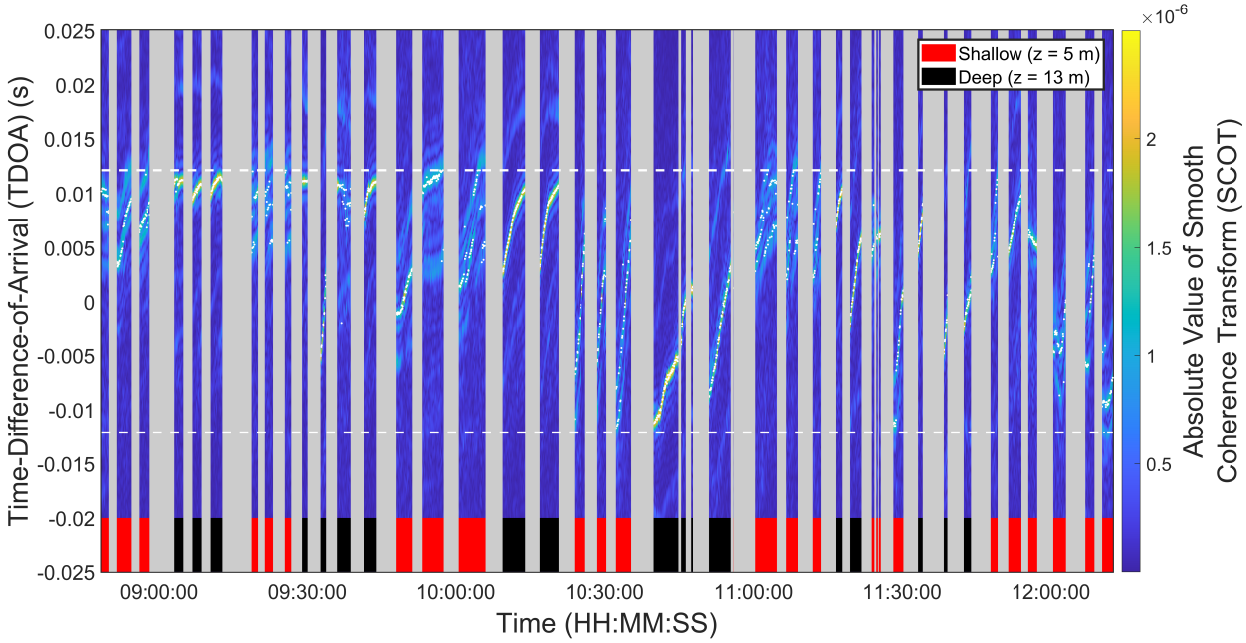

Figure 3.5. TDOA cross-correlogram between receiver $\vec{p}_0$ and $\vec{p}_1$ on September 7, 2019 when the controlled source was shallow (z = 5 m, red) or deep (z = 13 m, black). The highest SCOT value for each playback (white dot) and maximum TDOA based on array geometry (white dashed line) are also shown.

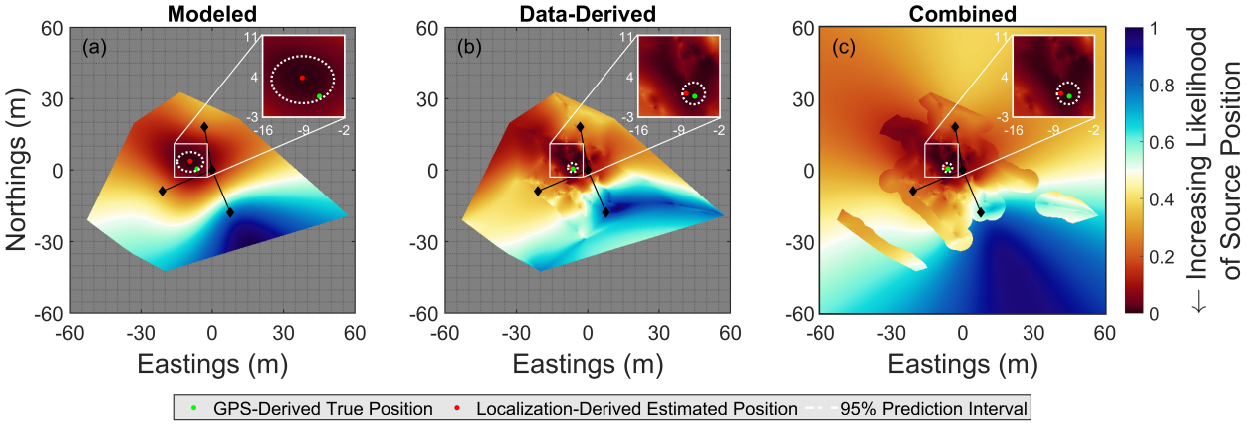

Figure 3.6. Ambiguity surfaces for a GPS-located, underwater controlled source (green circle) using (a) modeled and (b) data-derived replicas. These replicas were combined, as described in the Supporting Information, to produce the ambiguity surface shown in (c). The position estimate with highest probability (red circle) and 95% prediction interval (white dotted ellipse) are also shown. Black diamonds are receiver locations.

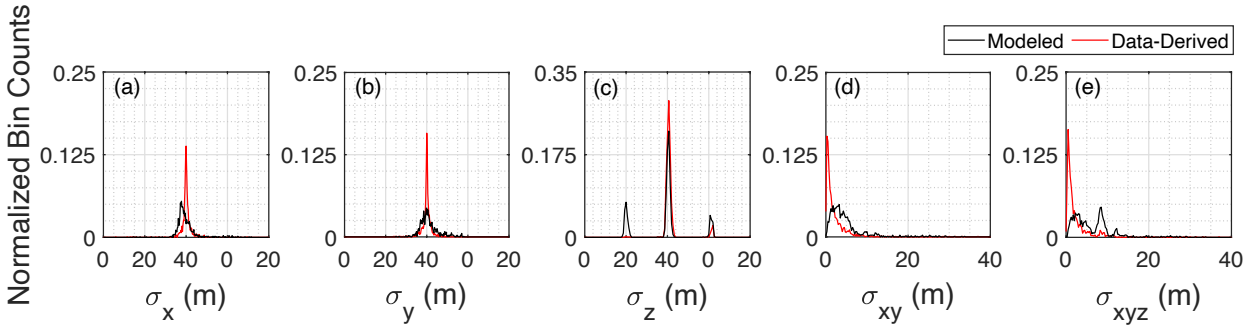

Figure 3.7. Error distributions in all Cartesian dimensions using modeled (black line) and data-derived (red line) replicas. Bins are normalized by the total number of playbacks.

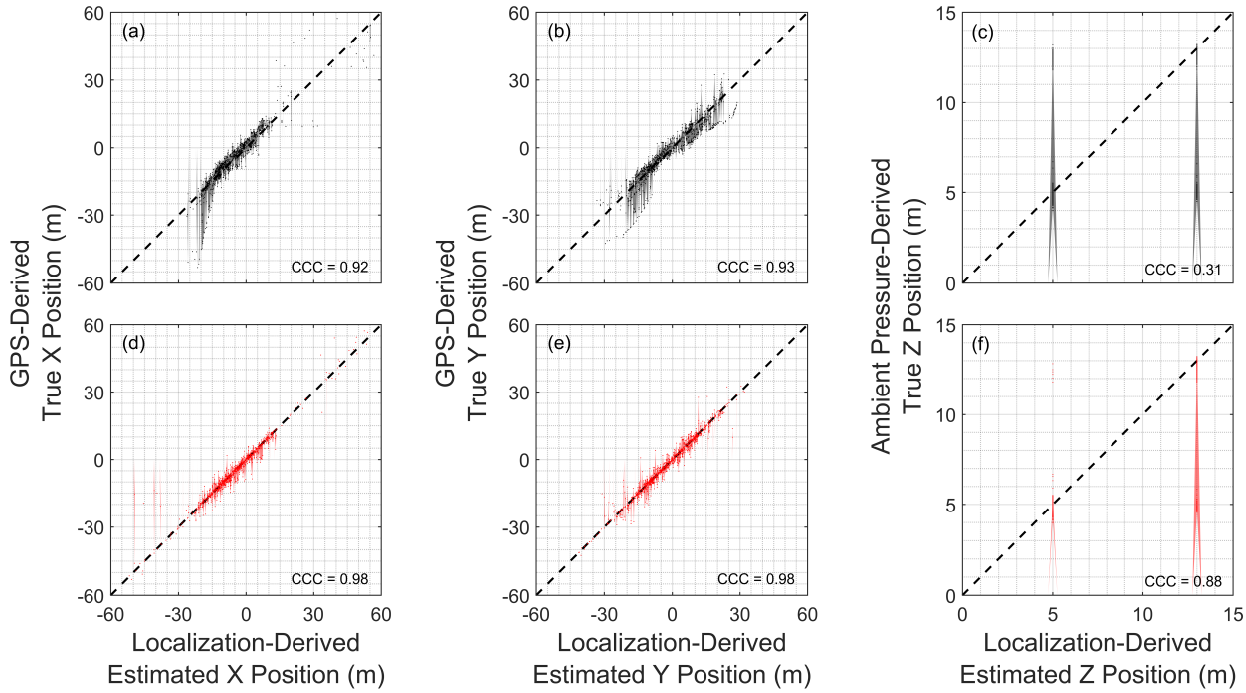

Figure 3.8. Localization-derived estimated position using (a)-(c) modeled and (d)-(f) data-derived replicas vs. GPS- or ambient pressure-derived true position. Dashed line is the 1:1 (45°) line of agreement. Shaded areas represent 95% prediction intervals. CCC is Lin's concordance correlation coefficient.

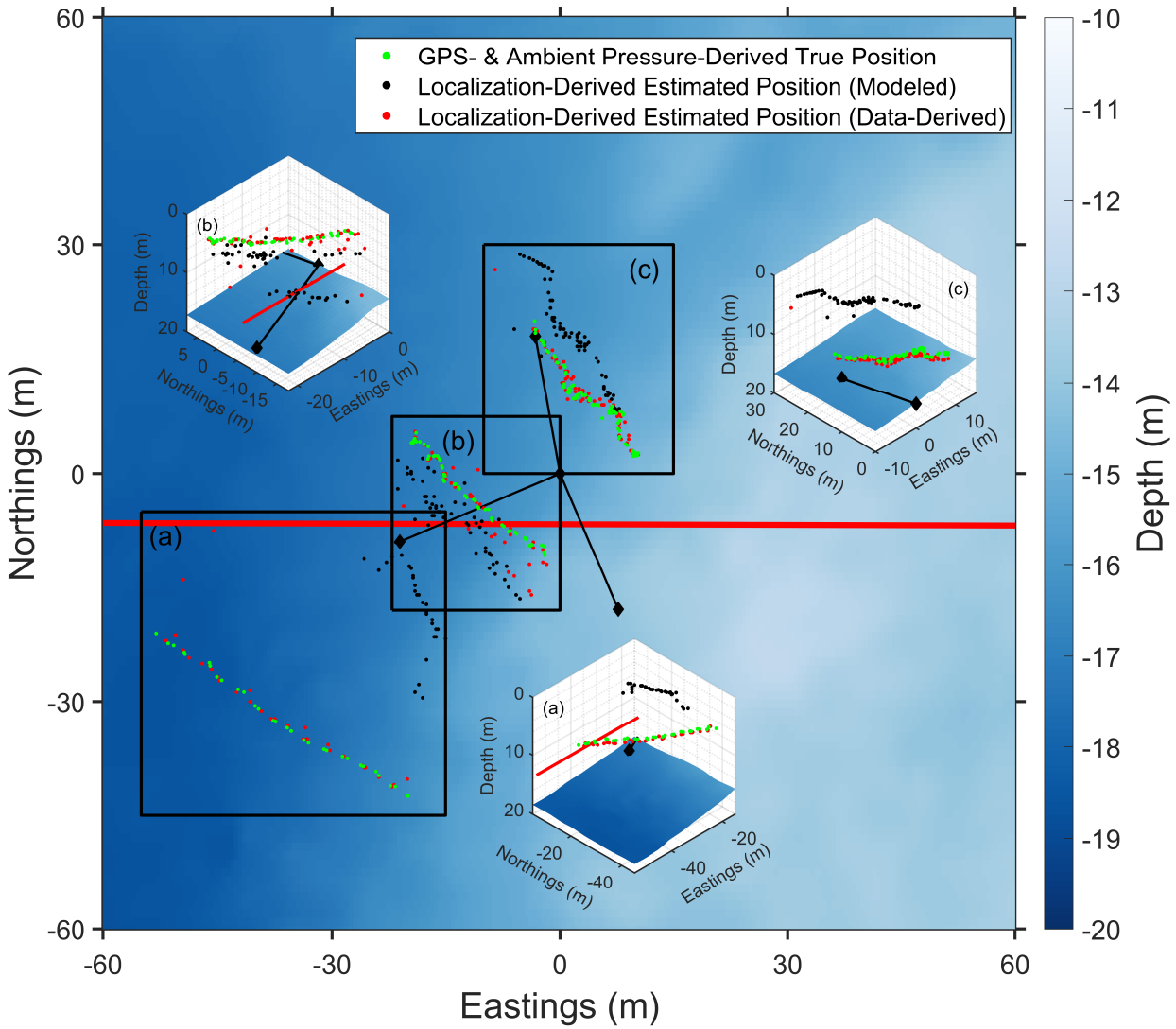

Figure 3.9. Example of localization-derived estimate positions of playbacks located (a) outside and (b) inside the footprint of the array, as well as (c) along the perimeter of the array using modeled (black dot) and data-derived (red dot) replicas. GPS- and ambient pressure-derived true positions are shown in green. Insets show 3D view. Black diamonds are receiver locations. Red line shows northern boundary of the South La Jolla State Marine Reserve.

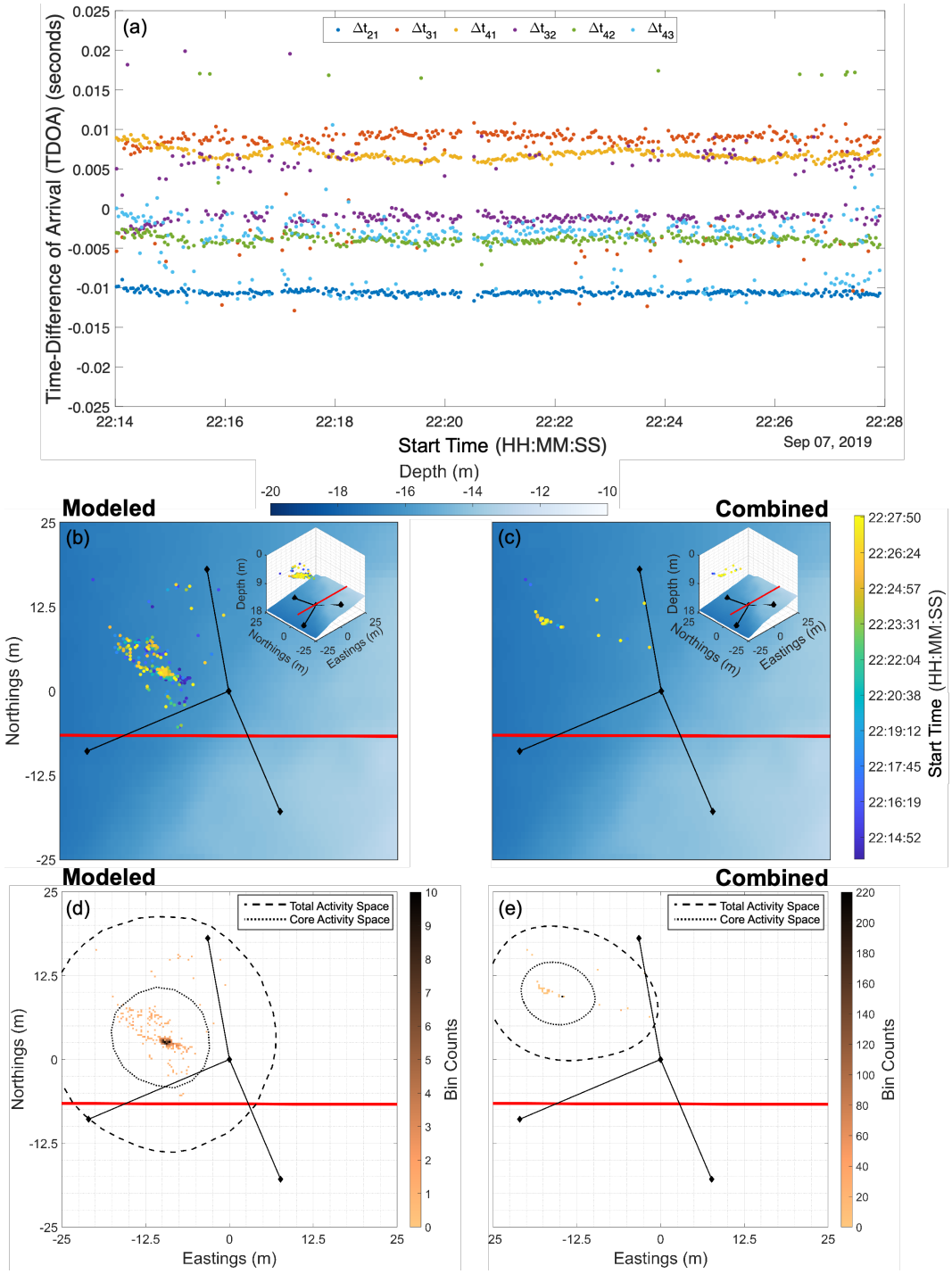

Figure 3.10. (a) TDOA vs. start time of Fish #1's calls. Location estimates (dots) of Fish #1 determined by localizing their vocalizations using (b) modeled or (c) combined replicas. Color of dots indicates the start time of the call. Inset shows 3D view. Number of calls per bin in the search grid using (d) modeled or (e) combined replicas. Total (dashed line) and core (dotted line) activity space are shown. Black diamonds are receiver locations. Red line shows northern boundary of the South La Jolla State Marine Reserve. All times are local (Pacific Daylight Time).

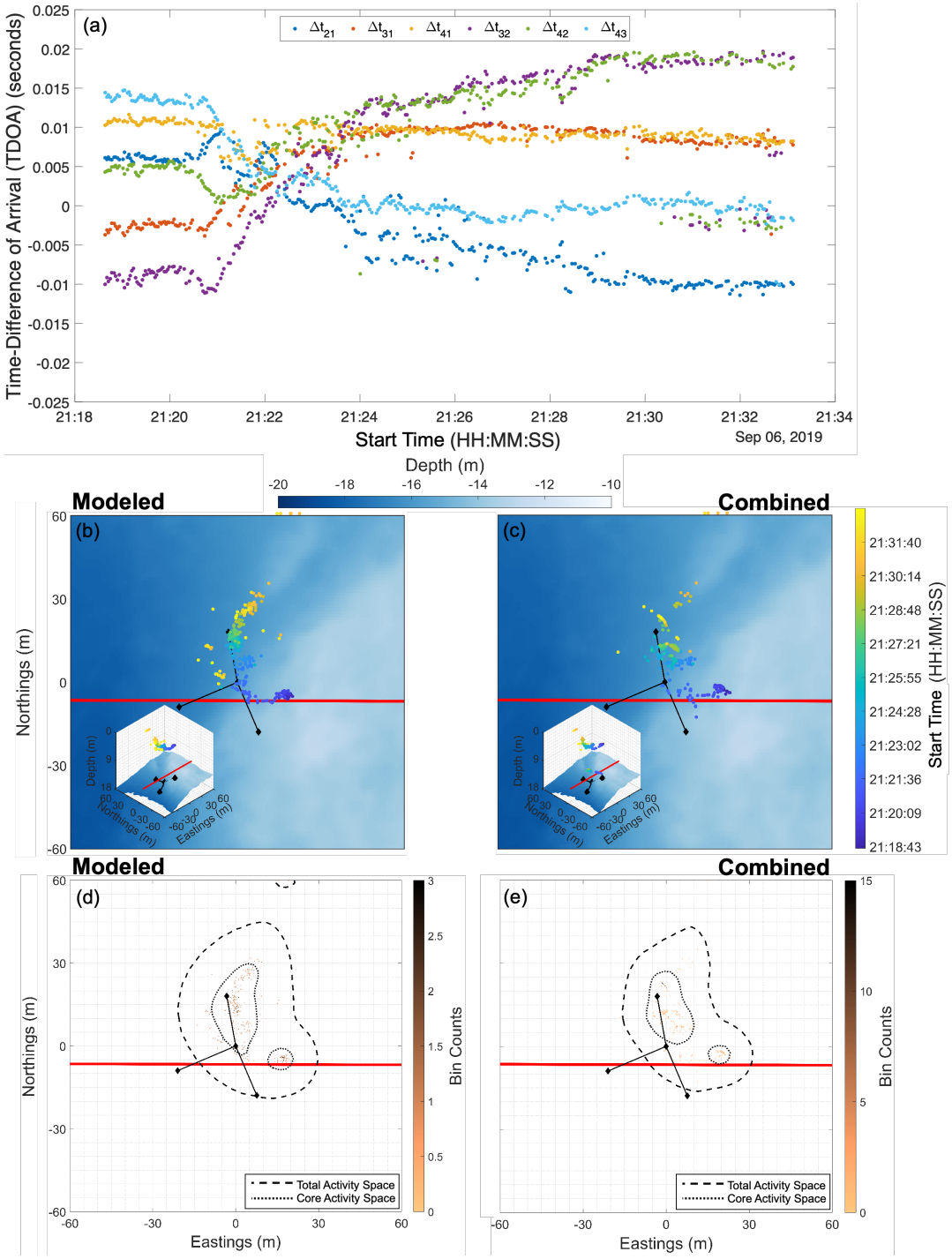

Figure 3.11. (a) TDOA vs. start time of Fish #2's calls. Location estimates (dots) of Fish #2 determined by localizing their vocalizations using (b) modeled or (c) combined replicas. Color of dots indicates the start time of the call. Inset shows 3D view. Number of calls per bin in the search grid using (d) modeled or (e) combined replicas. Total (dashed line) and core (dotted line) activity space are shown. Black diamonds are receiver locations. Red line shows northern boundary of the South La Jolla State Marine Reserve. All times are local (Pacific Daylight Time).

Table 3.1. Summary of previous published studies that localize individual fish using their sounds.

	Number of Receivers	Array Configuration	Receiver Depth (m)	Localization Error Estimation Method	Localization Error	Localization Dimensionality	Total Number of Calls Localized	Number of Individual Fish
Cummings et al. (1964)	3	equilateral triangle with receivers ~46 m apart	~20	none reported	not reported	2D	~43	not reported
Parsons et al. (2009)	4	equilateral triangle with receivers 120 m apart; two receivers separated vertically by 5 m at one location	5 to 23	playback of fish call (n = 16)	mean ± SD = 3.36 ± 1.22 m	3D	302	3
Parsons et al. (2010)	1		18.3	none reported	not reported	2D/3D	40	1
Locascio & Mann (2011)	5	linear array with receivers 0, 8, 24 and 56 m apart; fifth laterally offset	7	none reported	removed calls whose error was > 1.5 m	2D	1025	6
Yamato et al. (2017)	4	receivers separated by 0.37 m; two pairs of receivers oriented 90˚ to each other	7.7	simulation	0.076 mm	2D	~125	not reported
Mouy et al. (2018)	6	octahedron with receivers 1 m apart	3	simulation	< 1 m inside array; > 1 m outside array	3D	9	1
Putland et al. (2018)	4	linear array with receivers 5.6, 3 and 8.1 m apart	2.4 to 3.4	simulation	< 2 m between 33˚ to 148˚	2D	1,352	7
K. C. Wilson et al. (2019)	6	18-40 m spacing between receivers	24 to 33	22 kHz pinger (n = 18) & simulation	2-5 m near center of array, 7-15 m near perimeter	2D	34,883	not reported
Pagniello (2021)	4	equilateral triangle with receiver in center; receivers 18 to 23 m from center	13 to 17	playback of fish call (n = 1116)	median ± MAD = 1.2 ± 0.72 m	3D	654	2

Table 3.2. Latitude, longitude, depth, and sensitivity of receivers.

Receiver	Latitude (˚N)	Longitude (˚W)	Depth (m)	Sensitivity (dB re 1 V/µPa)
$\vec{p}_0$	32.8263	-117.2902	15.85	-165.2
$\vec{p}_1$	32.8262	-117.2904	16.15	-164.3
$\vec{p}_2$	32.8261	-117.2901	13.72	-165.5
$\vec{p}_3$	32.8264	-117.2902	16.76	-165.5

Table 3.3. Descriptions and estimates of the sources of localization error.

Source of Error	Estimated Magnitude	Description
σ_{GPS}	± 1 m	Garmin GPS device's estimated position error, a measurement of horizontal position error based upon dilution of precision and satellite signal quality.
σ_{source}	± 2 m (shallow) or ± 4 m (deep)	Source position error due to drift. $\sigma_{source} = length\ of\ rope * \sin\left(\cos^{-1}\frac{depth}{length\ of\ rope}\right)$
$\sigma_{receiver}$	± 2 m	Total receiver position error. $\sigma^2_{receiver} = \sigma^2_{GPS} + \sigma^2_{buoy}$
σ_{buoy}	± 1 m	Receiver position error due to the displacement of the surface buoy by currents.
σ_{sync}	0	Receiver synchronization error.
σ_c	± 9 m/s	Sound speed error estimated from sound speed profile.
σ_t	± 0.49 ms	Theoretical timing error from equation (1) as defined by Woodward (1964).
σ_{multi}	± 9.7 ms	Multi-path propagation error due to incorrect association of a direct-path signal at one receiver with a reflected signal on another or two reflected signals at different receivers.
σ_{ray}	-5.69 x 10^{-5} to -4.31 x 10^{-10} s	Deviation in time of arrival between curved and straight path when sound speed changes linearly with depth. Defined in Spiesberger & Fristrup (1990) as: $\delta T \cong -\frac{\left(\frac{\partial c(z)}{\partial z}\right)^2 L^3}{24\, c_1^3}$ where $\frac{\partial c(z)}{\partial z}$ is the slope of the sound speed profile, L is the distance between the source and receiver and c_1 is the sound speed at the source depth.

Table 3.4. Summary statistics for localization error distributions in each dimension using modeled and data-derived replicas.

Dimension(s)	Median (m)		Median Absolute Deviation (m)		Minimum (m)		Maximum (m)		Lin's Concordance Correlation Coefficient	
	Model	*Data*	*Model*	*Data*	*Model*	*Data*	*Model*	*Data*	*Model*	*Data*
x	-1.30	0.01	1.56	0.61	-25.6	-34.1	31.5	29.5	0.92	0.97
y	0.15	0.05	2.13	0.59	-14.9	-16.1	18.0	16.9	0.93	0.98
z	0.12	0.24	0.33	0.24	-8.20	-7.79	8.51	8.41	0.31	0.88
xy	3.47	1.06	1.62	0.76	0.12	0.003	33.8	37.1	0.78	0.94
xyz	5.17	1.20	3.00	0.72	0.36	0.07	33.8	37.1	0.74	0.93

Table 3.5. Call parameters for calls produced by two fish.

	Fish #1				**Fish #2**			
	Mean ± SD	*n*	Minimum	Maximum	Mean ± SD	*n*	Minimum	Maximum
Call Duration (s)	0.29 ± 0.02	395	0.13	0.35	0.32 ± 0.03	318	0.24	0.44
Inter-Call Interval (ICI) (s)	2.30 ± 0.91	394	0	11	2.74 ± 1.47	317	1.59	12
Peak Frequency (Hz)	349 ± 23	395	322	387	369 ± 43	318	240	533
3 dB Bandwidth (Hz)	197 ± 12	395	172	272	211 ± 36	318	173	423
6 dB Bandwidth (Hz)	309 ± 16	395	280	430	320 ± 54	318	268	536
10 dB Bandwidth (Hz)	403 ± 45	395	355	628	453 ± 95	318	354	851
SL (dB re: 1 µPa at 1 m peak-to-peak from 245 to 1255 Hz)	147 ± 4	336	140	176	151 ± 4	318	137	164
SL (dB re: 1 µPa at 1 m RMS from 245 to 1255 Hz)	128 ± 2	336	124	142	134 ± 4	318	118	142

Table 3.6. Behavioral metrics for two fish derived from localized calls computed with either the modeled or combined replica library.

	Fish #1								**Fish #2**							
	Modeled Replica Library				*Combined Replica Library*				*Modeled Replica Library*				*Combined Replica Library*			
	Mean ± SD	*n*	Min	Max	Mean ± SD	*n*	Min	Max	Mean ± SD	*n*	Min	Max	Mean ± SD	*n*	Min	Max
Swim Speed (cm/s)	178 ± 349	335	0	4521	101 ± 166	335	0	895	209 ± 409	317	0	2885	164 ± 274	317	0	2510
Total Activity Space (m^2)	933	1			387	1			2298	1			1751	1		
Core Activity Space (m^2)	169	1			79	1			437	1			355	1		
Number of Calls in MPA	0	336			0	336			13	318			7	318		

Supporting Information for: **Three-dimensional localization and tracking of individual fish using *in situ* sound playbacks in a complex shallow-water environment**

S1. Coordinate System and Array Geometry

We have defined a left-handed coordinate system such that θ is the azimuth in degrees, ϕ is the elevation in degrees and R is the range in meters (Supplementary Figure 3.1a). The corresponding local geographical directions for the Cartesian coordinates *x*, *y* and *z* are longitude or eastings (*E*-*W*), latitude or northings (*N*-*S*) and depth (*D*), respectively. The local azimuth angle is measured counterclockwise from *E* to *N* while the local elevation angle is measured counterclockwise from *E* to *D*.

The passive acoustic array was arranged in a two-dimensional tetrahedron configuration centered at the origin. Such an array design is omni-directional, with equivalent localization performance in all directions. A receiver was placed at each apex of the tetrahedron at a distance of approximately 20 m from the center receiver. As such, this formed a 20-m aperture array with four receivers to enable the localization of low-frequency sounds (Supplementary Figure 3.1b). The corresponding array position vectors $\vec{p}_m$, $m = 0, \ldots, M-1$, are defined as:

$$\begin{cases} \vec{p}_0 = [0 \quad 0 \quad 0], \\ \vec{p}_1 = \left[-\frac{\sqrt{3}}{2}d \quad -\frac{d}{2} \quad 0\right], \\ \vec{p}_2 = \left[\frac{\sqrt{3}}{2}d \quad -\frac{d}{2} \quad 0\right], \\ \vec{p}_3 = [0 \quad d \quad 0], \end{cases} \tag{S1}$$

where $d = 20$ m is the length of each arm of the array and $M = 4$ is the number of receivers

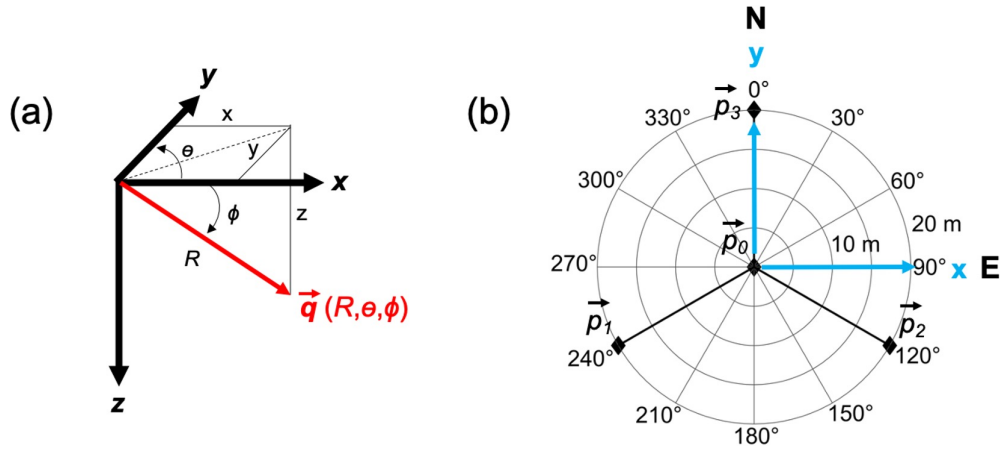

Supplementary Figure 3.1. (a) Left-handed coordinate system used for the localization scenario. (b) 2D configuration of passive acoustic system. Black diamonds are receiver locations defined in equation (S1).

S2. Acoustic Data Processing and Call Parameters

The start and end times of each sound playback was manually identified in spectrograms using *Triton*, a Matlab-based (The Mathworks, Inc., Boston, MA) acoustic data display and analysis software program (Wiggins, 2003). Spectrograms of the acoustic data were generated by dividing the time series into equal-length segments of 8192 samples with 90% overlap. A Kaiser-Bessel window of $\alpha = 2.5$ was applied to each segment before taking its fast Fourier transform (FFT) and averaging the squared magnitude of the FFT of overlapped, windowed segments. The overall sensitivity (-78 dB re 1μPa/counts) of the passive acoustic recorder was applied to the spectrograms to generate calibrated values of the spectral density (dB re 1μPa^2/Hz). When a signal of interest was identified, the mean of the signal across all receivers was subtracted from the signal on each receiver. The signal was also filtered between 245 and 1255 Hz (i.e., 5 Hz above and below its maximum and minimum frequency) using an 8th-order, bandpass IIR filter with a passband ripple of 1 dB.

Spectrograms of all the acoustic data from September 6 to 7, 2019 were manually reviewed for fish sounds whose frequency and temporal characteristics closely resemble those used during playbacks. When fish sounds were identified, their start time, end time and frequency bandwidth were manually logged using the Logger feature in *Triton*. Call duration $T_{90\%}$ was taken as the time between the 5% and 95% points on the cumulative energy curve. Inter-call interval between successive calls by the same fish was also computed. Pressure spectral density (dB re 1μPa^2/Hz) curves were generated to estimate peak frequency as well as 3-, 6- and 10-dB bandwidths (Hz), which describe the distribution of acoustic pressure as a function of frequency.

Source level (SL_{dB}) (dB re 1 µPa at 1 m) for the full duration of the fish call was estimated from the received level (RL_{dB}) (dB re 1 µPa):

$$SL_{dB} = RL_{dB} + 20\log_{10}\left(\frac{d}{1\,m}\right) + 10\log_{10}\left(\frac{r-d}{d}\right), \qquad (S2)$$

where d is the transition range at which geometrical spreading transitions from spherical to cylindrical taken as the depth of the seafloor and r is the horizontal distance between the fish and the corresponding

receiver. The value of both d and r was calculated using the localization-derived position estimate of the fish computed using the combined replica library and receiver $\vec{p}_2$ (i.e., the receiver where the received level of the call was highest). Received level was computed and reported as both root-mean-square (RMS):

$$RL_{RMS} = 20\log_{10}\left(\sqrt{\frac{1}{T_{90\%}}\int_{T_{90\%}} \mathrm{x_m}^2(t)\,dt}\right), \quad (S3)$$

and peak-to-peak (p-p) pressure level:

$$RL_{p-p} = 20\log_{10}\left(\max\left(\mathrm{x_m}(t)\right) - \min\left(\mathrm{x_m}(t)\right)\right). \quad (S4)$$

Received level was computed between 245 and 1255 Hz for each call. Based on *in situ* sound playbacks, we estimate that the SL error caused by localization error could range from 0 to 31 dB depending on the position of the source. Received and source level of the playbacks was computed in the same manner as RL_{RMS}. Additionally, noise level (NL) was computed by taking a 2 second sample after the playback occurred.

S3. Effect of Natural Neighbor Interpolation on Data-Derived Replica Fields

To examine the effect of the natural neighbor interpolation scheme on localization performance, sources located within 0.5 m of the signal of interest (i.e., the playback whose position we were attempting to estimate) were omitted from the replica library. The position of the signal of interest was estimated as described in Section 2.4.4 using this modified data-derived replica library. Additional modified data-derived replica libraries were generated by omitting positions located within 1, 2 and 5 m of the signal of interest, respectively. As the distance between the signal of interest and closest data-derived replica field increased, localization error also increased. When sources within 5 m from the signal of interest were omitted, localization performance using the modified data-derived replica library was nearly equal to localization performance using modeled replica library.

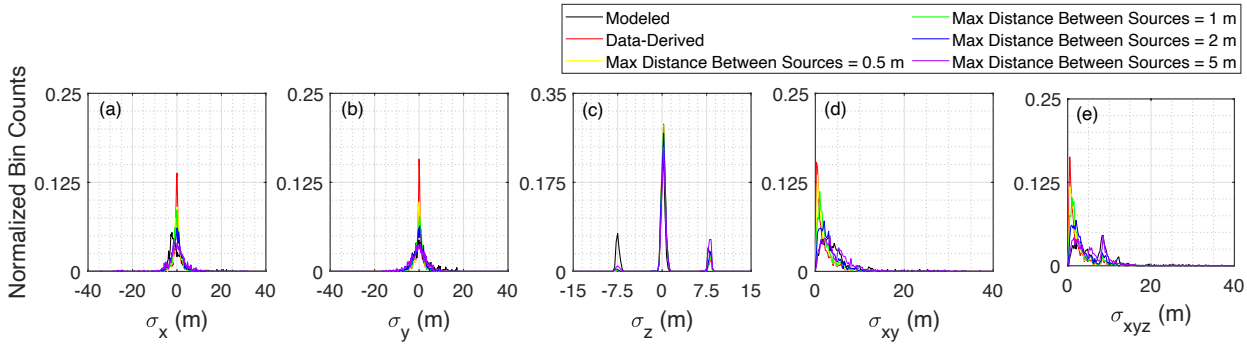

Supplementary Figure 3.2. Error distributions in the x-, y-, z-, xy- and xyz-dimensions for sources using modeled (black line) and data-derived (red line) replicas as well as modified replica libraries with sources located within 0.5 m (yellow line), 1 m (green line), 2 m (blue line) and 5 m (purple line) of the signal of interest omitted. Bins are normalized by the total number of playbacks.

S4. Localization Performance Metrics

Localization performance was quantified in terms of bias and variance. Bias, i.e., the mean of the estimated positions ($\vec{q}_{estimated}$) minus the true position ($\vec{q}_{true}$), describes systematic errors which change slowly over time and is a measure of central tendency. The scattering of localization-derived position estimates about their mean is described by the variance, which can be thought of as a measure of dispersion.

Error distributions were calculated by subtracting the true position from the localization-derived position in the x-, y- and z-dimensions, respectively. Additionally, these error estimates were combined to create single metrics $\sigma_{xy} = \sqrt{\sigma_x^2 + \sigma_y^2}$ and $\sigma_{xyz} = \sqrt{\sigma_x^2 + \sigma_y^2 + \sigma_z^2}$, whose distributions were also computed as described above. The normality of the resulting error distributions was tested using the Lilliefors test (Lilliefors, 1967). The test indicated that none of the distributions are normally distributed ($p < 0.001$). As such, median ($\tilde{x}$) and median absolute deviation (MAD) as well as maximum and minimum error values were computed as summary statistics for these distributions to describe the constant and random error. Lin's concordance correlation coefficient (CCC) (Lin, 1989) was also calculated to assess the degree of equivalence between the estimated position and the true position (i.e., the vertical departure from the 1:1 line of agreement). Lin's CCC ranges from -1 to 1, with perfect agreement at 1.

Prediction intervals were constructed by subtracting the 2.5th percentile from the 97.5th percentile of true positions at each grid point in the numerical search grid in the x-, y- and z-dimensions, respectively (Fig. 3.8). No intervals were computed at grid points with zero or one playback. These prediction intervals define the interval inside which it is 95% certain that the true position of the source will be at a given estimated position.

S5. Combined Replica Library for Living, Vocalizing Fishes

Modeled and data-derived replica libraries were combined to create a fully populated replica library to localize sounds naturally produced by living fish. We restricted the interpolation of the data-derived replica fields to a distance of 5 m from a playback location and eliminated instances when σ_{xy} was greater than 5 m. The remaining grid points without a corresponding data-derived replica field were assigned with the associated modeled replica fields such that six TDOA pairs (either modeled or data-derived) were associated with every point in the 481x481x2-point numerical search grid.

S6. Behavioral Metrics from Tracks of Vocalizing Fishes

Swimming speeds (cm/s) were computed as the three-dimensional distance traveled along a straight-line between successive, localized calls divided by the time elapsed between the start of those calls. We also counted the number of calls within the borders of the marine protected area as a proxy for the amount of time the fish may have spent in the South La Jolla State Marine Reserve.

The movement-based kernel estimation (MBKE) method was used to determine the general area utilized by vocalizing fish activity (Benhamou & Cornélis, 2010). This was computed using the R package adehabitatHR (Calenge, 2006). MBKE is a probabilistic method that assumes an animal moves according to a biased random walk to estimate activity space size (m^2) and shape that incorporates a temporal component (Benhamou, 2011). We defined the total and core activity area used as the area of 95% and 50% contours of the utilization distribution (UD) kernels, respectively, with variable smoothing parameter dependent on the time spent between each position estimate and localization error. The maximum duration between successive steps (T_{max}) to be used to compute the UD was set to the

maximum inter-call interval calculated. The parameter h_{min} was chosen to be the standard deviation of localization errors using either modeled or data-derived replica fields such that:

$$h_{min} = \sqrt{\frac{\sum(e_i-\mu)^2}{N}}, \quad (S5)$$

where $e_i = \sqrt{(\Delta PIx_i)^2 + (\Delta PIy_i)^2}$ (i.e., a single metric that combines the width of the prediction intervals in the x- and y-dimension derived from the *in situ* playbacks), μ is the mean of e_i and N is the number of observations. The smallest distance below which we considered that an animal was not moving was set to match the localization grid resolution such that L_{min} = 0.25 m.

S7. Localization Performance by Source Depth and Distance to the Center of the Array

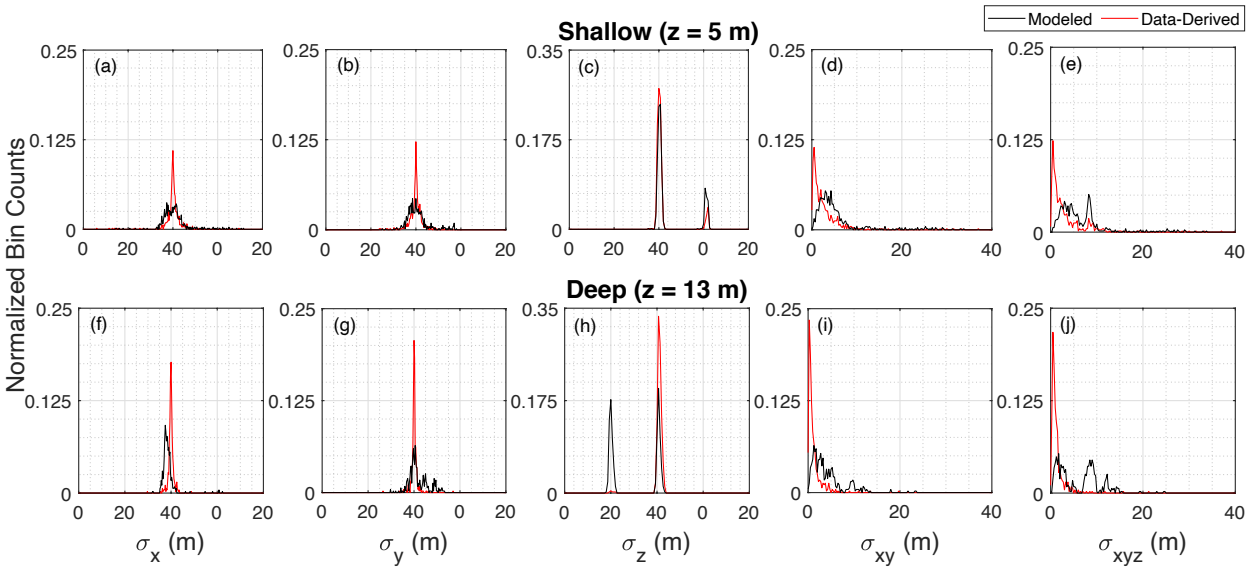

Supplementary Figure 3.3. Error distributions in the x-, y-, z-, xy- and xyz-dimensions for (a)-(e) shallow and (f)-(j) deep sources using modeled (black line) and data-derived (red line) replicas. Bins are normalized by the total number of playbacks of each type at each depth.

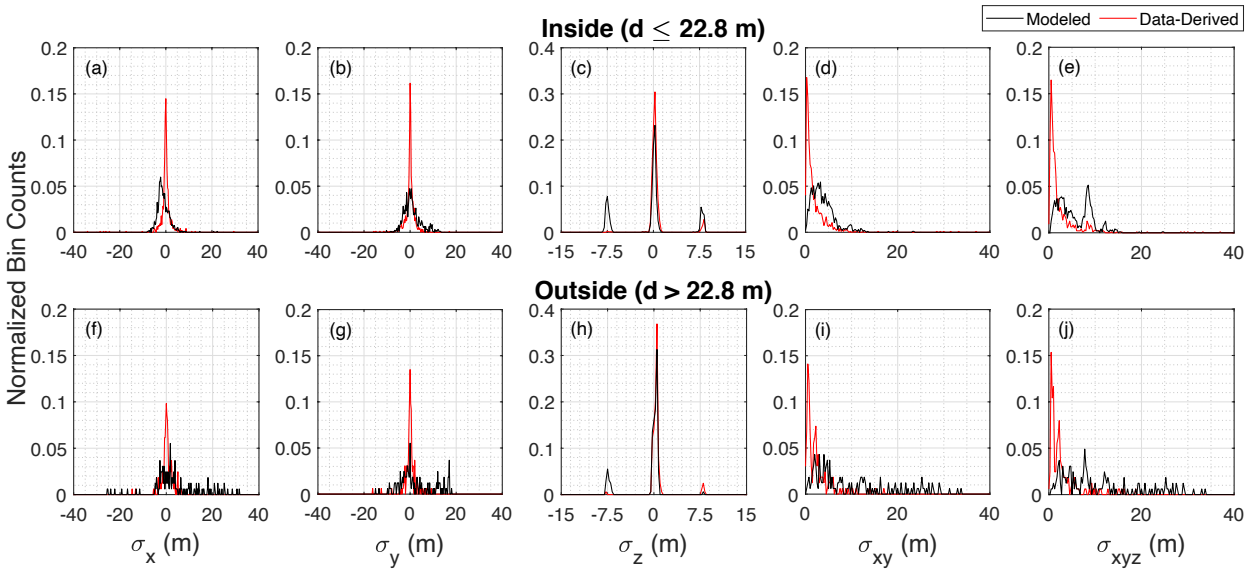

Supplementary Figure 3.4. Error distributions in the x-, y-, z-, xy- and xyz-dimensions for sources (a)-(e) inside and (f)-(j) outside of the array using modeled (black line) and data-derived (red line) replicas. Bins are normalized by the total number of playbacks inside and outside the array, respectively.

Supplementary Table 3.1. Summary statistics for localization error distributions in each dimension using modeled and data-derived replicas. Separate error distributions were computed for shallow and deep sources as well as sources played inside and outside of the receiver array based on the true position.

Dimension(s)	**Median (m)**		**Median Absolute Deviation (m)**		**Minimum (m)**		**Maximum (m)**		**Lin's Concordance Correlation Coefficient**	
	Model	*Data*	*Model*	*Data*	*Model*	*Data*	*Model*	*Data*	*Model*	*Data*
	Shallow (z = 5 m) (*n* = 647)									
x	-0.05	0.10	2.25	0.80	-25.8	-34.1	31.8	12.8	0.91	0.97
y	-0.22	0.04	2.20	0.88	-14.9	-16.1	18.0	13.1	0.93	0.98
z	0.24	0.10	0.29	0.23	-1.67	-1.67	8.51	8.41	0.04	-0.004
xy	3.79	1.61	1.50	1.14	0.32	0.03	34.0	37.1	0.78	0.94
xyz	5.10	1.71	2.70	1.17	0.49	0.07	34.0	37.1	0.73	0.93
	Deep (z = 13 m) (*n* = 469)									
x	-1.78	-0.04	0.85	0.42	-8.02	-10.2	22.2	8.70	0.94	0.99
y	0.56	0.06	1.93	0.33	-10.2	-9.71	13.1	16.9	0.93	0.99
z	-0.13	0.38	1.04	0.18	-8.20	-7.83	1.16	1.21	0.03	0.06
xy	2.91	0.65	1.67	0.41	0.12	0.003	23.5	19.8	0.76	0.95
xyz	5.26	0.86	3.51	0.42	0.36	0.07	24.7	21.1	0.76	0.93
	Inside Array (d ≤ 22.8 m) (*n* = 953)									
x	-1.51	0.01	1.33	0.57	-8.02	-34.1	22.2	12.8	0.94	0.95
y	0.21	0.06	1.97	0.59	-10.2	-15.8	13.1	16.9	0.94	0.97
z	0.12	0.22	0.35	0.24	-8.20	-7.83	8.51	8.41	0.25	0.87
xy	3.25	0.99	1.45	0.70	0.12	0.002	23.5	37.1	0.79	0.84
xyz	4.83	1.16	3.07	0.69	0.36	0.07	24.7	37.1	0.76	0.80
	Outside Array (d > 22.8 m) (*n* = 163)									
x	1.59	0.14	3.77	0.81	-25.8	-14.9	31.8	6.39	0.91	1.00
y	-0.07	-0.003	4.17	0.59	-14.9	-16.1	18.0	11.0	0.91	0.99
z	0.32	0.40	0.24	0.18	-7.79	-0.46	8.04	8.33	0.45	0.85
xy	5.76	1.51	4.75	1.15	0.35	0.05	34.0	16.9	0.41	0.95
xyz	7.58	1.68	4.70	1.07	0.61	0.12	34.0	18.7	0.41	0.95

References

Benhamou, S. (2011). Dynamic approach to space and habitat use based on biased random bridges. *PLoS ONE*, *6*(1). doi:10.1371/journal.pone.0014592

Benhamou, S., & Cornélis, D. (2010). Incorporating Movement Behavior and Barriers to Improve Kernel Home Range Space Use Estimates. *Journal of Wildlife Management*, *74*(6), 1353–1360. doi:10.2193/2009-441

Calenge, C. (2006). The package 'adehabitat' for the R software: A tool for the analysis of space and habitat use by animals. *Ecological Modelling*, *197*(3–4), 516–519. doi:10.1016/j.ecolmodel.2006.03.017

Lilliefors, H. W. (1967). On the Kolmogorov-Smirnov Test for Normality with Mean and Variance Unknown. *Journal of the American Statistical Association*, *62*(318), 399–402. doi:10.1080/01621459.1967.10482916

Lin, L. I. (1989). A Concordance Correlation Coefficient to Evaluate Reproducibility Author (s): Lawrence I-Kuei Lin Published by : International Biometric Society Stable URL : http://www.jstor.org/stable/2532051 REFERENCES Linked references are available on JSTOR for thi. *Biomatrics*, *45*(1), 255–268.

Wiggins, S. (2003). Autonomous Acoustic Recording Packages (ARPs) for long-term monitoring of whale sounds. *Marine Technology Society Journal*, *37*(2), 13–22. doi:10.4031/002533203787537375